NBSIR 77-1280 (R)

FILE CO

DO NOT REM

DEVELOPMENT, TESTING AND EVALUATION OF MHD-MATERIALS

RECEIVED
DATE 7/21/77
OTP

Quarterly Report

for the period April – June 1977

H. P. R. Frederikse, T. Negas and S. J. Schneider

Inorganic Materials Division
Institute for Materials Research
National Bureau of Standards
Washington, D. C. 20234

Date Published: June 30, 1977

Table of Contents   Page

ABSTRACT

Electrode design and fabrication as well as post-test characterization received much attention during this reporting period. Several new methods for joining the ceramic to the metal base are being considered, including a thick cermet layer and a mechanical attachment. A series of 11 anode-cathode pairs (5 different designs, 3 different materials) are being fabricated (with outside assistance) for a test in the AVCO generator under slagging conditions.

An appreciable amount of time has been spent in consultation with Westinghouse, Battelle and APS Materials Inc., in connection with the planning of Phase III of the U-02 testing program.

A number of electrode/insulator modules that have been tested in the MIT rig were analyzed at NBS (ANL, GE and NBS designs).

The large volume of viscosity data, collected over the last 4 years, are presently being analyzed and presented in the form of a comparison with a "base slag composition" (half-way between Illinois #6 and Rosebud).

Previous data of Halstead on the vapor pressure of K_2SO_4 together with results of new NBS measurements have been carefully compared and evaluated. The saturation pressures of K_2SO_4 appear to be about 5 times lower than previously assumed, which has important implications for seed-slag separation procedures.

In the assessment of alloys for downstream components attention has been focussed on mechanical strength and resistance to H_2S-attack.

Objectives and Scope of Work

The overall objective of this program is to obtain chemical and physical definition of high temperature materials which have shown promise for use in coal-fired open-cycle MHD power systems. Major problem areas in which investigations will be concentrated are:

1. Characterization of coal slag and its effects on system components and performance at prototype temperatures.

2. Development of electrode materials which provide adequate performance over extended periods of time.

3. Insulating materials which limit thermal losses and are resistant to prolonged thermal and erosion effects.

4. Preheater materials which can withstand the operating modes of separately and directly fired operation.

5. Seed recovery methods from slag which are technically and economically feasible.

6. Phase equilibria and diffusion rates of seed in slag and the corrosive action of combination on system components and materials.

7. Durability of prototype MHD sub-systems.

The program is designed to contribute to the solution of these problems by providing much needed data on candidate materials and by evaluating test samples and structures that have been subjected to real or simulated MHD conditions. The activities are grouped under six tasks:

G. Program Management Coordination (Assisting ERDA in coordination, planning and review of the various MHD-Materials Development Programs).

H. U-02 Materials Testing and Characterization (Coordination of U-02 Test Activities, Phase I). (Terminated June 30, 1976).

I. Operational Design Properties (viscosity, electrical conductivity, vaporization).

J. Corrosion by Seed and Slag (phase equilibria, diffusion).

K. Materials Testing and Characterization (test coordination, pre- and post-test analysis).

L. Assessment of Steam Plant Components (corrosion resistance of metals and alloys).

Summary of Achievements (April-June 1977)
(completed Milestones-See Work Statement for FY 1977)

Third Quarter accomplishments in terms of the projected milestones of the NBS-ERDA contract are listed below. ERDA directives requesting change of direction or emphasis (electrodes for U-25, characterization of electrodes for other contractors, etc.) have necessitated some changes in the chronological order of projected targets.

1c. Planning meetings and consultation sessions have been held to prepare for the U-02 materials test (Phase III) to be conducted in early 1978.

2. A number of NBS staff members particpated in project reviews, preparation of program plans, etc.

4a. Measured the viscosity of a New Hampshire flyash (AVCO) and a number of synthetic slags.

10b. Determined first versions of the phase diagrams for the quaternary systems $K_2O-Al_2O_3-SiO_2-MgO$ and $K_2O-Al_2O_3-SiO_2-CaO$.

13a. Measured the K_2SO_4 vapor pressure over K_2SO_4 (c,l).

19a. The electrical conductivities of a [60% spinel (MAFF-31)-40% Cr]- cermet and of a (not-so-insulating) sample of $SrZrO_3$ were determined.

30a. Measurements have been initiated on diffusion of iron from Mg-Al-Fe spinel into MgO.

39b. Electrode/insulator modules were designed, fabricated (outside NBS) and prepared for testing in various MHD test facilities (MIT, AVCO).

39c. Samples of 35 materials, that are being used by ERDA contractors for MHD-electrodes, insulators and preheaters, have been characterized at NBS by means of X-ray diffraction with respect to their phase composition.

40c. Optical and S-E-Microscopy as well as X-ray diffraction have been used for the evaluation of 3 electrode assemblies (NBS, ANL and GE) tested at MIT.

43a. Compiled a list of mechanical properties of promising alloys in particular for steam super heater application.

Coal Slag Properties Related to MHD, Conference on High Temperature Sciences Related to Open-Cycle,Coal-Fired MHD Systems, Argonne Natl. Lab., 4/6/77, W. Capps.

Some Vapor Pressure Data on K_2O Containing Substances, Conference on High Temperature Sciences Related to Open-Cycle, Coal-Fired MHD Systems, Argonne National Lab., 4/6/77, E. R. Plante.

Status of MHD Materials, Conf. on High Temperature Science Related to Open Cycle, Coal-Fired MHD Systems, Argonne Natl. Lab., 4/6/77, S. J. Schneider.

The Second Joint Test of a U.S. Electrode System in the USSR U-02 Facility, G. Rudins, S. J. Schneider, T. Negas, B. R. Rossing, J. L. Bates, G. P. Telegin, T. Bordina, O. Zamislov and V. Zalkind, 16th MHD Symp., Pittsburgh, PA May 16-18, 1977.

Electrodes and Insulators: Design and Materials Considerations, H. P. R. Frederikse and W. R. Hosler, 16th MHD Symp., Pittsburgh, PA, May 16-18, 1977.

Some Properties of Coal Slags of Importance to MHD, 16th MHD Symp., Pittsburgh, PA, W. Capps, May 16-18, 1977.

Interaction of MHD Seed (K_2O) with Multicomponent Oxide Solids and Liquids, L. P. Cook, E. R.Plante, C. L. McDaniel, T. Negas, and R. S. Roth, American Ceramic Society Meeting, Chicago, Il., April 25, 1977.

Task G. PROGRAM MANAGEMENT AND COORDINATION (S.J. Schneider)

1. Program Review and Consultation Activities

    S. J. Schneider participated in the regular ERDA-MHD staff meetings
and in assorted program review/coordination meetings and briefings. The
meetings included:

    1. ANL MHD Conference (invited speaker) April 4-6
    2. Program review at Montana Tech and Montana State University -May 2-6
    3. 16th MHD Symposium (presentation of paper on the US-USSR
        Phase II Test - Pittsburgh, May 16-18)
    4. Materials Ad Hoc Working Group Meeting (U-02 Phase III) April 7
    5. Steering Committee - US-USSR Program
    6. Technology Task Force - US-USSR Cooperative Program

The conclusions and recommendations resulting from these meetings are
reflected in reports to ERDA, through direct consultation with ERDA staff
or through documents published elsewhere.

    NBS receives on a regular basis, MHD technical reports and proposals
for review. During this period NBS provided 3 such evaluations.

    Part of the NBS experimental program involves characterization of
materials component elements tested in various MHD test rigs and facilities
throughout the United States (and USSR). In order to expedite the dessemina-
tion of this information, NBS has instituted a separate reporting system in
addition to the regular Quarterly submissions. The system consistes of the
following elements: 1. Telephone report to submittor after initial
examination, 2. Follow-up letter report, and 3. Detailed report (if warranted)
to submittor and ERDA. The detailed report will be distributed to general
contractors on an as needed basis as determined by ERDA; however highlights
of the detailed report will be abstracted and published in the NBS Quarterly
reports. In addition, general overall summary reports will be compiled from
time to time and published in appropriate journals and special editions.

    Inquiries regarding the status of any particular characterization or
requests for additional assistance should be directed to:

    A. Perloff 301-921-2900

    alternates
    T. Negas 301-921-2843
    W. Hosler 301-921-2940

2. US-USSR Cooperative Program

    a. U-25 Electrode Program

    Because of its importance this activity will have, in the coming
months, renewed emphasis. NBS responsibilities and accomplishments are
reported elsewhere in this report.

b. US-USSR Materials Program Activities

During this reporting period the US-USSR Ad Hoc Materials Working Group held several informal meetings concerning the implementation of the Phase III test at the U-02 in Moscow. The overall activity is being managed by Westinghouse; other participating groups include NBS, Battelle NW, GE, and ANL. The present schedule calls for proof-testing of candidate electrode systems at the Westinghouse facility in August-September 1977, delivery of the finished electrode wall to Moscow in November-December 1977 and actual testing in January 1978 (note scheduled dates are tentative and may be changed).

Upon the completion of the Phase III test the Materials Working Group will cease its activities as a separate entity; its functions will be incorporated into the efforts of the newly formed Task Force on MHD Technology Development (US-USSR).

In addition to the above, the Joint US-USSR chapter on materials (Status Report) has been again revised to incorporate new information provided by the USSR. It is believed that this will be the last version and that the chapter is "ready to go to press."

Task I.   OPERATIONAL DESIGN PROPERTIES

1.   Viscosity of Coal Slags   (W. Capps and D. A. Kauffman, Inorganic Glass Section)

Introduction

    Part of the program of characterizing MHD materials is the preparation
of synthetic slags and the determination of viscosity of these and of any
real slags furnished to NBS by other contractors.

Slag Preparation and Viscosity Measurement

1.   A power plant flyash from a New Hampshire coal was sent to NBS by
Mr. Stan Petty, AVCO-Everett Research Laboratory. A melt was made and
its viscosity was determined and is shown in Fig. 1 along with the analysis
furnished by AVCO.

2.   Twenty synthetic slags from the NBS studies were sent to Dr. James Anderson
at Montana State University for use in his program. Three specimens were
sent to Mr. Harry Rausch at the G. E. Valley Forge Space Center.

3.   Systematic additions were made to NBS Base Composition, K-884, to
determine the viscosity dependence on concentration of silica, alumina,
iron-oxide, etc. Preliminary results are shown in Figs. 2, 3 and 4.
Findings to date indicate (1) a nearly linear, large, positive dependence
on silica concentration, (2) a small negative dependence on alumina, and
(3) a large, negative, nearly linear dependence on the amount of iron
oxide. Although opposite in sign, the rate of change due to iron is the
same as the silica rate.

4.   Two talks were given: "Coal Slag Properties Related to MHD" was given
at the High Temperature Chemistry Symposium at Argonne National Laboratory
in April and "Some Properties of Coal Slags of Importance to MHD" was given
at the 16th Symposium on Engineering Aspects of MHD at the University of
Pittsburgh in May. An abstract of the talk will be printed in the pro-
ceedings.

Future Work

    The series described in paragraph 3 above will be continued to determine
the effects on viscosity of calcium and magnesium oxides.

    This new data together with an extensive bank of earlier data will be
used to improve equations and/or develop a suitable graphical method for
purposes of prediction of viscosity of coal slags from ash analyses.

*NOTE: Compositions of melts referred to in Figures 2, 3 and 4 appear
        in Table I.

Table 1

Coal Slag Compositions (wt. %)

NBS Melt No.	SiO_2	Al_2O_3	Fe_2O_3	CaO	MgO	
K-884	47.77	21.76	16.58	10.57	3.32	Base
K-887	52.77	19.68	14.99	9.56	3.00	+5% SiO_2
K-901	57.77	17.59	13.41	8.55	2.68	+10% "
K-913	42.77	23.84	18.16	11.58	3.64	-5% "
K-915	37.77	25.93	19.75	12.60	3.96	-10% "
K-921	45.33	25.76	15.73	10.03	3.15	+5% Al_2O_3
K-926	50.83	16.76	17.63	11.25	3.53	-5% "
K-931	53.88	11.76	18.70	11.92	3.74	-10% "
K-933	44.90	20.45	21.58	9.94	3.12	+5% Fe_2O_3
K-934	42.04	19.15	26.58	9.30	2.92	+10% "
K-953	39.18	17.84	31.58	8.67	2.72	+15% "
K-955	50.63	23.06	11.58	11.20	3.52	-5% "
K-958	53.49	24.36	6.58	11.84	3.72	-10% "

POWER PLANT FLY-ASH from a New Hampshire coal.

K-929

		wt.%
SiO_2	42	
Al_2O_3	25	
Fe_2O_3	15 - FeO 1.5
CaO	5.8	
MgO	3.1	
Na_2O	2.9	
K_2O	3.4	

xls

VISCOSITY (log$_{10}$ poises)

TEMPERATURE (C)

Fig. I.
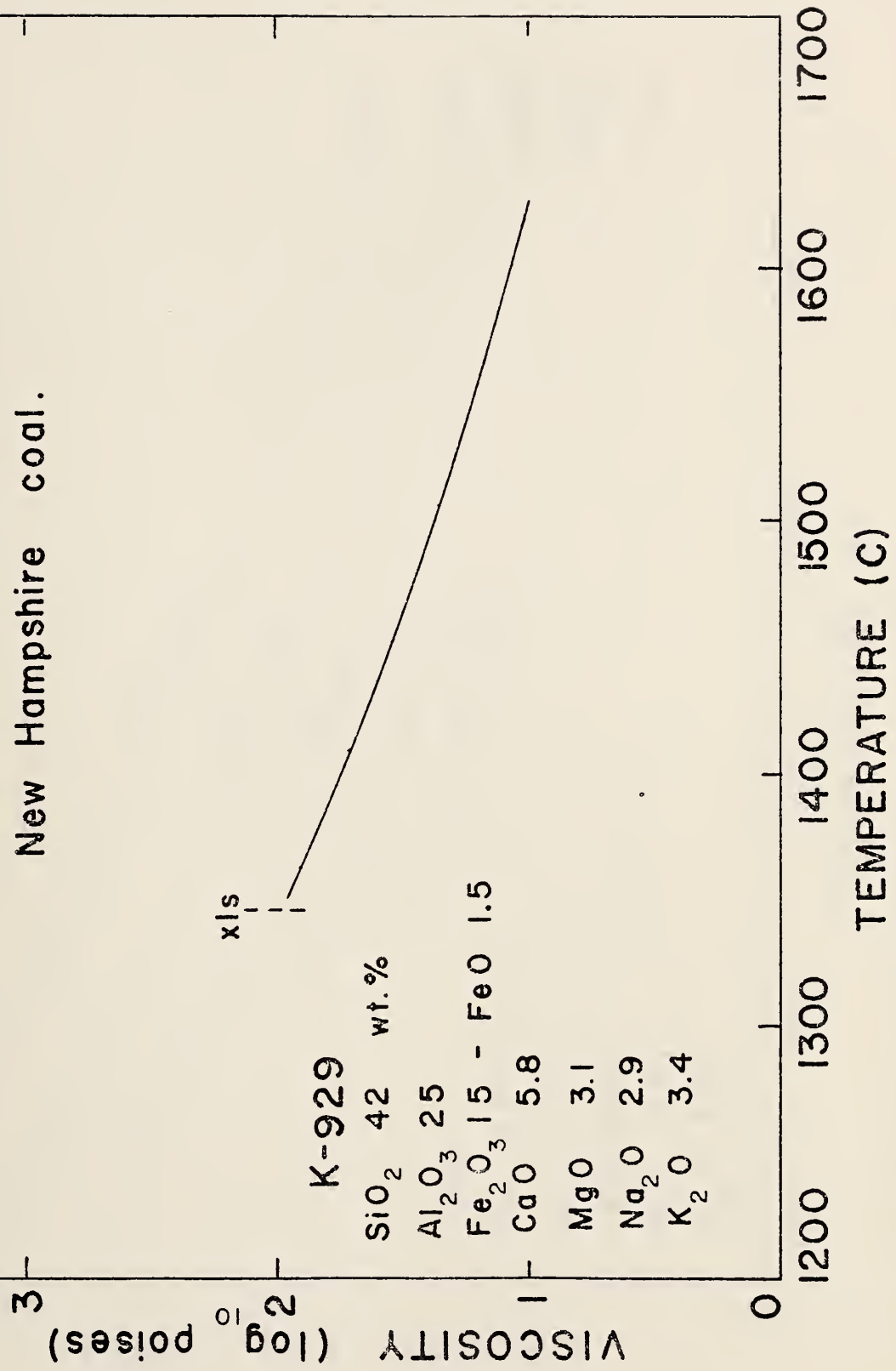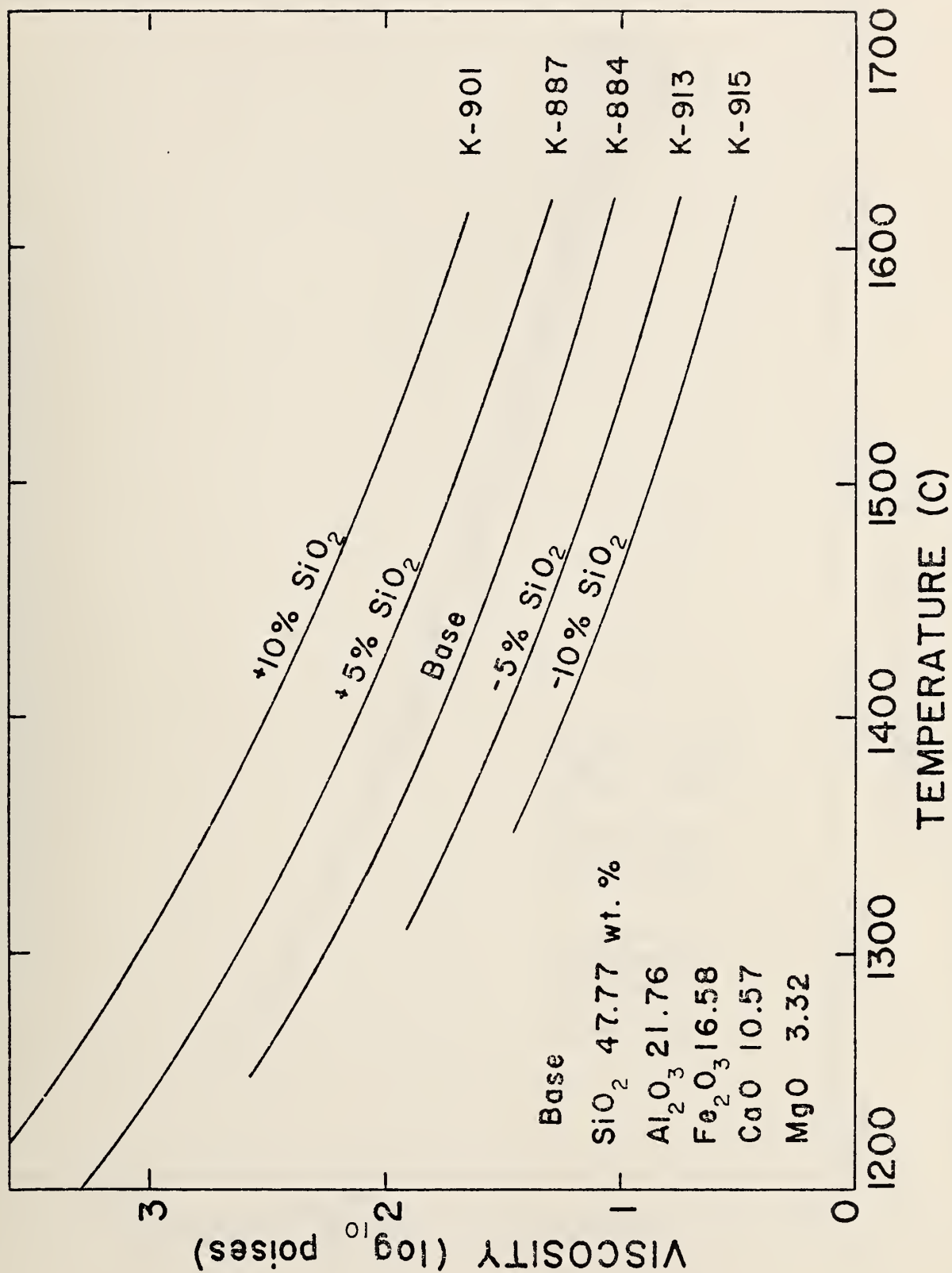
EFFECT OF SILICA

Fig. 2

Fig.3. EFFECT OF ALUMINA

K-931 -10% Al_2O_3
K-926 -5 % Al_2O_3
K-884 Base
K-921 +5% Al_2O_3
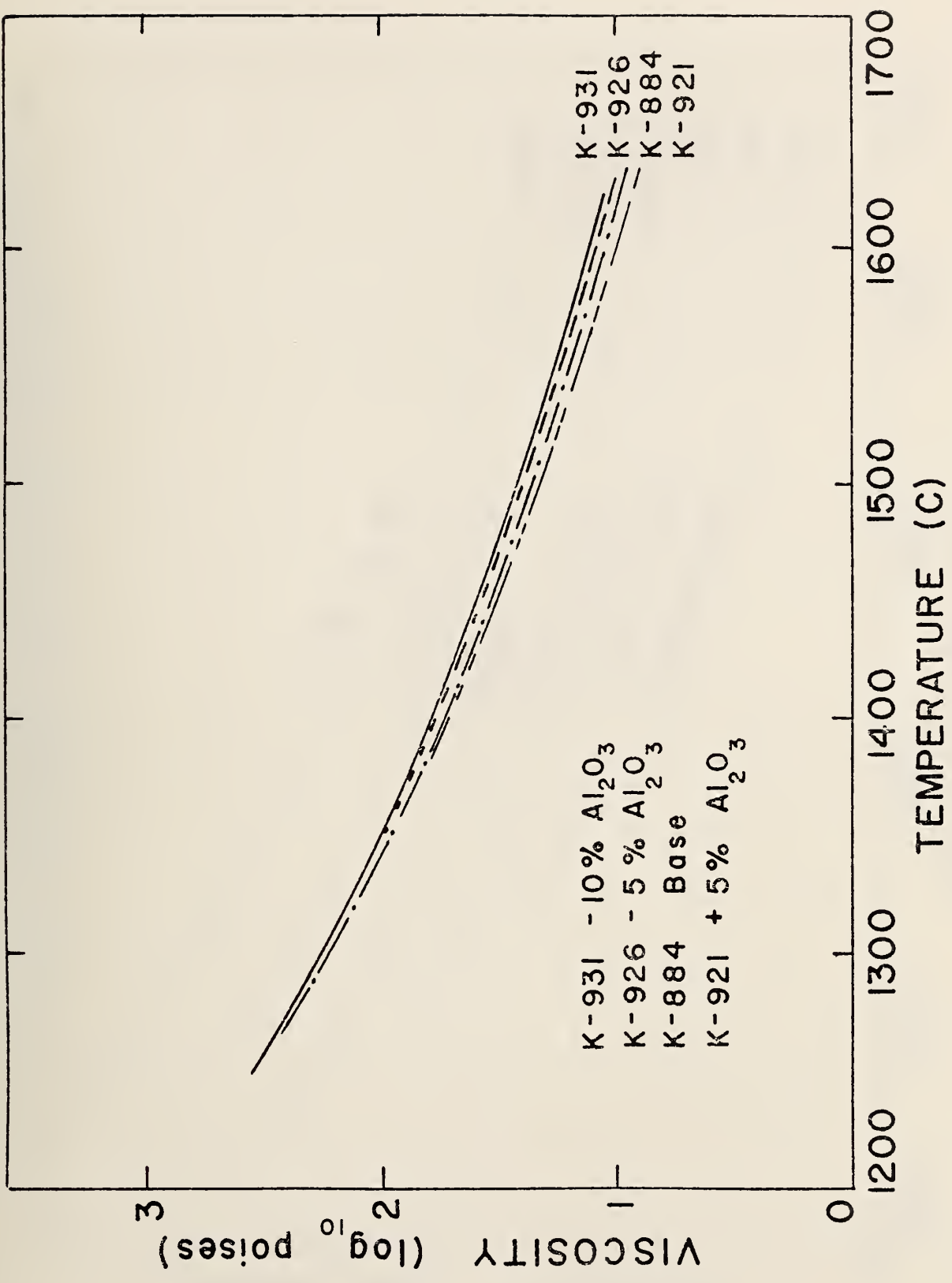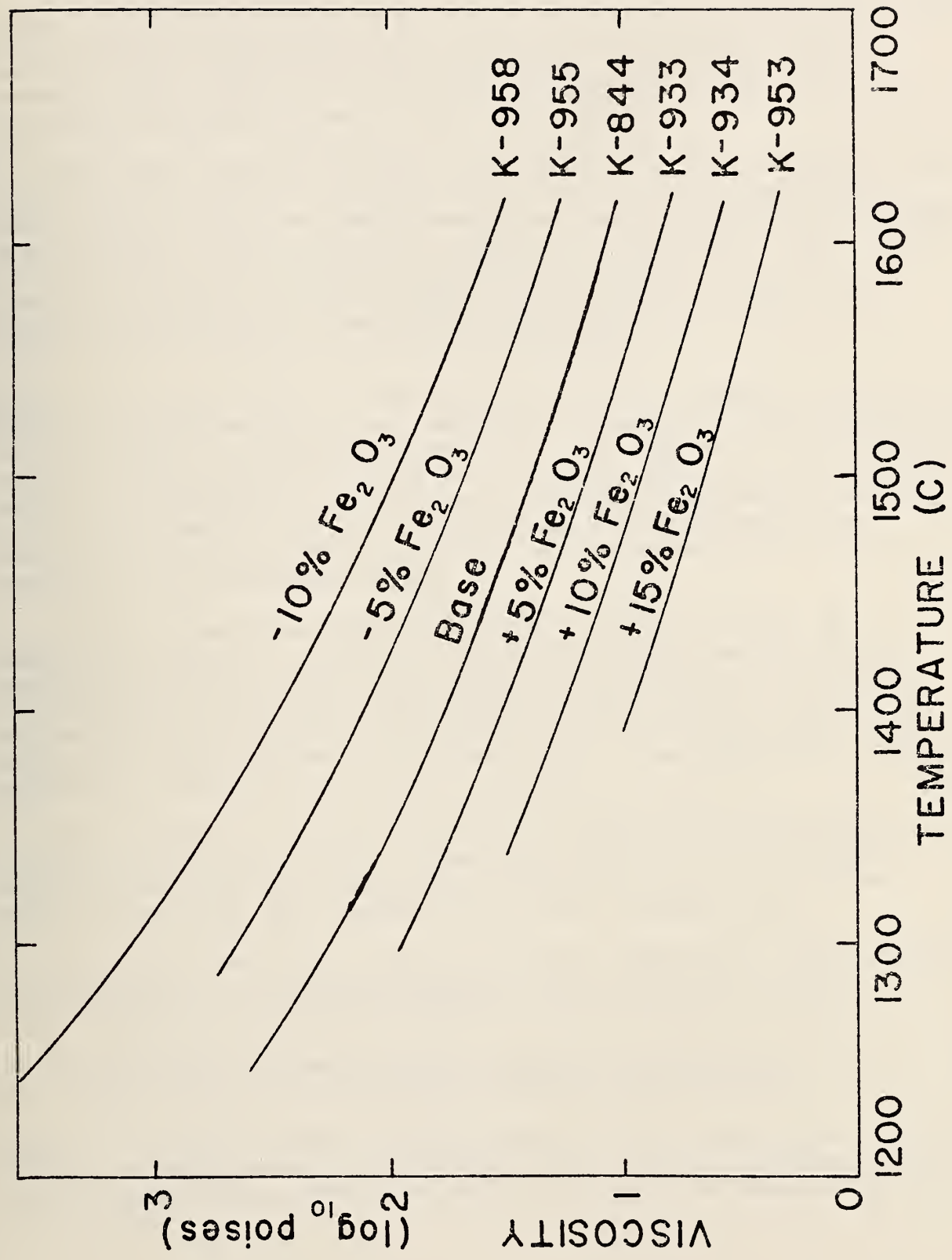
Fig. 4.   EFFECT OF IRON OXIDE

2. <u>Electrical Conductivity</u> (W. R. Hosler and A. J. Armstrong)

<u>LaCrO$_3$</u>. After the electrical conductivity measurements on arc plasma sprayed LaCrO$_3$ + 5% MgO were completed (see Jan.-March 1977 quarterly report) small hair-like crystals were seen to have grown between the electrical contacts. These crystals were removed and examined by scanning electron microscopy and energy dispersive x-ray (EDX) analysis.

The crystals were of two types: small rods (0.5-5.0 μm diameter) and larger crystals (10-20 μm diameter) which were acicular in appearance. Both types of crystals were approximately the same composition as determined by EDX analysis. They were mostly composed of Mg and Cr with a few percent of Si and Ni present. The presence of silica is detrimental to the electrical conductivity and high temperature strength of LaCrO$_3$. The source of these impurities should be eliminated in order to provide the best possible material for use as an MHD electrode.

<u>Cermet</u>. A sample of MAFF-31 (3MgAl$_2$O$_4$:Fe$_3$O$_4$) + 40% Cr cermet was sprayed in a free stand by APS Materials Inc., Dayton, OH. A portion of this material was tested at several temperatures between 700 °C and 1500 °C. After each high temperature treatment which lasted for from two to six hours, the sample was cooled to room temperature. Electrical conductivity measurements were made at the high temperature and then at room temperature to determine the deleterious effect of oxidation. Conductivity measurements were made using very high current densities (15A/cm^2).

Although measurable oxidation is known to occur in Cr metal at temperatures above 900 °C in air, no significant change was seen in room temperature electrical conductivity until the sample had been subjected to a temperature of 1215°C. Room temperature values ranged from 1000 to 600 ohm^{-1}cm^{-1} after treatment at temperatures up to 1133 °C. After treatment at temperatures between 1215 °C and 1535 °C, room temperature electrical conductivity values fell from 126 to 55 ohm^{-1}cm^{-1}. (Fig. 5).

This Cr-MAFF-31 cermet has been used in several electrode designs as a lead-out material for MAFF-31. The chromium provides the necessary electrical conductivity at temperatures below 600 °C as well as a lower thermal conductivity than the Hastelloy B metal previously used.

Electrical conductivity values at elevated temperatures ranged between 300-400 ohm^{-1}cm^{-1} at temperatures between 730 °C and 1468 °C. At 1535 °C a sharp decrease in electrical conductivity was seen (35 ohm^{-1}cm^{-1}).

After removal, the sample still possessed considerable strength and there were no apparent cracks despite repeated thermal cycling.

<u>SrZrO$_3$</u>. A sample of SrZrO$_3$ designated SZ-CE0104 was received from Westinghouse Research and Development Lab., Pittsburgh, PA. This was a sintered piece which was single phase material of good crystallinity but appeared slightly pink in color.

The electrical conductivity of the sample was measured as a function of temperature and several partial pressures of oxygen. The results are shown in Fig. 6. The electrical conductivity of this sample would be too high to be effective as an insulator material for high temperature use in an MHD generator. Although the data is in general agreement with that given in "Introduction to Ceramics", by W. D. Kingery, H. K. Bowen and D. R. Uhlmann, there is the possibility of the high conductivity being due to impurities present. So far no chemical analysis was made.

Another sample of known high purity has been received and measurements are in progress.

10^3 1727°C 1545 1393 1265 1156 1060 977 903 838 780 727

CONDUCTIVITY (OHM-CM)

10^2

10^1

5   6   7   8   9   10

$$\frac{10^4}{T(K)}$$
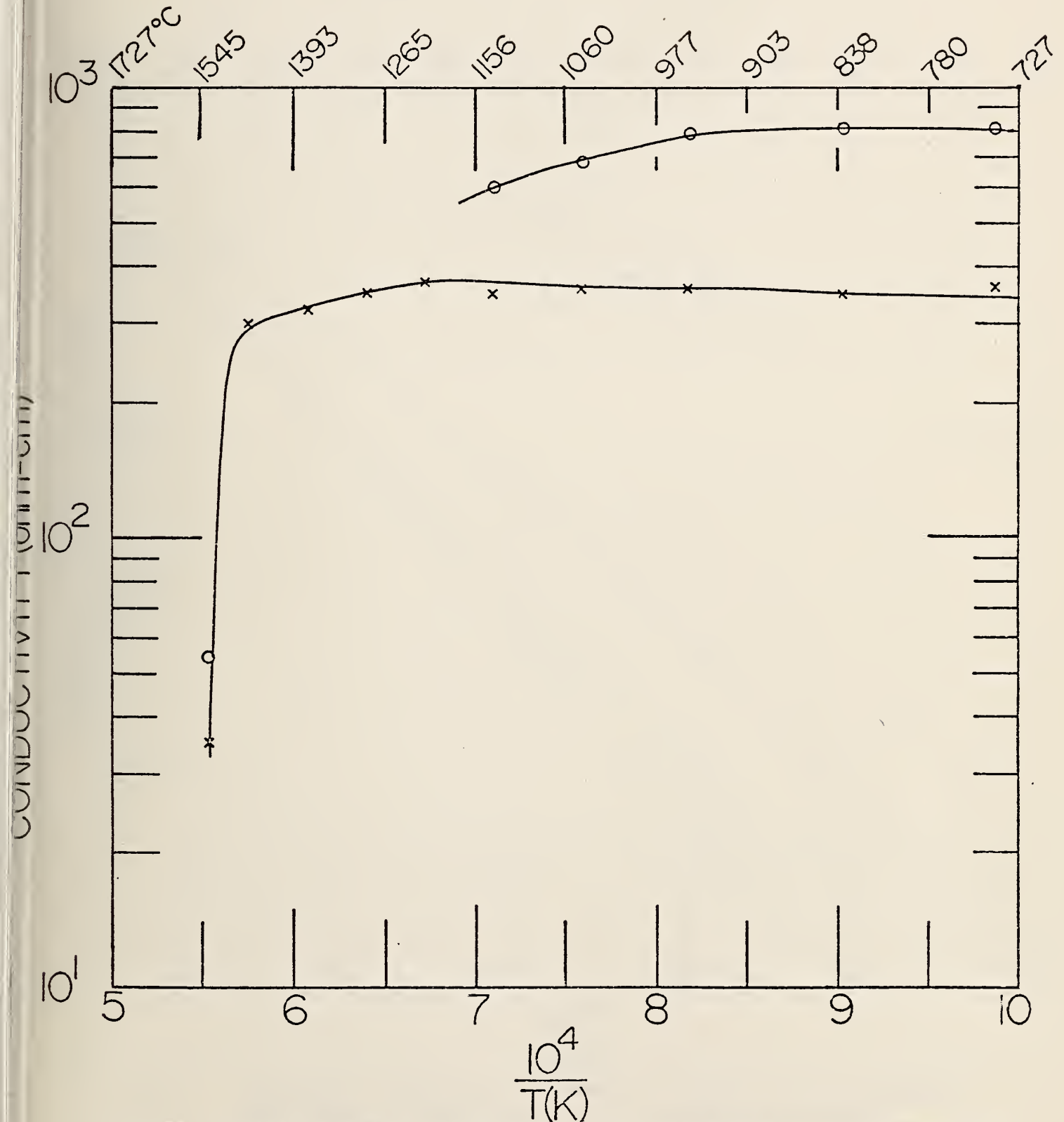
Fig. 5 . Crosses represent the conductivity of the cerment at high temperatures.
Circles indicate the room temperature conductivity after treatment
at the temperature shown on the abscissa.
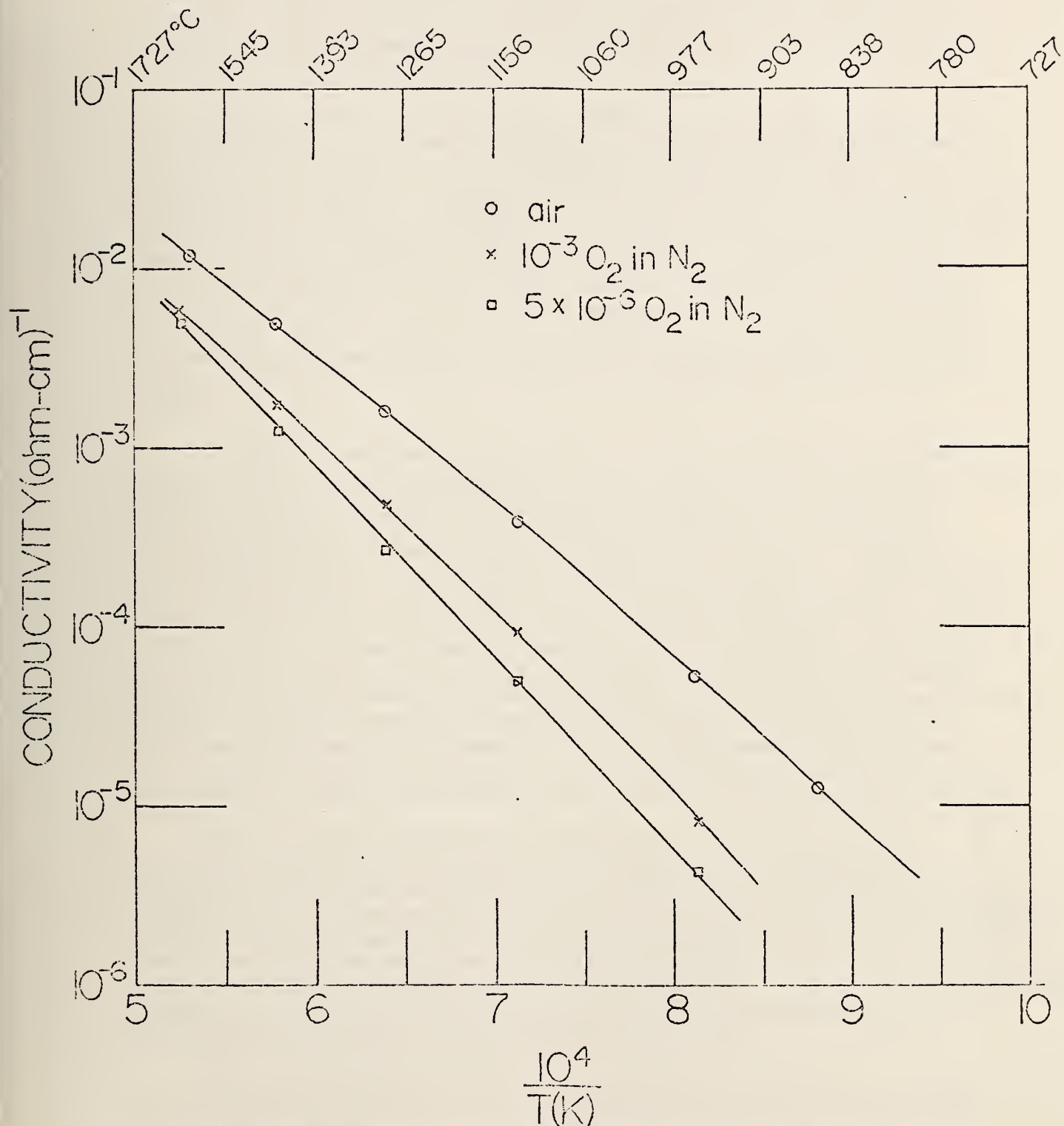
Fig. 6. Electrical conductivity of a sample of SrZrO$_3$ from Westinghouse (SZ-CE0104). Sintering time, temp. & atmos. not given.

3. Vaporization and Dissociation Studies on K_2SO_4 (E. R. Plante)

The vaporization program has been involved in the determination of K(g) pressures over various K_2O-containing materials. The purpose of these measurements has been to provide data which can be used for predicting the equilibrium concentration of K_2O in slag solutions and to predict the temperatures and K(g) pressures at which MHD structural materials will resist corrosion.

Although the molecule K_2SO_4(g) does not enter directly into these considerations, it is one of the more important K bearing molecules at temperatures from 1600 - 2200K and plays a significant role in defining the activity of K_2O in the vapor phase as well as the condensation temperature of K_2SO_4. A comprehensive review article on the vaporization thermodynamics of K_2SO_4 by Eliezer and Howald (1) was recently presented. Their critical evaluation of the existing data concluded that the most reliable measurements were probably those of Halstead (2); a viewpoint with which we and most of the MHD community probably agree. However, the lack of reliable measurements confirming his data and a review (3) of the vapor pressures of K_2O-containing substances important to MHD made it appear that some measurements to confirm his results were in order.

Halstead's measurements were made using the gravimetric Knudsen method below, and the transpiration method above the melting point. (1349 K) His Knudsen data were obtained using cells pressed from equimolar mixtures of $A\ell_2O_3$ and MgO. He recognized potential problems due to cell porosity and/or reaction of the K_2SO_4 with the cell. Measurements were therefore made using cells in which the inner or outer surface was covered with Pt. Since these latter results agreed with the former, it was concluded that the Knudsen cells were both non-porous and unreactive to K_2SO_4(c). The transpiration results were not regarded by Halstead to be as trustworthy as the Knudsen results because of difficulties in obtaining vapor pressures independent of flow rate at higher temperatures (1668K). However, within the experimental error, the vapor pressure data were in reasonable agreement with a vapor pressure equation based on the Knudsen data extrapolated into the liquid range by correcting for the change in slope and intercept due to the heat and entropy of fusion.

While Halstead recognized the potential errors due to porosity of the Knudsen cell and/or reaction with $A\ell_2O_3$ or MgO, the presence of $A\ell_2O_3$ is a common factor in both his transpiration and Knudsen experiments. Although it is not known whether the rate of reaction would be sufficiently high to cause serious error it can be predicted from data in the JANAF (4) tabulation and some measurements previously reported from this laboratory (5) that the reaction of K_2SO_4 with $A\ell_2O_3$ to form $K_2O \cdot 9A\ell_2O_3$ is thermodynamically favorable. These are additional reasons why new measurements of the vapor pressure of K_2SO_4 were considered worthwhile.

There is no doubt that the overall vaporization behavior of K_2SO_4 can be described in terms of the sublimation or vaporization reaction,

$$K_2SO_4(c, \ell) = K_2SO_4(g)$$

and the dissociation reaction,

$$K_2SO_4(c, \ell) = 2K(g) + SO_2(g) + O_2(g)$$
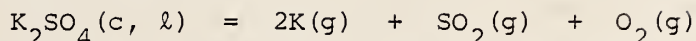
The existence of $K_2SO_4(g)$ molecules has been demonstrated through previous mass spectrometric measurements (6, 7) as well as some recent observations in our own laboratory and indirectly by the observation that the measured pressure is greater than that predicted for the decomposition pressure alone. It is worth noting that decomposition pressures involving well characterized vapor species and condensed phases can generally be calculated from thermodynamic data more accurately than they can be measured. The major question therefore concerns the relative importance of the vaporization and dissociation reactions. Concentrations of other species in the gas phase such as K_2O, KO, and SO_3 can be shown to be minor (< 1%) in comparison.

<u>Experimental Measurements</u> (In collaboration with C. Olson and T. Negas)

Mass effusion measurements were made using the Mettler Microbalance System. The K_2SO_4 sample was NBS-ICTA Standard Reference Material 760. The effusion cell was constructed of Pt and had an effusion orifice .020" in diameter. Weight loss data were obtained at fixed temperature and recorded in the form weight *vs* time. Linear portions corresponding to m/t were selected and used to calculate apparent pressures. The rate of vaporization observed corresponds to that due to effusion of $K(g)$, $O_2(g)$ and $SO_2(g)$ as well as $K_2SO_4(g)$. The observed rate of evaporation can be used to calculate an apparent $K_2SO_4(g)$ pressure using the equation

$$P = \frac{m}{cat} \sqrt{\frac{2\pi RT}{M}}$$

in which m/t is the weight loss per unit time, a is the area of the effusion orifice, c is the Clausing factor, R is the gas constant, T is the absolute temperature and M is the molecular weight of K_2SO_4. Comparison of the apparent pressure with the calculated dissociation pressure shows that a correction for effusion of dissociation products is necessary.

The contribution of dissociation products to the apparent $K_2SO_4(g)$ pressure can be shown to be

$$\delta P_{K_2SO_4} = P_K/2 \sqrt{M_{K_2SO_4}/M_K}$$

Here, $M_{K_2SO_4}$ and M_K are the molecular weights, and P_K is the potassium pressure from the dissociation reaction under Knudsen flow conditions which can be determined from the relationship,

$$P_K = (K_{eq}/.290)^{1/4}$$

in which K_{eq} is the equilibrium constant for the dissociation reaction. Values of P_K were obtained at 100K intervals using data from the JANAF (4) tables. Least square lines for use above or below the melting point were obtained using 3 calculated pressures at 100K intervals above or below the melting point respectively. The data are given in table 2 which lists the temperature in K, the apparent K_2SO_4 pressure in atmospheres, the corrected K_2SO_4 pressure in atmospheres, and the third law heat of sublimation at 298K. The third law heats were calculated using the recent Gibbs function data made available by Gurvich *et al* (8).

The second law heat of sublimation calculated by least squares using the method of Cubicciotti (9), the above Gibbs functions, and based on data below the melting point is 81140 ± 1960 cal mol^{-1} compared to the average third law heat of 81780 ± 60 cal mol^{-1} indicating good agreement between the entropies of K_2SO_4(g) (45.313 estimated from molecular constant data by Gurvich (8) *vs* 45.820 ± 1.547 determined by the second law method at 298K). The errors quoted are standard errors. The standard heat of formation of K_2SO_4(g) at 298K is -261760 cal mol^{-1} based on our average third law heat and the JANAF (4) value of -343540 cal mol^{-1} for the standard heat of formation of K_2SO_4(c). ERDA contractors wishing to use the standard heat of formation of K_2SO_4(g) given here should also use the Cp data for K_2SO_4(g) given by (8).

Careful analysis of the data points above the melting point show that they are incorrect because of unknown systematic error (they give rise to a negative heat of fusion for example) so they were excluded from consideration in calculating the second and third law heat.

According to our data and analysis the saturation pressure of K_2SO_4 is about 1/5 the value measured by Halstead. This may have important implications in design considerations for seed-slag separation in MHD systems. As a rough guess, we estimate that this will increase the condensation temperature of K_2SO_4 in an MHD system by about 50K.

Future Work:

During the next quarter measurements on the K pressure over $K_2O-SiO_2-Al_2O_3$ solutions will be continued. Additional measurements on K_2SO_4 using a larger effusion hole are planned in order to extend the temperature range in which measurements of the vapor pressure below the melting point are possible and to confirm the present results. Measurements by mass spectrometry on $KFeO_4$ will be attempted.

TABLE 2

K$_2$SO$_4$ Vapor Pressure Data

T°K	P apparent (atm)	P corrected (atm)	ΔH°$_{298}$(cal)
1271	5.01-6	3.98-6	81267
1316	1.25-5	9.65-6	81383
1271	4.00-6	2.97-6	82007
1196	7.75-7	6.16-7	81572
1221	1.44-6	1.14-6	81566
1246	2.38-6	1.81-6	81851
1271	4.40-6	3.37-6	81688
1296	7.27-6	5.44-6	81821
1321	1.28-5	9.62-6	81650
1196	7.27-7	5.68-7	81765
1221	1.29-6	9.87-7	81906
1246	2.18-6	1.61-6	82141
1296	7.27-6	5.44-6	81821
1321	1.20-5	8.82-6	81878
1345[a]	1.94-5	1.41-5	81847
1370[a]	3.18-5	2.32-5	81617
1351[a]	2.23-5	1.63-5	81729
1319	1.06-5	7.55-6	82182
1270	3.90-6	2.89-6	82020
1396[a]	5.15-5	3.74-5	81423
1420[a]	8.24-5	6.05-5	81091

[a] Above melting point, not used in second or third law analysis.

21

References

1. I. Eliezer and R. A. Howald, J. Chem. Phys., 65, 3053 (1976).

2. W. D. Halstead, Trans. Farad. Soc., 66, 1966 (1970).

3. E. R. Plante, Proceedings of the Conference on High Temperature Science Related to Open-Cycle, Coal-Fired MHD Systems, ANL-77-21 (1977).

4. JANAF Thermochemical Tables, Dow Chemical, Midland, Michigan.

5. E. R. Plante, C. D. Olson, and T. Negas, Sixth International Conference on Magnetohydrodynamic Power Generation, Washington, DC, 211 (1975).

6. P. J. Ficalora, O. M. Uy, D. W. Muenow, and J. L. Margrave, J. Amer. Ceram. Soc., 51, 574 (1968).

7. L. N. Gorokhov, High Temperature Technology, Proceedings of the Third International Symposium on High Temperature Technology, Butterworths, London, U. K. (1967).

8. L. V. Gurvich, O. V. Dorofeeva and V. S. Yungman, Proceedings of the Conference on High Temperature Science Related to Open-Cycle, Coal-Fired MHD Systems, ANL-77-21 (1977).

9. D. Cubicciotti, J. Phys. Chem., 70, 2410 (1966).

TASK J.   CORROSION AND DIFFUSION PROCESSES

1.   Seed-Slag Interactions

a.   Compositional Variations in $KAlO_2$-SiO_2 Based Materials (L. Cook, W. Brower)

To investigate the behavior of $KAlO_2$-SiO_2 based compounds at high temperatures, container metals suitable for preparation of sealed capsules in experiments above 1800°C were sought. Experiments with Ta and Mo were performed, using $(KAlO_2)_{70}(SiO_2)_{30}$, prereacted at 1600°C. Capsules were loaded and welded in an inert atmosphere. Experiments were performed under a forming gas atmosphere in an inductively heated graphite susceptor with zirconia packing. Temperature reached $\sim2200\pm100$ °C for about 10 min. The tantalum capsule ruptured and showed extensive signs of reaction (Figure 1). Reaction products appear to be free of K_2O, although this may have been completely volatilized. The tantalum reaction product is rich in Al_2O_3 (apparently no other elements besides Ta, and possibly O). The reaction has occurred both on the inside and the outside of the capsule - a thin layer of unreacted Ta is still present between reaction crusts. Whether the capsule rupture preceded reaction or whether rupture occurred because of reaction on the inner surface is uncertain. The latter seems unlikely, because there is no strong sign of reaction adjacent to the melted $(KAlO_2)_{70}(SiO_2)_{30}$. Rupture may have been caused by hydrogen embrittlement rendering the Ta incapable of withstanding the increased internal pressure at 2200° C - reaction was then possibly caused by contact of $(KAlO_2)_{70}(SiO_2)_{30}$ with forming gas. Further experiments using different atmospheres will test the feasibility of using Ta.

The molybdenum tubing worked much better in the same experiment (Figure 2-a). The capsule held, and no significant evidence of reaction between capsule walls and $(KAlO_2)_{70}(SiO_2)_{30}$ was detected (Figure 2-b). Energy dispersive x-ray spectra of melt showed no detectable Mo; spectra of tubing adjacent to melt showed no detectable K. A thin unidentified skin a fraction of a micron thick was seen adhering to the Mo wall adjacent to melt in some areas (Figure 2-c). Presumably this is an $MoSiO_2$-related substance. It appears that Mo will be acceptable for sealed high temperature studies of $KAlO_2$-based materials. Reaction with other components such as CaO will also be tested.

b.   Thermochemistry of the CaO-K_2O-Al_2O_3-SiO_2 System (L. Cook)

Experimental work conducted in the last quarter together with published data have been used to construct the working model of sub- solidus compatibilities in the system CaO-K_2O-Al_2O_3-SiO_2, shown in Figure 3. This system is especially important in understanding the

Fig. 1. Fractured surface of Ta capsule with $(KAlO_2)_{70}(SiO_2)_{30}$ sealed inside, run at ∿2200 °C in forming gas. Remainder of melt is visible in bottom (40X).

Fig. 2 a. Mo capsule, experiment identical to Fig. 1. Melt in bottom of capsule (35X).

Fig. 2 b. Contact between melt and Mo (1400X).

Fig. 2 c. Thin skin adhering to Mo wall (left) at interface
with melt (right) 7000X).

process of seed capture by western coals, some of which are markedly more CaO-rich than bituminous midwestern and eastern coals. This latter point is clear from comparison of Figures 4 and 5, CaO-SiO_2-Al_2O_3 "projections" of multicomponent analyses of bituminous and sub-bituminous coals, respectively. Also shown on these diagrams are projected tie lines between phases, taken from Figure 3. The chemical systems most important for study, in relation to the compositional distribution of natural coal ashes from the U.S. are thus apparent. Noteworthy is the difference in distribution of analyses between the two coal types. CaO in bituminous coals has a well defined distribution about a maximum of $\sim$ 3 mole % (Figure 4). CaO in sub-bituminous coals shows no tendency for a well-defined distribution, with values spread between 1 and 40 mole % (Figure 5). This conclusion is reinforced by the "average" analyses of five Montana coal formations (with standard deviations), included for purposes of comparison in Figure 5. In spite of the above difference, a marked similarity between the two types of coals is apparent in mole % $SiO_2/(SiO_2+Al_2O_3)$ ratios (Figure 6). The great majority of analyses fall between 0.67 (the projected composition of $KAlSiO_4$) and 0.80 (the projected composition of $KAlSi_2O_6$), with well defined medians at $\sim$ 0.77 and $\sim$ 0.75 for bituminous and sub-bituminous coals, respectively. Referring to Figure 5, many of the western type coals fall within the projected area of the system $CaSiO_3$-$CaAl_2Si_2O_8$-$KAlSi_2O_6$. It is for this reason that a study of this system is proposed as an important step in understanding the behavior of western coal slags in the channel (revised milestone 17-e). For the bituminous coals, iron is a much more important component than CaO, as discussed below.

A thermodynamic analysis of the CaO-K_2O-Al_2O_3-SiO_2 system is being conducted in conjunction with experimental determination of invariant vaporization equilibria in the system and measurement of potassium activities in melts of invariant composition. This analysis is being done with the following assumptions:

a) subsolidus equilibria are as in Figure 3

b) solid solutions involving substitution of K_2O do not occur with the exception of $Ca_2Al_2SiO_7$-$KCaAlSi_2O_7$, which is assumed ideal up to the maximum of 20 mole %

c) other solid solutions are not significant in this analysis

d) within each four phase volume, potassia chemical potentials in the system and potassia "activities" in the gas phase in equilibrium with condensed phases (defined as $P_K^2 \cdot P_{O_2}^{1/2}$) are fixed by a uniquely defined univariant vaporization equation (Table 1). This is true up to the temperature of invariant melting and is a reasonable extrapolation <u>for melts of invariant composition</u> up to plasma temperatures.

The value of this type of analysis lies in the correlation between the subsolidus (for which reliable thermochemical data are available) and the realm of plasma/slag interaction.
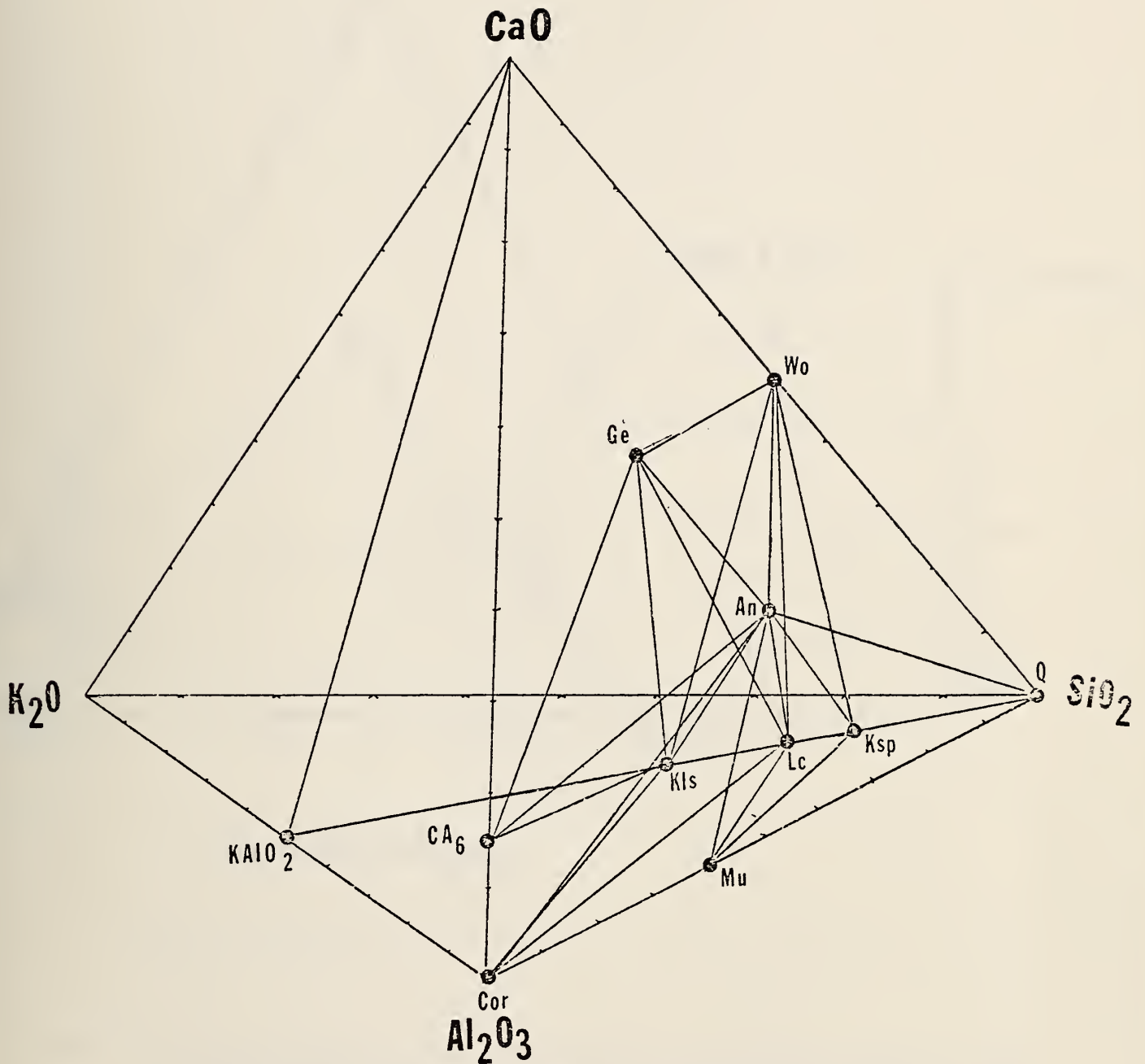
Fig. 3.   Working model of subsolidus equilibria for the system
$CaO-K_2O-Al_2O_3-SiO_2$ (mole %). Abbreviations as in Table 1.
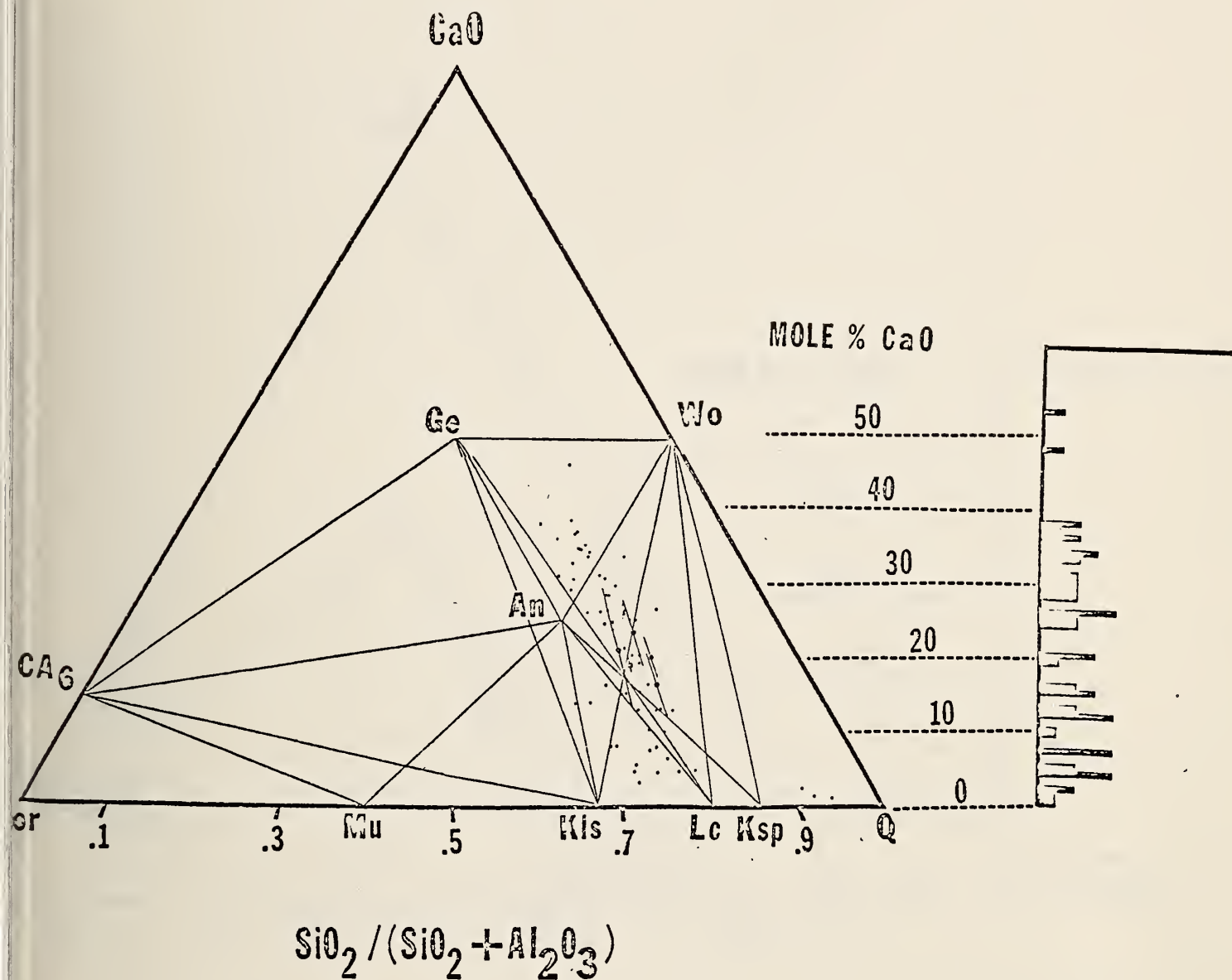
Fig. 4. CaO-Al$_2$O$_3$-SiO$_2$ projection of analyses for bituminous coals (Bureau of Mines Bulletin 567) in relation to subsolidus equilibria. Data point labelled I corresponds to "average" Illinois #6 coal (A. Postelthwaite, Pers. communication to W. Brower, 1976).
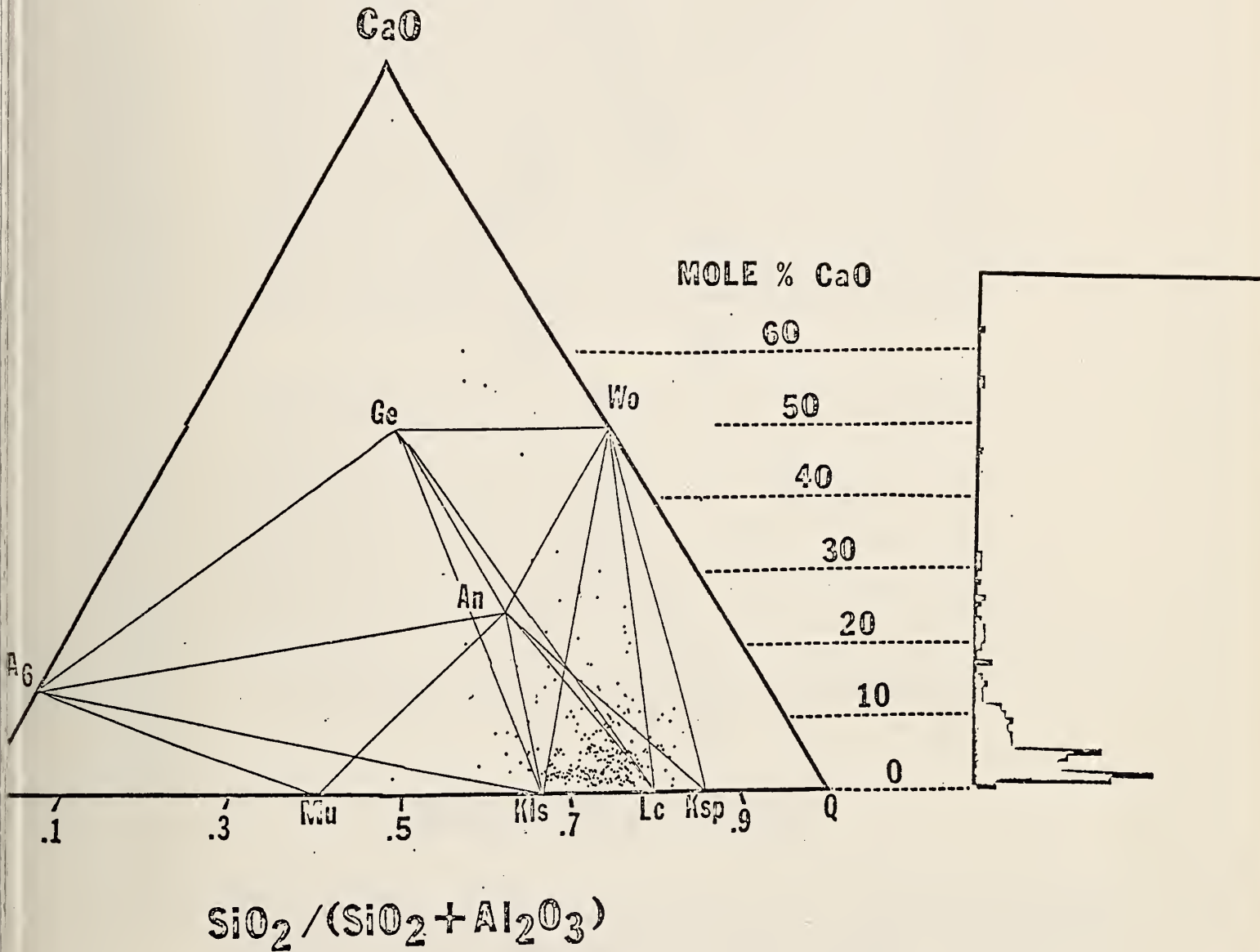
Fig. 5. CaO-Al$_2$O$_3$-SiO$_2$ projection of analyses for sub-bituminous coals, lignites and unclassified western coals (Bureau of Mines Bulletin 567) in relation to subsolidus equilibria. Data points with bars show "average" and standard deviations of five Montana coals (after Diebold).
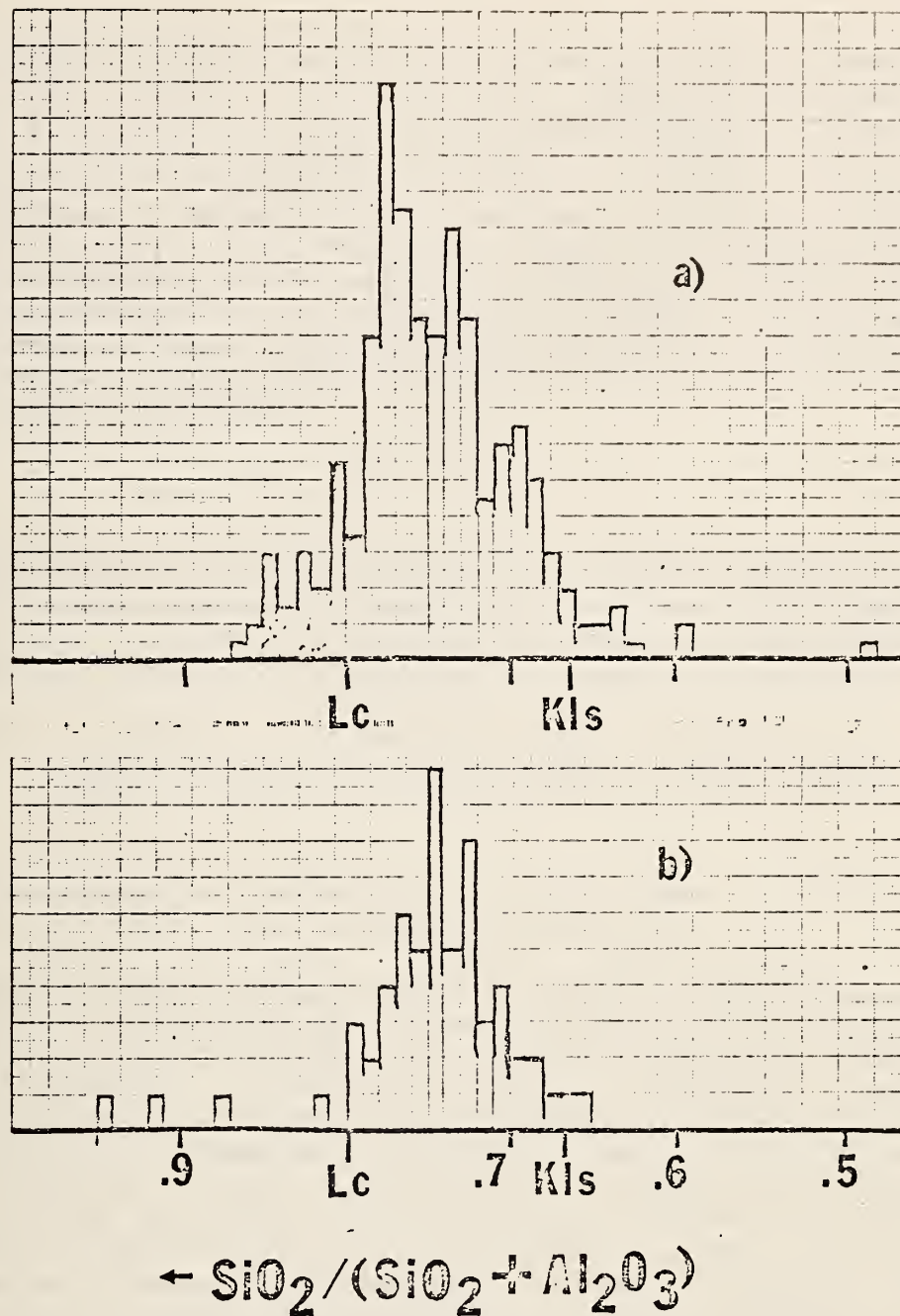
Fig. 6. Mole % silica to silica-plus-alumina ratio in recalculated analyses, U.S. coal ashes (Bureau of Mines Bull. 567). Grouped according to bituminous (a) and sub-bituminous or lower (b) rank. Kls and Lc indicate projected compositions of $KAlSiO_4$ and $KAlSi_2O_6$, respectively.

Calculated equilibrium curves for invariant melts in three of the volumes shown in Figure 3, corresponding to reactions 3-a, 4-a, and 7-a of Table 1 are given in Figure 7. The compositions and invariant temperatures of these melts can only be estimated at present; it is expected that these will be established during the next quarter. The upper reaction curve in Figure 7, corresponding to reaction 7-a in Table 1, is nearly coincident with that calculated for the eutectic melt between $K_2Si_2O_5$, $KAlSiO_4$ and $KAlSi_2O_6$, which contains $\sim$ 45 wt % K_2O. However a problem has been encountered in the thermochemical analysis, in that topological relationships of Figure 3 imply the following order of decreasing μ_{K_2O} in the compositional volumes of Table 1: 4, 3, 2, 1, (5, 7), (6, 8), 9, 11, 10. Given that

$$\mu_{K_2O} = \mu^\circ_{K_2O} + RT \ln P_{K_2O},$$

a similar relationship should hold among calculated potassium pressures. The relation among curves in Figure 7 is in the order of decreasing P_{K_2O}: 7-a, 3, 4. It is hoped that measurements during the next quarter, with continued thermodynamic analysis, will resolve this problem.

Reference: F. Diebold, 1977, Characterization of Coal for Open Cycle MHD Powder Generation System, Project Review, MERDI, Contract EF-77-C-01-2524.

c. Thermochemistry of the $MgO-K_2O-Al_2O_3-SiO_2$ System (L. Cook)

Figure 8 shows a working model for subsolidus compatibilities in the system $MgO-K_2O-Al_2O_3-SiO_2$, derived principially from the work of Schairer (1954) and Luth (1967), with limited experimental verification in this laboratory. The importance of MgO as a component of western-type coal slags, when recalculated on a mole % basis, is apparent from Figure 9, a $MgO-SiO_2-Al_2O_3$ "projection". MgO content ranges up to 20-25 mole %, with a maximum at $\sim$ 7 mole %. By contrast, bituminous coals (Figure 10) usually contain less than 5 mole % MgO, with a maximum at $\sim$1.5 mole %. The system $MgO-K_2O-Al_2O_3-SiO_2$ is thus important primarily in studying the behavior of western coal slags in the channel, but also in corrosion studies involving seed, slag and $MgAl_2O_4$ or similar insulators. Nearly all the sub-bituminous coals project within the $Mg_2SiO_4-KAlSiO_4-KAlSi_2O_6$ system, only partially studied by Luth (1967).

A preliminary thermodynamic analysis of the $MgO-K_2O-Al_2O_3-SiO_2$ system has been initiated as a prelude to further determination of invariant equilibria in the system and measurement of potassia activities in melts of invariant composition. This analysis is being completed with assumptions similar to a, b, c, d in the analysis of the $CaO-K_2O-Al_2O_3-SiO_2$ system above.
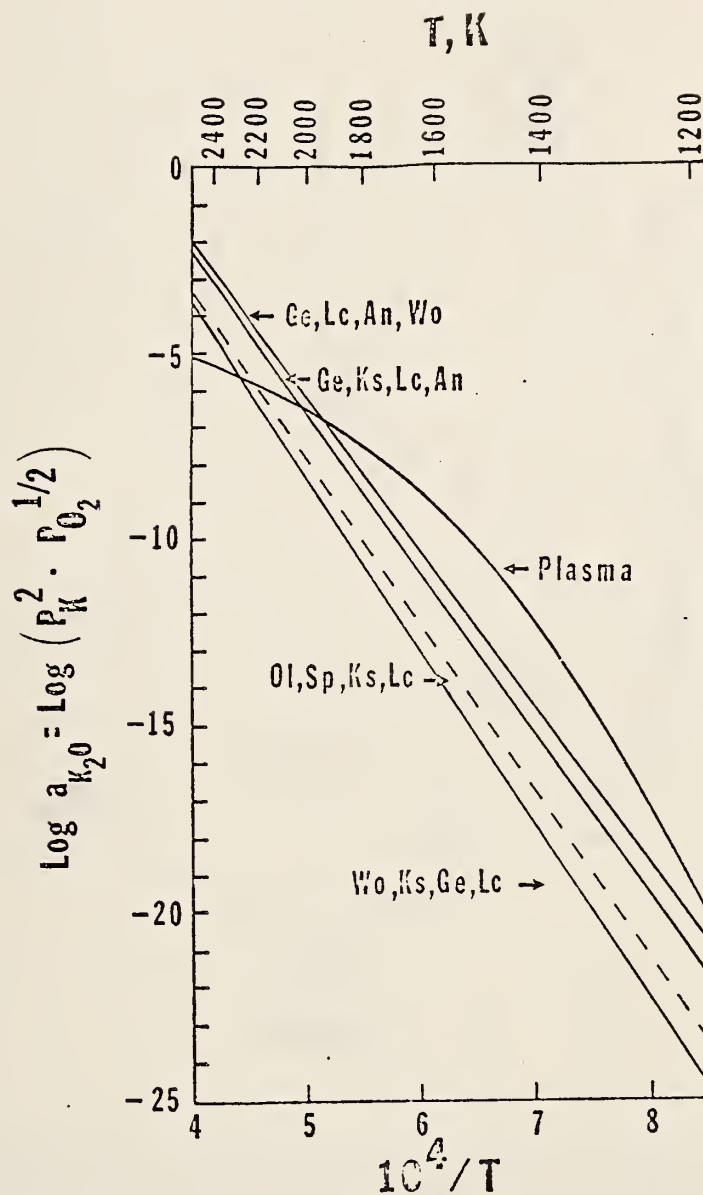
Fig. 7. Calculated potassium pressures as a function of temperature for
selected invariant melts in four-phase volumes in the systems
$CaO-K_2O-Al_2O_3-SiO_2$ and $MgO-K_2O-Al_2O_3-SiO_2$ (dashed) in relation
to seeded plasma (1 wt % K_2CO_3) curve (supplied by E. R. Plante).
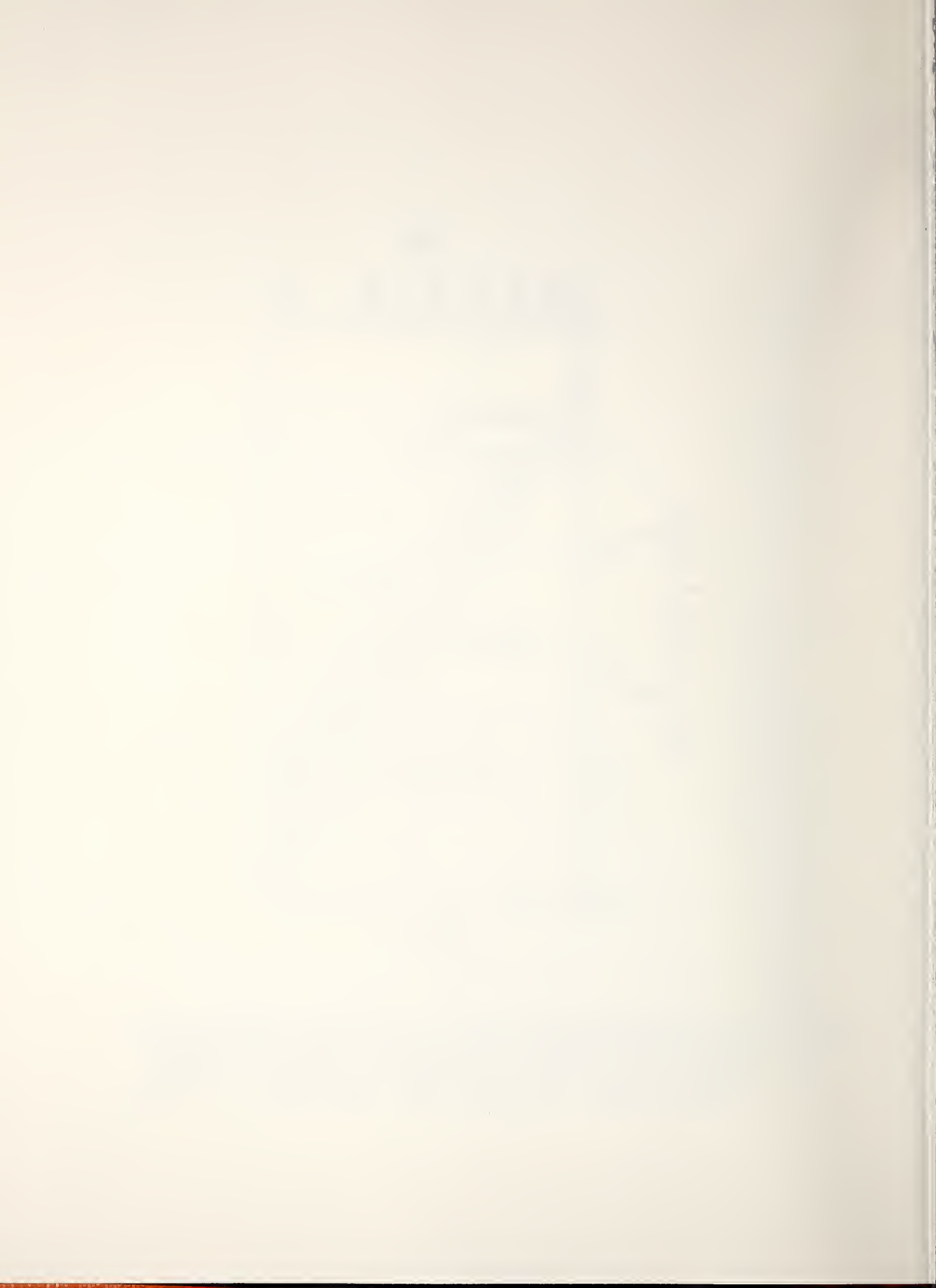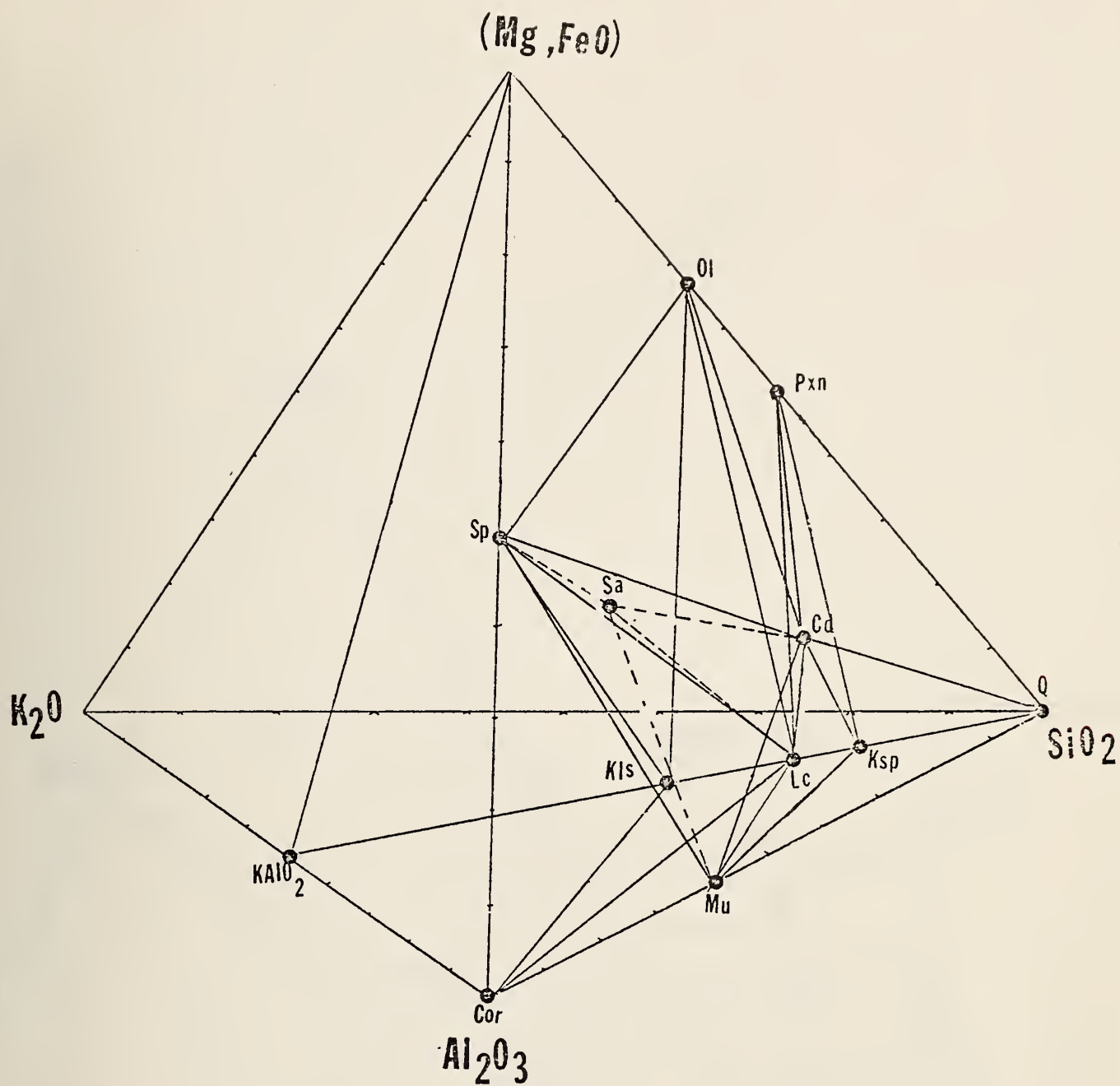
Fig. 8. Working model of subsolidus equilibria for the system $(Mg,Fe)O-K_2O-Al_2O_3-SiO_2$ (mole %). Abbreviations as in Table 1, as well as:

(M,F) Sp $= (Mg, Fe)Al_2O_4$

(M,F) Sa $= (Mg, Fe)_4Al_{10}Si_2O_{23}$

(M,F) Cd $= (Mg, Fe)_2Al_4Si_5O_{18}$

Ol $= (Mg,Fe)_2SiO_4 = (Fo,Fa)$

Pxn $= (Mg,Fe)SiO_3 = (En,Fs)$
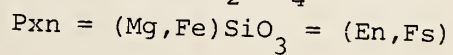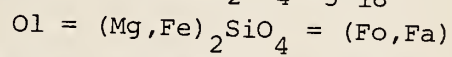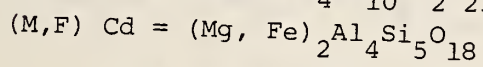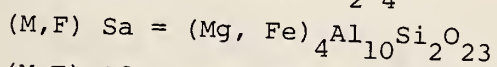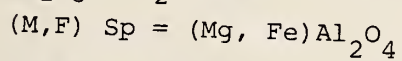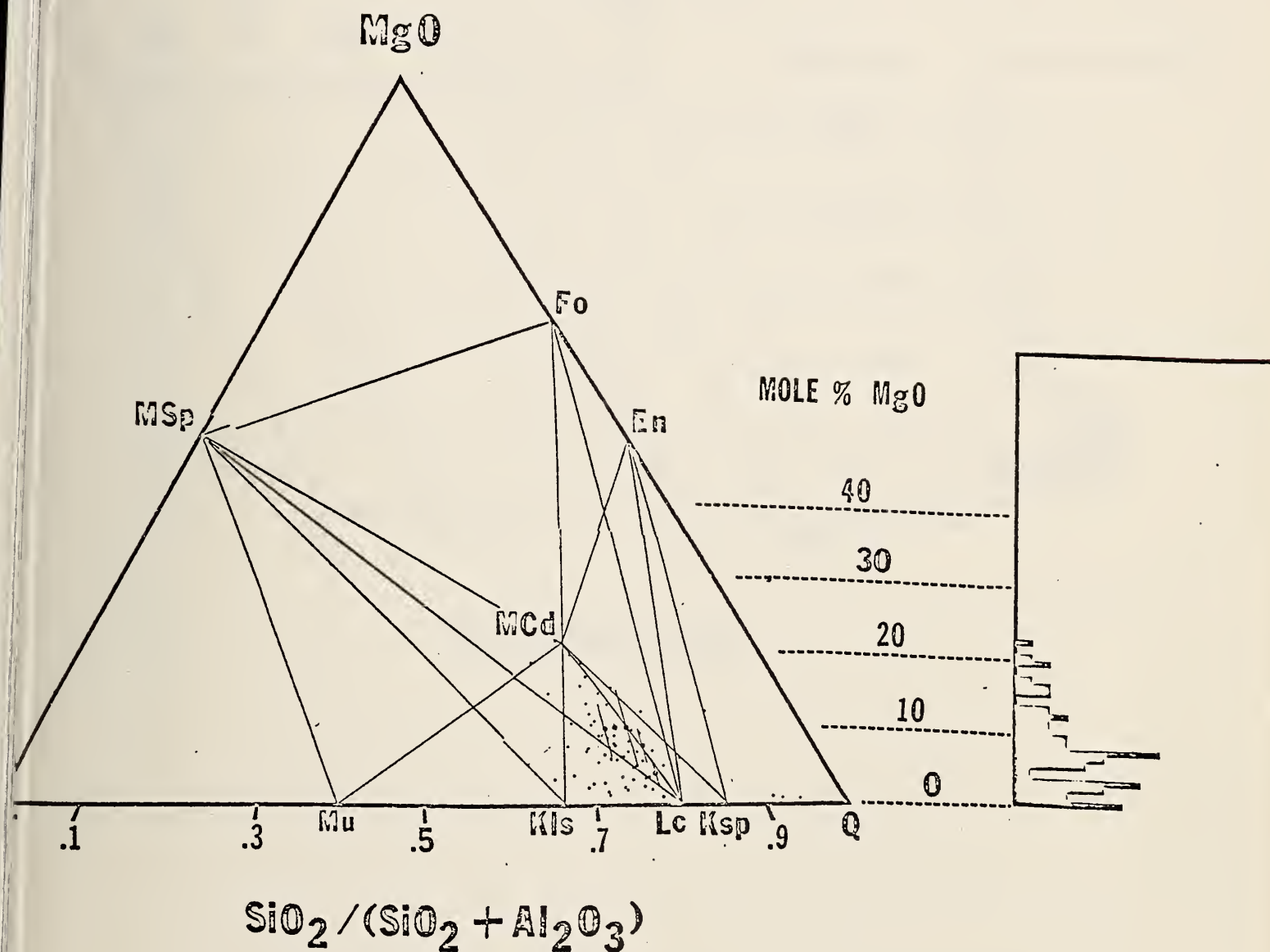
Fig. 9. MgO-Al$_2$O$_3$-SiO$_2$ projection of analyses for sub-bituminous coals, lignites and unclassified western coals - see Fig. 5.
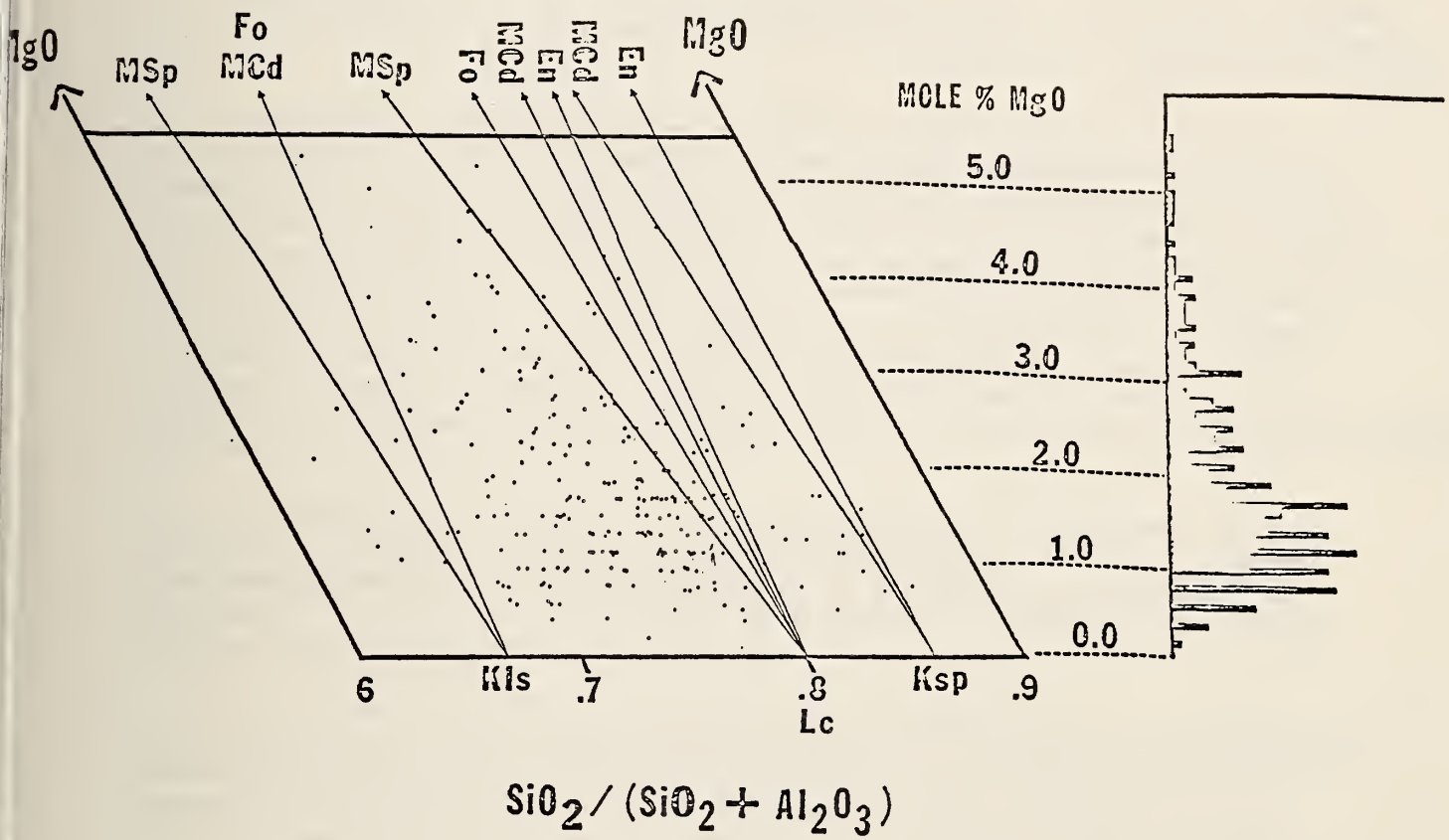
Fig. 10. MgO-Al$_2$O$_3$-SiO$_2$ projection of analyses for bituminous coals.

One curve, calculated for the invariant melt in the volume $(Mg)_2SiO_4$-$MgAl_2O_4$-$KAlSiO_4$-$KAlSi_2O_6$, or (Ol/Sp/Kls/Lc) is shown on Figure 7. This volume encompasses one of the largest compositional spaces in the system and is therefore significant. The position of the equilibrium curve lies close to the lower of those for the CaO-system.

References: J.F. Schairer, J. Amer. Ceram. Soc. <u>37</u>, 501-33 (1954)

W.C. Luth, J. Amer. Ceram. Soc. <u>50</u>, 174 (1967).

d.   <u>Thermochemistry of the FeO_x-K_2O-Al_2O_3-SiO_2 System</u>   (R.S. Roth, T. Negas,
C. McDaniel, H. Parker,
H.I. Yoo, L. Cook and D.B. Minor)

To obtain a preliminary working model for this system under low to moderate P_{O_2} pressure (prevalent in the higher temperature MHD regime, where $Fe^{+2} > Fe^{+3}$), substitution of Fe for Mg is assumed thermodynamically ideal (see Figure 8) so that subsolidus relations for Mg-phases also apply to Fe^{+2}-phases (this assumption breaks down in the SiO_2-rich region). Coal ash analyses and tie lines are shown in the FeO_x-Al_2O_3-SiO_2 projections of Figures 11 and 12. As noted above, FeO_x is an important constituent of bituminous coals, comprising typically from 5-25 mole %. FeO_x in sub-bituminous coals is somewhat variable, with a maximum at $\sim$ 6 mole %. The majority of analyses of both coal types project within the Fe_2SiO_4-$KAlSiO_4$-$KAlSi_2O_6$ system, for which data are lacking.

A thermodynamic analysis of the FeO_x-K_2O-Al_2O_3-SiO_2 system has been begun as a prelude to study of invariant equilibria, according to methods outlined above for MgO- and CaO-systems. Calculation of the effect of adding Fe^{+2} to the volume Ol/Sp/Kls/Lc indicates a rather marked lowering of the curve in Figure 7.

The K_2O-FeO_x system is under detailed investigation. T. Takahashi, K. Kuwabara and Y. Kase [Denki Kagaku, <u>43</u> (5) 273 (1975)] recently published chemical and electrical data for this system. Our preliminary data are generally in accord with the above although melting temperatures appear to be higher than reported. For example, the compound $KFeO_2$ (hydrolyzes at room temperature in air) is reported to melt congruently near 1325°C whereas our experiments reveal melting above 1600°C. Most interesting is the β-alumina type phase in this system (solid solution between $K_2O \cdot 6Fe_2O_3$ and $K_2O \cdot 6.8Fe_2O_3$). We have identified the unknown compound reported at $K_2O \cdot 10Fe_2O_3$ by the above workers as a β"'-alumina type phase. The electrical conductivity of these β-alumina related phases is shown to approach 1 $(ohm\text{-}cm)^{-1}$ at 100°C. These data prompted us to prepare several ceramic specimens for preliminary measurements of electrical conductivity. The base composition, $K_2O \cdot 7Fe_2O_3$ was selected either pure or doped with TiO_2 or Ta_2O_5. Powders were prepared from K_2CO_3 and Fe_2O_3 which were mixed, calcined at 800°C and remixed. Discs were cold-pressed then isostatically pressed and sintered at 1300°C covered with a powder of identical composition (to minimize K_2O loss). The doped materials suffered from substantial grain growth but remained suitable for preliminary measurements. High
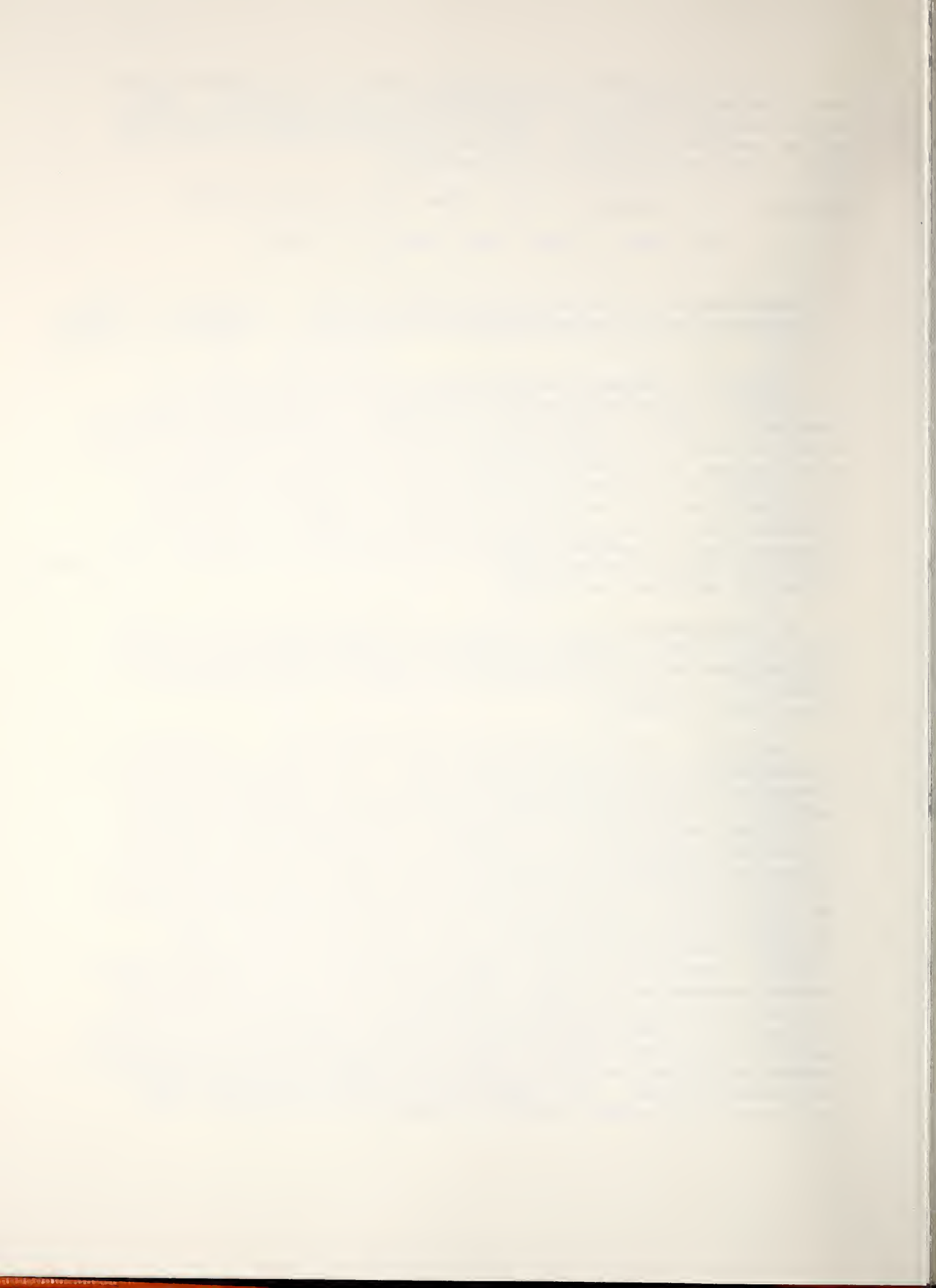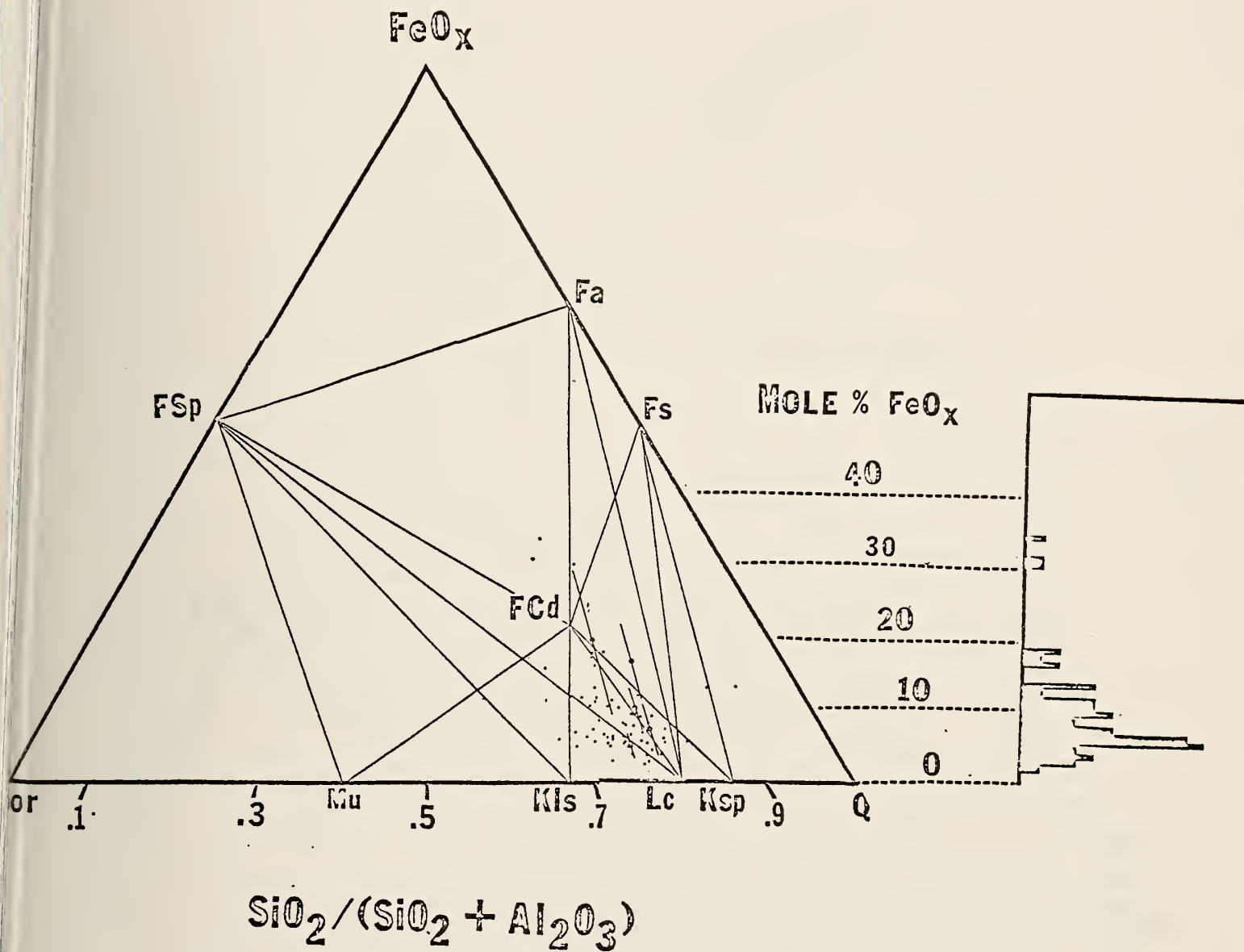
Fig. 11. FeO_x-Al_2O_3-SiO_2 projection of analyses for sub-bituminous coals, lignites and unclassified western coals, see Fig. 5.
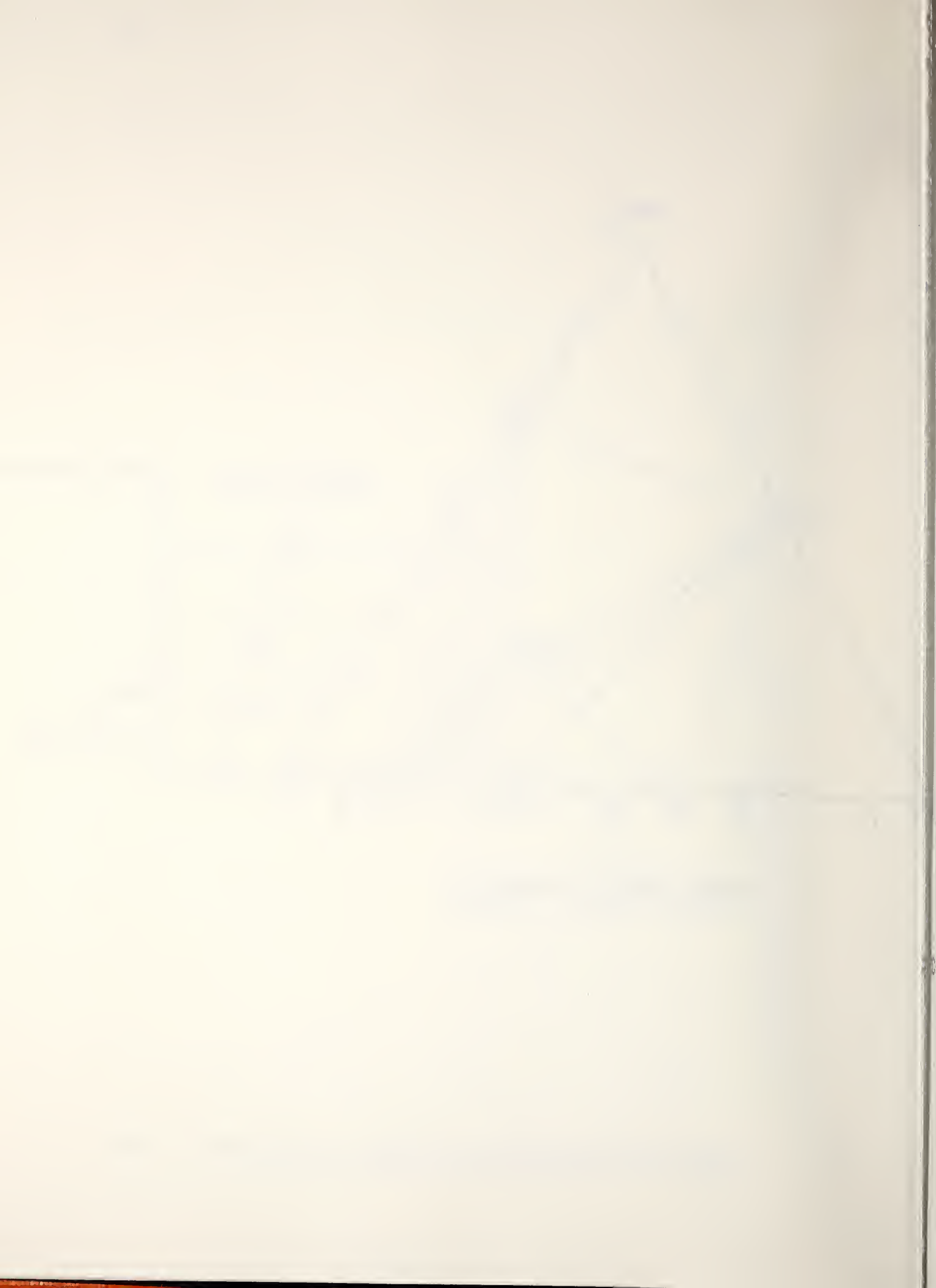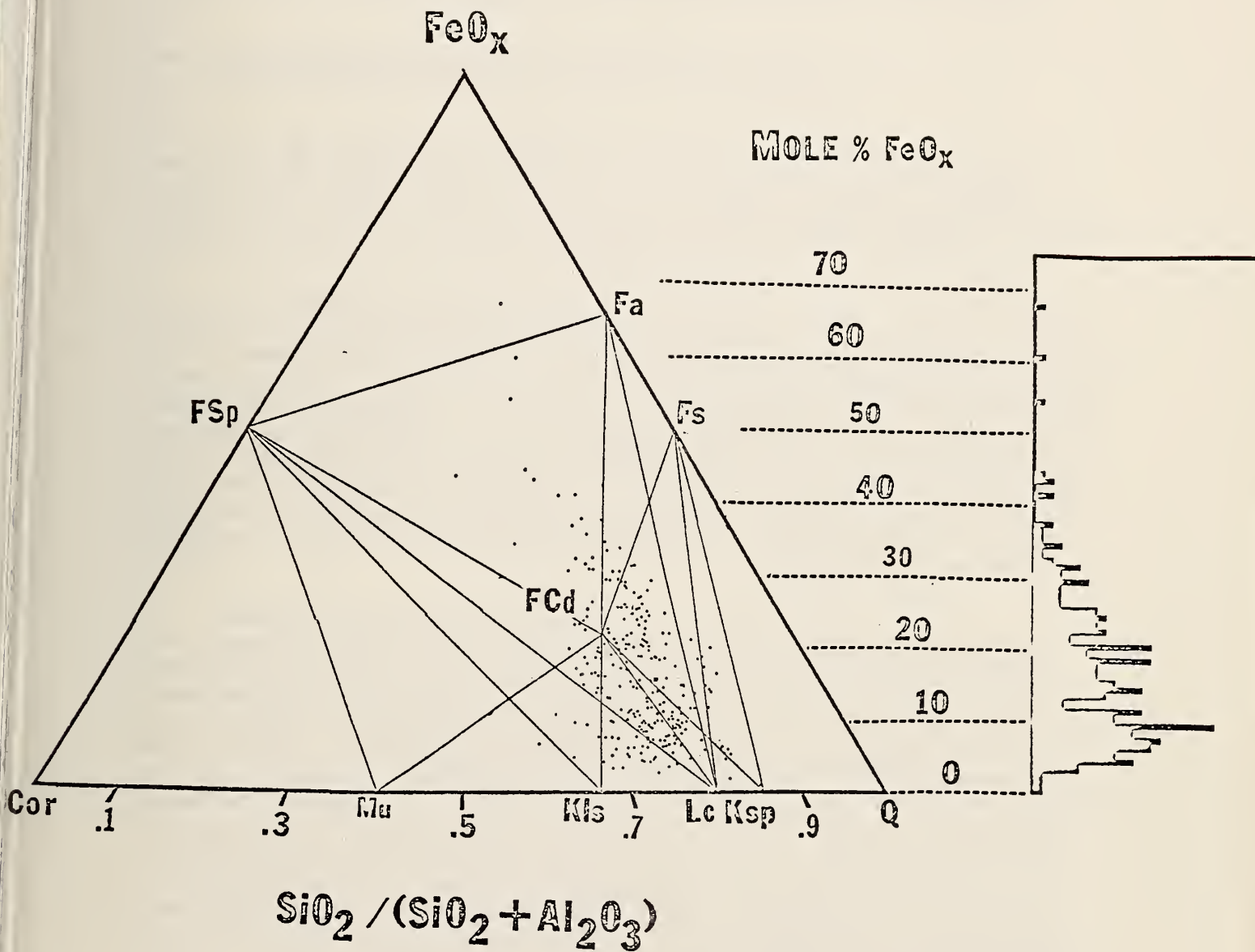
Fig. 12. FeO$_x$-Al$_2$O$_3$-SiO$_2$ projection of analyses for bituminous coals.

density bodies probably will have to be fashioned by hot-pressing.

Work is also being concentrated in the subsystems $KFeO_2$-SiO_2 and $KAlSiO_4$-$KFeSiO_4$. The $KFeO_2$-SiO_2 system is analogous in most respects to the $KAlO_2$-SiO_2 system (see previous Quarterly Reports). Solid solution of ~20 mol % SiO_2 in $KFeO_2$ stabilizes a cubic cristobalite-like phase with a=7.84A. A body centered tetragonal phase, $K_{1+x}Fe_{1+x}Si_{1-x}O_4$ (a=9.09, c=5.33A), occurs at ~43% SiO_2. $KFeSiO_4$ develops at low temperatures with the hexagonal kalsilite structure (a=5.278, c=8.824A) and transforms reversibly at 945°C to a new orthorhombic variant (a=9.155, b=5.433, c=59.61A). At about 25% $KAlSiO_4$ a new distorted form of kalsilite was found in the $KAlSiO_4$-$KFeSiO_4$ system. This form is monoclinic with a=10.70, b=8.55, c=10.65A and $\beta \cong 120°$.

e. Implications of Research on Seed-Slag Interactions (L. Cook)

The application of experimental studies to the understanding of natural coal slags, especially the differences in behavior between eastern and western coals, is clear from examination of Figures 4, 5, 6, 9, 10, 11 and 12. It should be emphasized, that when considering the chemistry, data are most meaningful when treated on a mole % basis.

By studying melts of invariant composition within the significant volumes of the multicomponent MHD slag system CaO-MgO-FeO_x-K_2O-Al_2O_3-SiO_2, it is expected that a maximum of information can be gathered per unit time expended. This work will allow construction of a working model for seed/slag interaction, once potassium concentrations have been measured, related to subsolidus - derived potassium pressures, and converted to potassium activity coefficients. This work will be closely correlated with more detailed investigation of specific systems, and correlated when possible with direct measurement of potassium vapor pressures. Most important is the continuing investigation of the K_2O-FeO_x-Al_2O_3-SiO_2 system.

Presently available MHD channel slag analyses representing compositions which appear to have been least contaminated by reaction with channel components are given in Table 2. They contain from 15-25 mole % K_2O. These analyses are plotted in Figures 13 and 14 on (CaO, FeO_x)-SiO_2-Al_2O_3 "projections". All channel slags appear to differ from the parent coal ash by having a significant enrichment in Al_2O_3 and a possible slight depletion in FeO_x. From these limited data and the compositional analysis given in Figures 4, 5, 6, 9, 10, 11 and 12, suggestions for the average compositions of channel slag produced under MHD operation by "typical" bituminous and sub-bituminous coals can be given, as in Table 3. It is to be emphasized that these are suggested only as reasonable working models and exceptions and local variations are expected to be the rule (see Figure 15). Particularly important are the effects of temperature and P_{O_2}. Not all channel slag analyses and especially those in Table 2
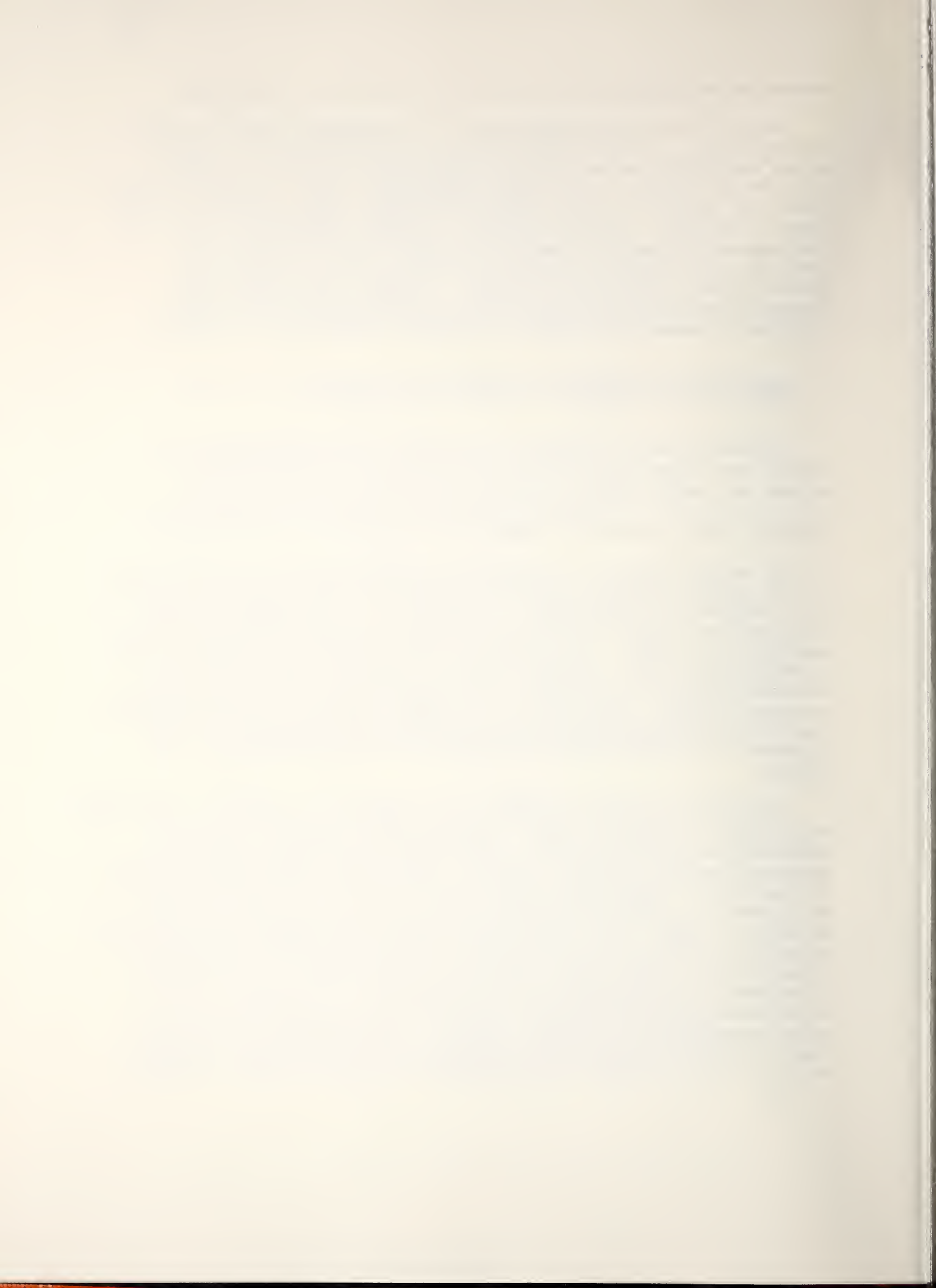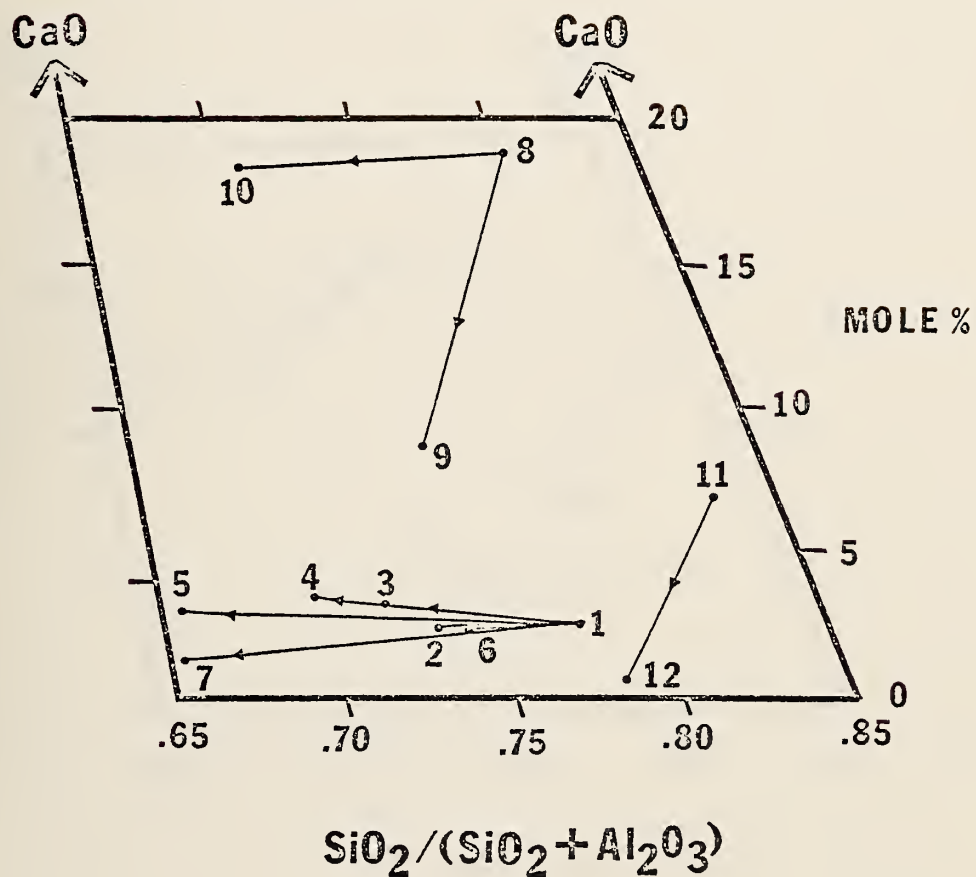
Fig. 13.   CaO-Al₂O₃-SiO₂ projection of channel slag analyses given in
Table 2
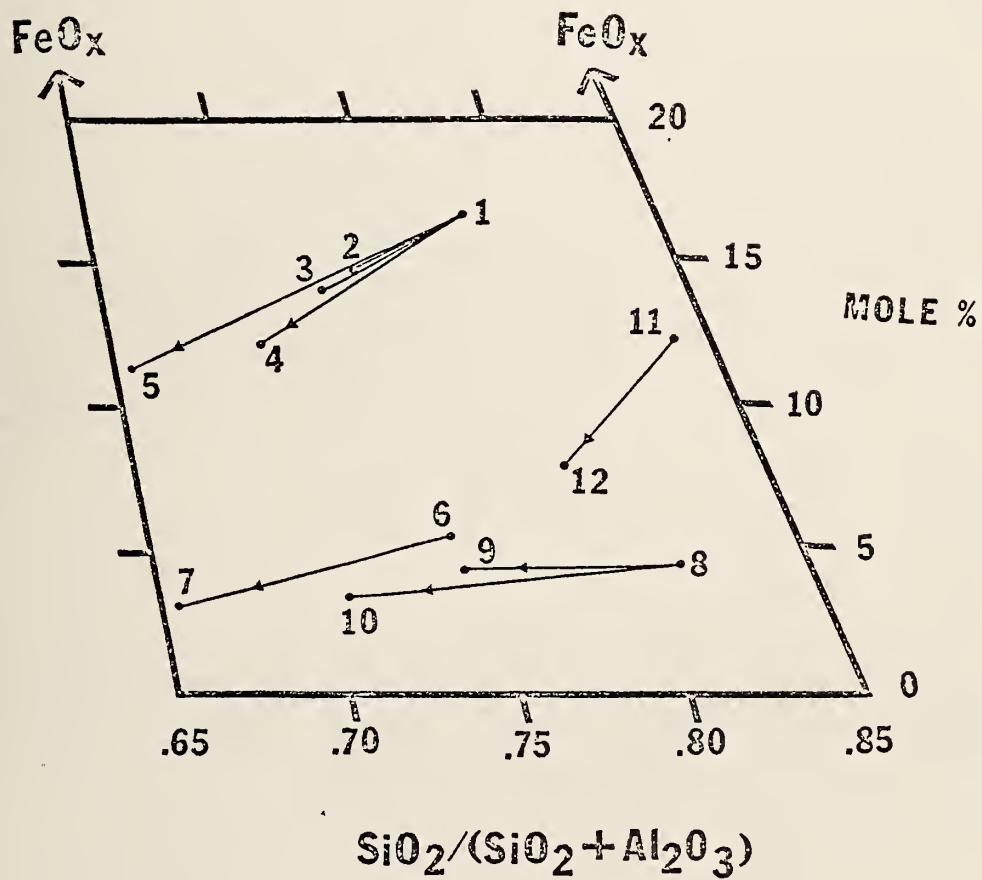
Fig. 14. FeO_x-Al_2O_3-SiO_2 projection of channel slag analyses given in Table 2.
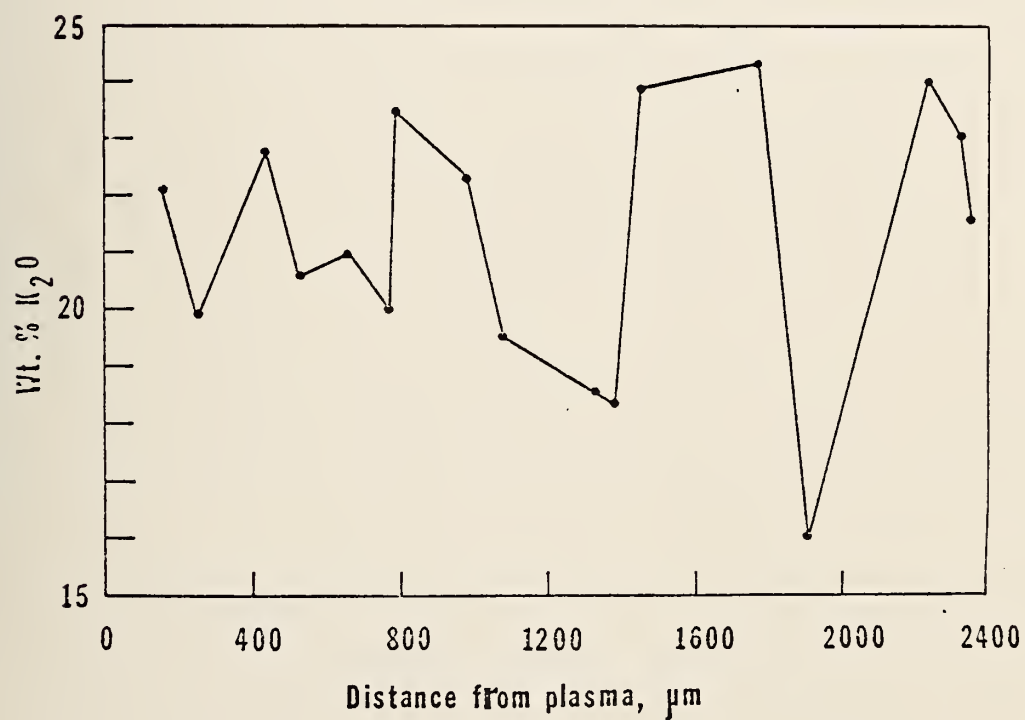
Fig. 15. Variation in K_2O content across a specimen of channel slag from AVCO Mark VI generator (S. Petty, pers. comm. to W. Hosler, 1975).

lend support to the idea that high CaO slags have a lower propensity for K_2O absorption. It may be that more data are needed before the effects suggested by Cook et al. (1976) to exist in synthetic compositions can be evaluated, especially for compositions with more than 30 mole % (CaO + FeO + MgO).

An important point is that modeling of channel slag by systems with $KAlSiO_4$ and $KAlSi_2O_6$ as components (25.0 and 16.7 mole % K_2O, respectively) is required (Figure 6 and Table 2).

Reference: L.P. Cook, E.R. Plante, T. Negas, R. Roth, C. Olson, 1976, Crystallization and Vaporization Studies on Synthetic Coal Slag Compositions: Proc. 15th Symp. Eng. Aspects MHD, Philadelphia.

Table 1. Gas-Solid Equilibria in the System $CaO-K_2O-Al_2O_3-SiO_2$
(apply also to invariant melts).

	Four Phase Volume	Vaporization Equilibrium
1	$Kls/Cor/CA_6/An$	$2Kls + CA_6 = 1An + 6Cor + 2K + 1/2\ O_2$
2-a	$Kls/CA_6/Ge/An$	$34Kls + 12Ge = 1CA_6 + 23An + 34K + 17/2\ O_2$
2-b	$Kls/CA_6/(Ge)_{.8}(KGe)_{.2}/An$	$46Kls + 20(Ge)_{.8}(KGe)_{.2} = 1CA_6 + 35An + 50K + 25/2\ O_2$
3-a	$Kls/Lc/Ge/An$	$1Kls + 1Lc + 1Ge = 2An + 2K + 1/2\ O_2$
3-b	$Kls/Lc/(Ge)_{.8}(KGe)_{.2}/An$	$12Kls + 6Lc + 10(Ge)_{.8}(KGe)_{.2} = 18An + 20K + 5\ O_2$
4-a	$Kls/Lc/Ge/Wo$	$5Kls + 2Wo = 1Ge + 3Lc + 2K + 1/2\ O_2$
4-b	$Kls/Lc/(Ge)_{.8}(KGe)_{.2}/Wo$	$42Kls + 18Wo = 10(Ge)_{.8}(KGe)_{.2} + 24Lc + 16K + 4\ O_2$
5	$Kls/Lc/Cor/An$	$4Kls = 2Lc + 1Cor + 2K + 1/2\ O_2$
6	$Lc/Cor/Mu/An$	$2Lc + 5Cor = 2Mu + 2K + 1/2\ O_2$
7-a	$Lc/Ge/An/Wo$	$3Ge + 4Lc = 5An + 1Wo + 4K + O_2$
7-b	$Lc/(Ge)_{.8}(KGe)_{.2}/An/Wo$	$30(Ge)_{.8}(KGe)_{.2} + 30Lc = 42An + 12Wo + 36K + 9\ O_2$
8	$Lc/Ksp/An/Wo$	$1Wo + 5Lc = 3Ksp + 1An + 2K + 1/2\ O_2$
9	$Lc/Ksp/Mu/An$	$16Lc = 1Mu + 10\ Ksp + 6K + 3/2\ O_2$
10	$Ksp/Mu/An/Q$	$6Ksp = 1Mu + 16Q + 6K + 3/2\ O_2$
11	$Ksp/An/Wo/Q$	$1Wo + 2Ksp = 5Q + 2K + 1/2\ O_2$

$Kls = KAlSiO_4$ = kalsilite
$Lc = KAlSi_2O_6$ = leucite
$Ksp = KAlSi_3O_8$ = potassium feldspar
$Cor = Al_2O_3$ = corundum
$Mu = 3Al_2O_3 \cdot 2SiO_2$ = mullite
$CA_6 = CaAl_{12}O_{19}$
$Ge = Ca_2Al_2SiO_7$ = gehlenite
$(Ge)_{.8}(KGe)_{.2} = (Ca_2Al_2SiO_7)_{0.8}(KCaAlSi_2O_7)_{0.2}$
$An = CaAl_2Si_2O_8$ = anorthite
$Wo = CaSiO_3$ = wollastonite
$Q = SiO_2$ = quartz

Table 2. Channel Slag Analyses (Recalculated on basis of 100 Mole % = $SiO_2+Al_2O_3+FeO_x+CaO+MgO$ or $SiO_2+Al_2O_3+FeO_x+CaO+MgO+K_2O$).

A. AVCO Mark VI Test 8/6/74[1]

	1 Parent Coal Ash	2 Burner Slag $(-K_2O)$	3 Channel Slag $(-K_2O)$	Burner Slag $(+K_2O)$	Channel Slag $(+K_2O)$
SiO_2	61.47	59.57	58.24	49.19	48.49
Al_2O_3	18.01	21.84	23.00	18.04	19.15
FeO_x	16.69	14.67	14.03	12.12	11.68
CaO	2.52	2.33	3.16	1.93	2.63
MgO	1.31	1.59	1.57	1.31	1.31
K_2O	--	--	--	17.43	16.75
$\dfrac{SiO_2}{(SiO_2+Al_2O_3)}$	.7734	.7317	.7169		

[1] AVCO Everett Res. Lab., Experimental MHD Powder Plant Development Program, Monthly Progress Report, October 1, 1974.

B. AVCO Mark VI Test 9/20/74[2]

	1 Parent Coal Ash	4 Cathode Slag $(-K_2O)$	5 Anode Slag $(-K_2O)$	Cathode Slag $(+K_2O)$	Anode Slag $(+K_2O)$
SiO_2	61.47	57.82	55.17	43.27	45.49
Al_2O_3	18.01	25.17	29.13	18.84	24.02
FeO_x	16.69	12.10	11.28	9.06	9.30
CaO	2.52	3.43	2.99	2.57	2.47
MgO	1.31	1.47	1.43	1.10	1.18
K_2O	—	--	--	25.17	17.54
$\dfrac{SiO_2}{(SiO_2+Al_2O_3)}$	.7734	.6967	.6544		

[2] AVCO Everett Res. Lab., Development Program for MHD Power Generation, Monthly Progress Report, November 1, 1974.

C. AVCO Mark VI B Test 4/29/75[3]

	Cathode Slag $(-K_2O)$	Anode Slag $(-K_2O)$	Cathode Slag $(+K_2O)$	Anode Slag $(+K_2O)$
SiO_2	64.82	63.47	52.00	53.79
Al_2O_3	23.59	25.99	18.92	22.03
FeO_x	6.58	4.77	5.28	4.04
CaO	3.28	3.89	2.63	3.30
MgO	1.73	1.88	1.39	1.59
K_2O	--	--	19.78	15.24

[3] AVCO Everett Res. Lab., Development Program for MHD Powder Generation, Progress Report Report No. 46, July 1, 1975.

D. Stanford Facility, Test #9, 1976[4]

	6 Parent Coal Ash	7 Channel Slag $(-K_2O)$	Channel Slag $(+K_2O)$
SiO_2	67.19	55.88	46.72
Al_2O_3	23.59	29.61	24.75
FeO_x	5.51	3.67	3.07
CaO	2.33	1.31	1.09
MgO	1.39	9.53	7.97
K_2O	--	--	16.40
$\dfrac{SiO_2}{(SiO_2+Al_2O_3)}$	.7401	.6536	

E. Stanford Facility, Test #11, 1976[4]

	8 Parent Coal Ash	9 Channel Slag $(-K_2O)$	Channel Slag $(+K_2O)$
SiO_2	56.73	54.69	45.96
Al_2O_3	13.41	19.03	15.99
FeO_x	4.42	4.28	3.60
CaO	18.89	8.78	7.38
MgO	6.55	13.22	11.11
K_2O	--	--	15.96
$\dfrac{SiO_2}{(SiO_2+Al_2O_3)}$	.8088	.7419	

[4] J.K. Koester, M.E. Rodgers, and K.R. Eustis, 1976, In Channel Observations on Coal Slags: Proc. 15th Symp. Eng. Aspects MHD, Philadelphia.

F. Stanford Facility, Test #12, 1977[5]

	8 Parent Coal Ash	10 Channel Slag $(-K_2O)$	Channel Slag $(+K_2O)$
SiO_2	56.80	50.23	42.58
Al_2O_3	13.42	21.03	17.83
FeO_x	4.38	3.38	2.87
CaO	18.87	18.27	15.49
MgO	6.52	7.09	6.01
K_2O	--	--	15.22
$\dfrac{SiO_2}{(SiO_2+Al_2O_3)}$	.8089	.7049	

G. Stanford Facility, Test #19, 1977[5]

	11 Parent Coal Ash	12 Channel Slag $(-K_2O)$	Channel Slag $(+K_2O)$
SiO_2	67.23	71.51	59.68
Al_2O_3	13.69	19.94	16.64
FeO_x	12.16	7.97	6.65
CaO	6.92	0.59	0.49
MgO	--	--	--
K_2O	--	--	16.54
$\dfrac{SiO_2}{(SiO_2+Al_2O_3)}$	.8308	.7820	

[5] J.K. Koester and R.M. Nelson, 1977, Electrical Behavior of Slag Coatings in Coal-Fired MHD Generators: Proc. 16th Symp. Eng. Aspects MHD, Pittsburg.

[*] Numbers above the analyses refer to data points in illustrations.
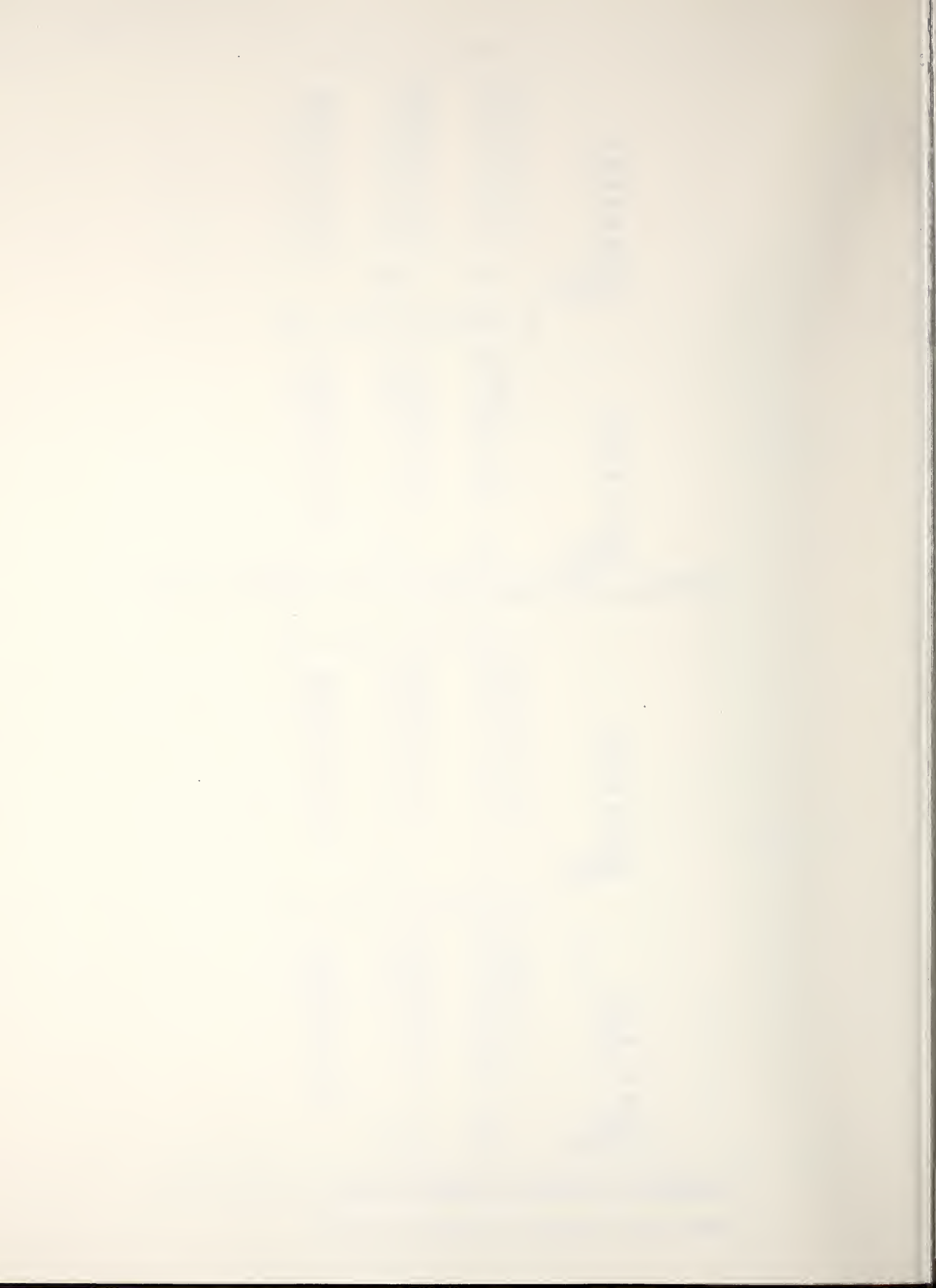
Table 3. Suggested Average Compositions for Modeling MHD
Channel Slag (Mole %).

	Western Coal	Eastern Coal
SiO_2	42.0	46.0
Al_2O_3	17.5	19.0
FeO_x	5.0	12.0
CaO	12.0	2.4
MgO	6.0	1.2
K_2O	17.5	19.4
	100.0	100.0
$\dfrac{SiO_2}{SiO_2+Al_2O_3}$	0.705	0.705
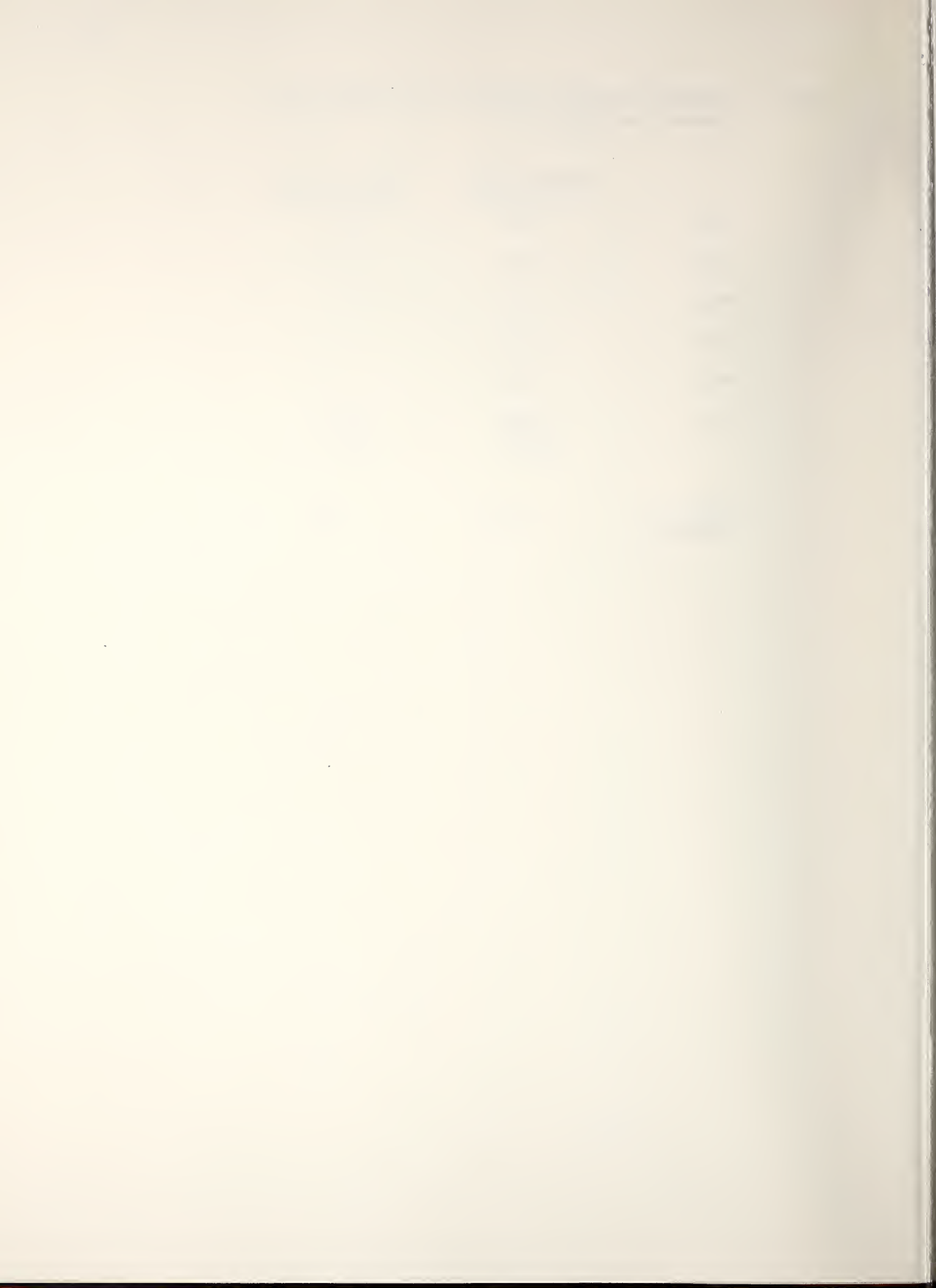
Diffusion in Insulator-Electrode Couples (A. J. Armstrong, E. N. Farabaugh
J. R. Manning)

Insulator-electrode couples, as described in the March 1977 report, have been made. These couples were heated at 1600 °C for 1, 10 and 100 hr. periods. Preliminary Fe diffusion data has been taken on a MAFF-31 – MgO couple.

Figs. 16, 17 and 18 are optical micrographs of MAFF-MgO couples heated for 100, 10 and 1 hour respectively. The 100 hr. test drove enough iron from the MAFF into MgO to cause a deep rust-colored discoloration of the whole of the MgO insulator. The 10 hr. test also produced a discolored band in the MgO as can be seen at the edge of the MgO (middle layer) in Fig. 17 The 1 hr. test produced a much narrower band in the MgO as can be seen by comparing Fig. 17 and 18.

In these couples the boundary between the insulator and electrode was marked by fine Pt wire placed between the two materials. Fig. 19 is a 100X SEM micrograph revealing that the MgO and MAFF were actually held apart ∿25 µm by the Pt wire. The wire is seen as the white appearing round spot about midway along the boundary of MgO (the coarse grained material) and the MAFF-31.

The Fe concentration profile in the MAFF and MgO as determined by SEM and EDX techniques is shown in Fig. 20. The boundary between the two materials is indicated by the long line. Note the decrease of Fe towards the edge of the MAFF as expected. We also see a hump in the Fe profile in the MgO about 75 µm from the boundary. In previous measurements on $MgAl_2O_4$-MAFF diffusion couples, we have also seen and reported such a hump in the Fe profile, but it was reported to lie in the electrode material. In question in those tests was the exact position of the electrode insulator interface. It was to locate the interface that the Pt wire markers were introduced.

On the basis of this preliminary data, it seems that the hump lies in the insulator material for this MgO-MAFF couple. Also, it appears that the fact that the electrode and insulator were not in intimate contact, did not inhibit diffusion of Fe from the MAFF into the MgO.

Profiles will be taken from the other couples and plotted. Particular attention will be paid to the position of any Fe hump relative to the insulator-electrode boundary.
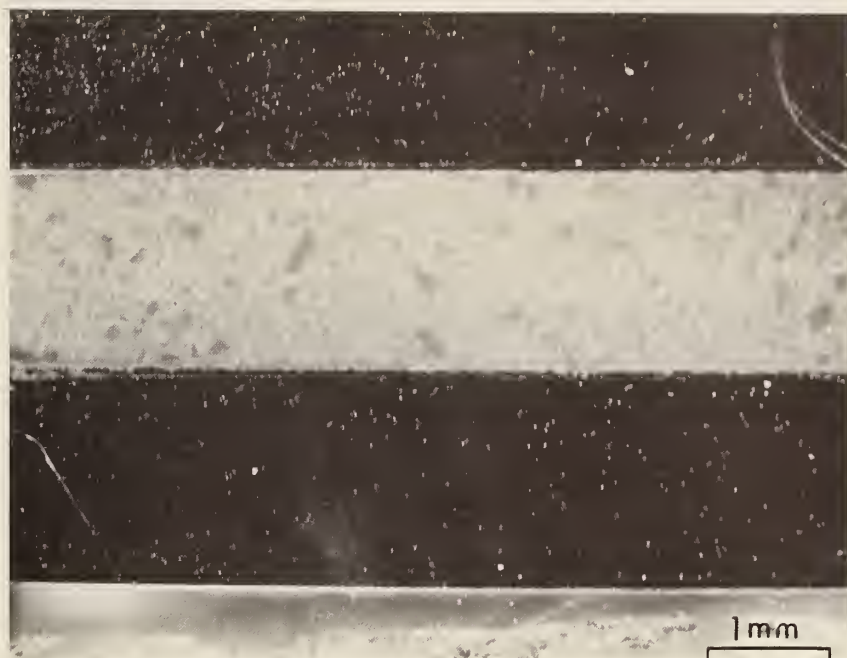
Fig. 16. Optical micrographs of MAFF-31-MgO couple tested for 100 hrs.
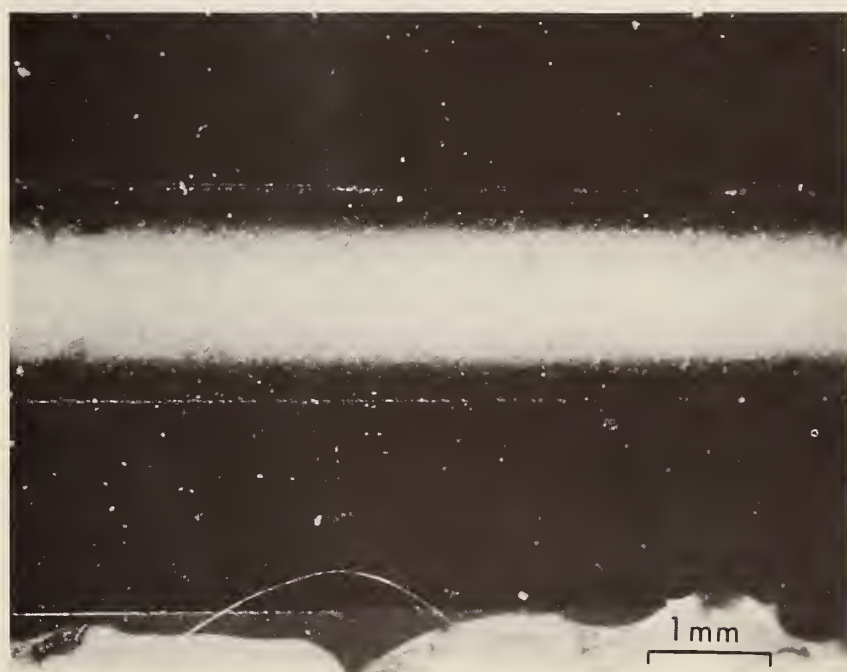
Fig. 17. Optical micrograph of MAFF-31-MgO couple tested for 10 hrs.
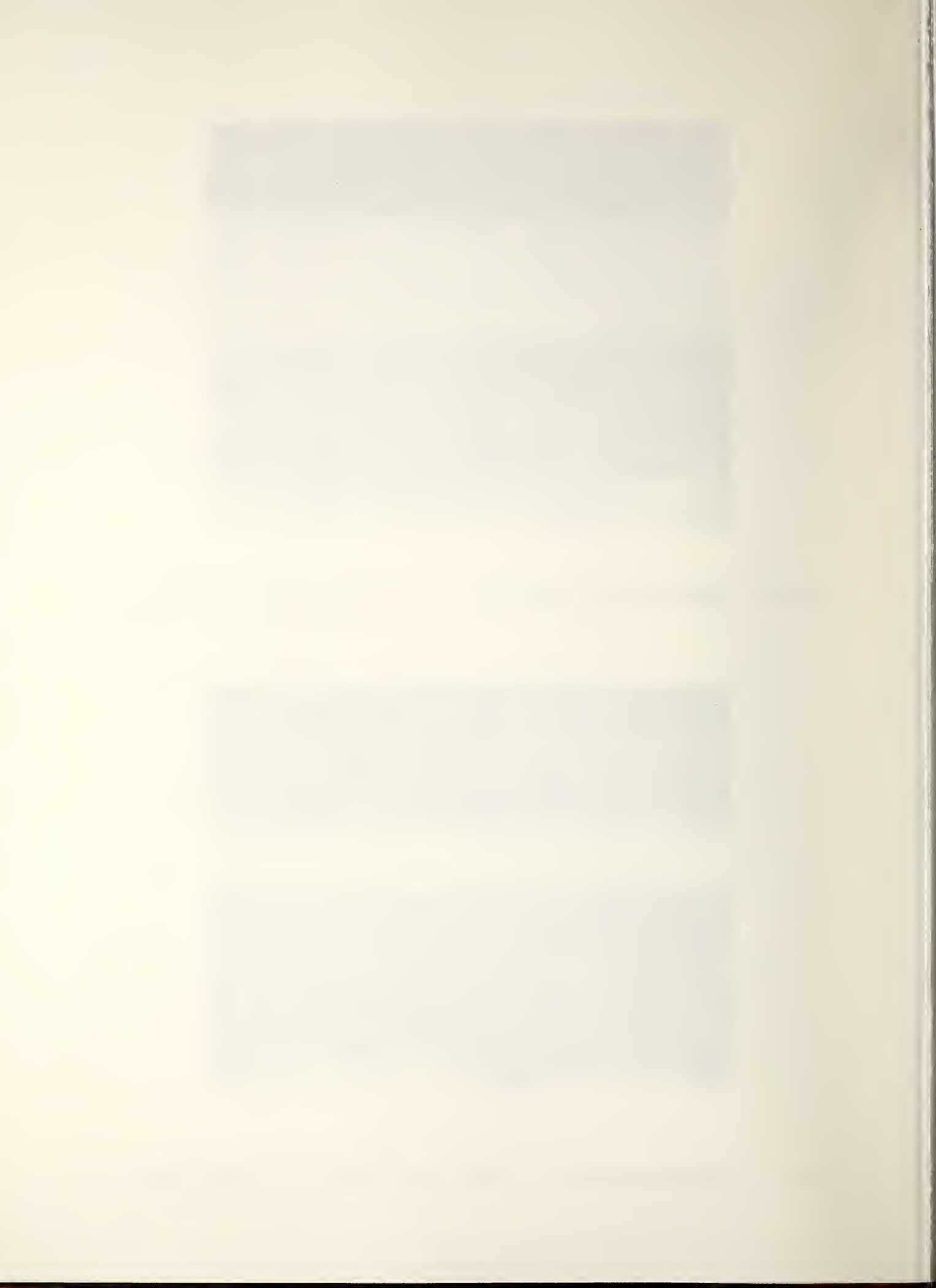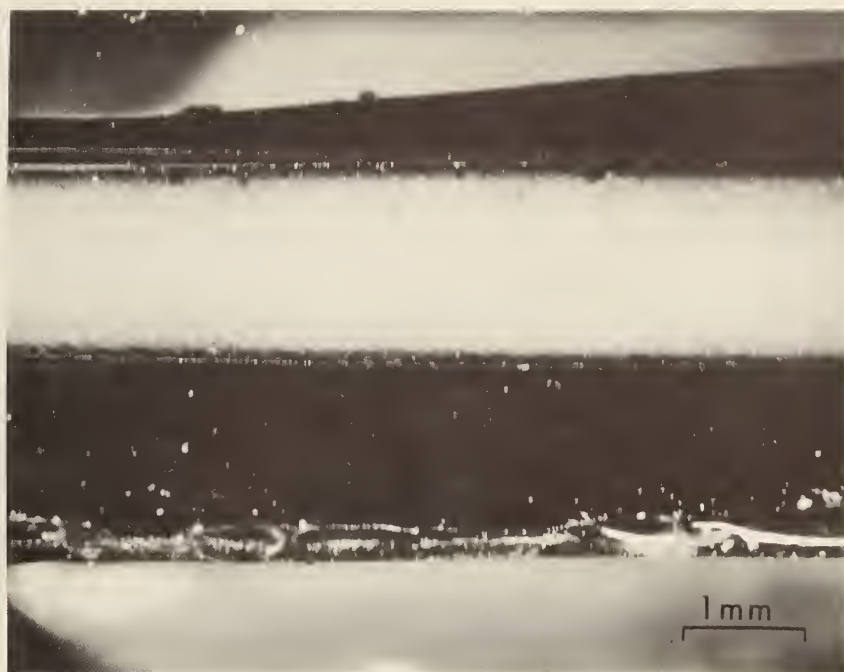
Fig. 18. Optical micrograph of MAFF-31-MgO couple tested for 1 hr.

Fig. 19. 100 SEM micrograph showing separation of MgO (coarse-ground material) and MAFF-31.
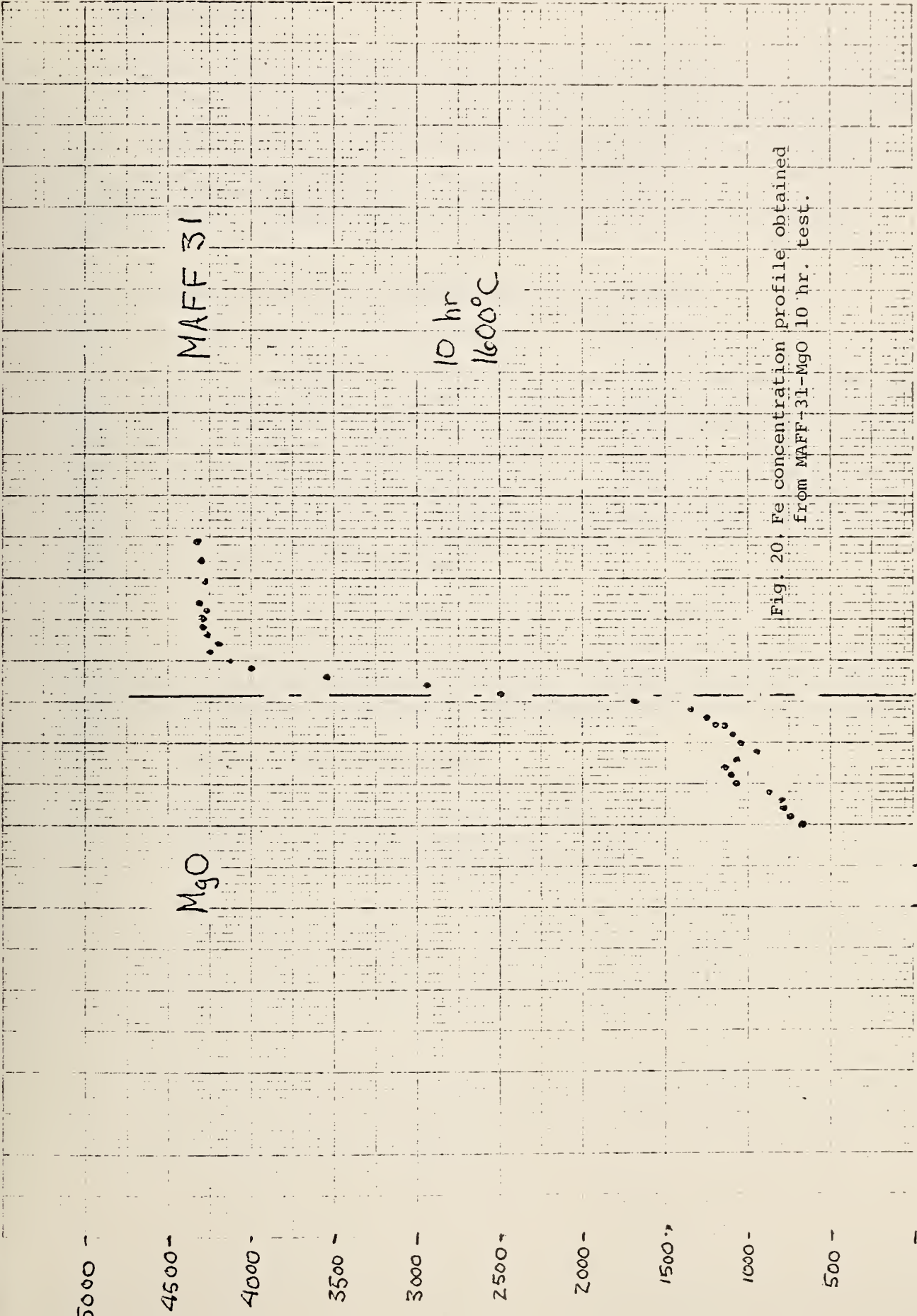
Fig. 20. Fe concentration profile obtained from MAFF-31-MgO 10 hr. test.

Task K.   Materials Testing and Characterization

1.   Introduction

During this reporting period an appreciable fraction of our efforts have been devoted to characterization of materials, design and fabrication of electrode/insulator modules, and evaluation of tested electrode assemblies. This includes structural analyses of ceramic powders and solid samples from various sources (sections 2a and 2b) consultations and preparations for future tests (section 3), results of the analyses on 3 electrode modules (TT/NBS, ANL and GE) tested in the MIT-rig (section 4a,b,c), as well as examinations of Fluidyne preheater materials (section 5a) and fly-ash (section 5b).

2.   Structural Analysis of Powdered and Solid Ceramics

a.   X-ray Diffraction of MHD Materials (C. L. McDaniel)

During this quarter we received over 35 materials (powders, dense ceramics, etc.) from various external sources. Most of these were fabricated ceramics, sinterable or sprayable powders or powders at various stages of processing. These were analyzed by powder x-ray diffraction methods. Data, transmitted to the appropriate source, are shown in Table 1 (following p. 52). Secondary phases (e.g., at grain boundaries, segregations, etc.) when present (depending on the phase and host material) at levels below roughly 3% are not detected by routine x-ray diffraction. If requested, samples will also be analyzed for minor phases using SEM/EDX methods.

b.   ANL U-02 Phase III Materials (T. Negas, C. L. McDaniel)

ANL delivered five materials related to their U-02, Phase III effort. X-ray diffraction analyses were requested. Treatment of these materials was fully documented by ANL and is summarized together with x-ray results below.

$$MHD \ \#1 - 18 \ m/o \ CeO_2 \cdot 82HfO_2$$

$$MHD \#2-4 - 9.7 \ m/o \ Y_2O_3 \cdot 16.3CeO_2 \cdot 74HfO_2$$

$$Powder - 18 \ m/o \ CeO_2 \cdot 82HfO_2, \ commercial$$
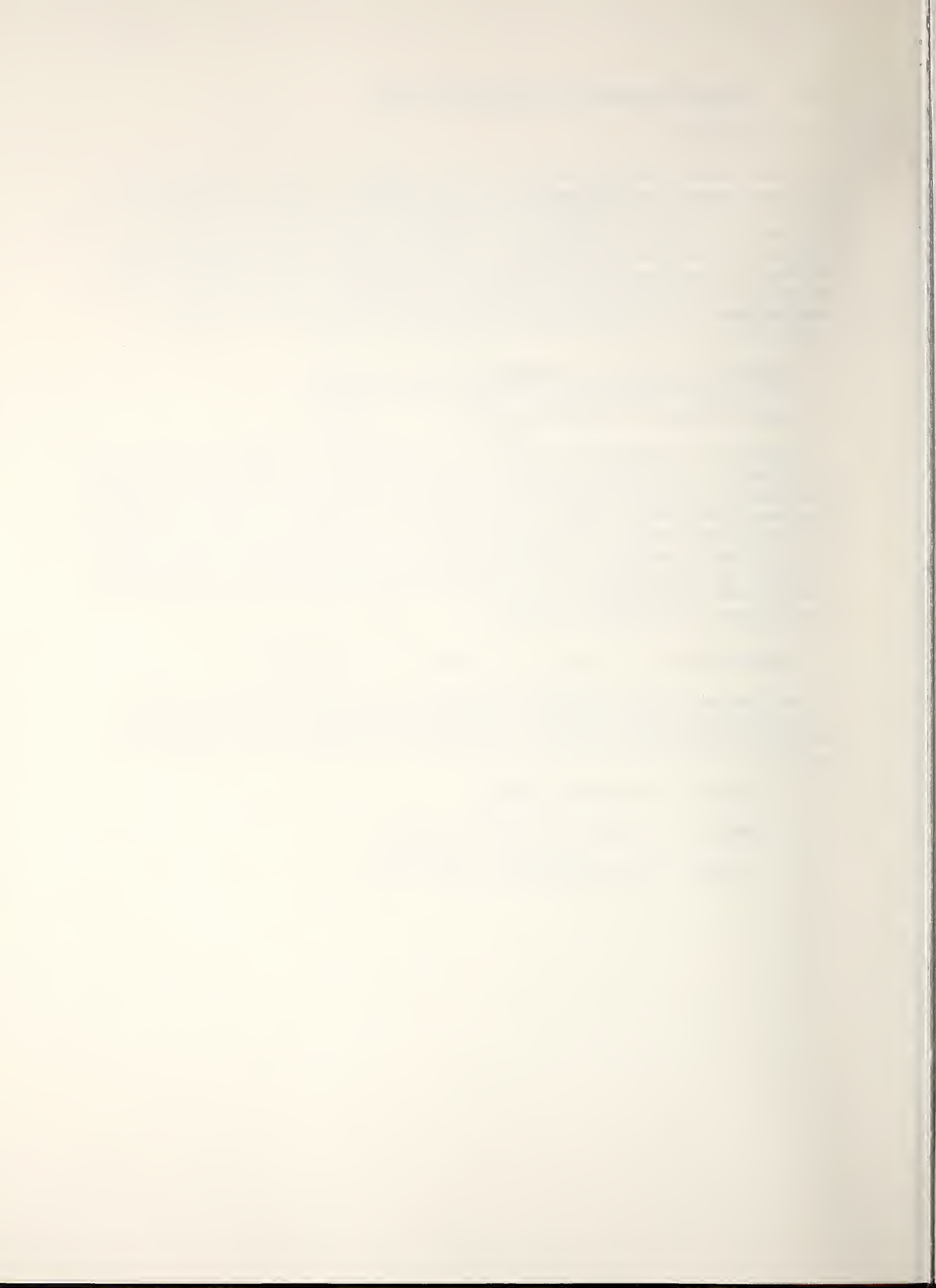
SAMPLE	TREATMENT	X-RAY RESULTS
Powder	none	Roughly equal proportions of monoclinic HfO_2-type solid solution plus a cubic or tetragonal phase rich in HfO_2. Broad x-ray lines suggest fine grain size and/or poor crystallinity
MHD #1	hot-pressed, vacuum $\sim$1500°C, 5600 psi, $\sim$40 min. Annealed in air 1000-1150°C. 90% dense	Monoclinic HfO_2-type solid solution with a trace of CeO_2
MHD #2	hot-pressed, vacuum, $\sim$1400-1435°, 5000 psi, $\sim$20 min. Annealed 1150°C in air. 95% dense	Cubic fluorite solid solution (HfO_2-rich) of excellent crystallinity (a=5.144A) plus monoclinic HfO_2 (<5%)
MHD #3	hot-pressed, vacuum $\sim$1300-1325°C, 5000 psi, $\sim$20 min. No anneal in air. 95% dense	Same as MHD #2 but with slightly more monoclinic HfO_2. Cubic phase has a=5.153A suggesting a somewhat lower HfO_2 content than in MHD #2.
MHD #4	hot-pressed, flowing Ar, 1300-1325°C, 5000 psi, $\sim$15 min. No anneal in air. 82% dense.	Cubic fluorite plus monoclinic HfO_2 (in roughly a 2:1 proportion) plus a trace of Y_2O_3. Not as well reacted as MHD #2 and #3.

3. <u>Preparation for Future Tests</u> (W. R. Hosler)

A considerable amount of time has been spent in consultation with Westinghouse on planning the materials aspects of <u>Phase III of U-02</u>. In particular, there has been close contact with APS Materials, Inc., Dayton, OH and Trans Tech, Inc., Gaithersburg, MD in an effort to obtain the best possible powders and sprayed material for certain electrodes in the Phase III design. It is necessary to maximize the density and obtain single phase pore-free material to reduce MAFF-31 oxidation and seed penetration. At the same time, resistance to fracture must be high. In arc plasma sprayed $LaCrO_3$(Mg) the density and resistance to fracture must also be maximized along with obtaining single phase pore-free material. A program has been initiated with APS Materials, using arc plasma sprayed powders from Trans Tech and others to study these requirements and develop these materials.

Several proof tests for Phase III U-02 are scheduled for August and September at Westinghouse R & D Lab., Pittsburgh, PA. Subsequent analysis of the electrodes will be made and the results will be used to determine the materials and electrode designs to be used for the Phase III test scheduled in Moscow in early 1978.
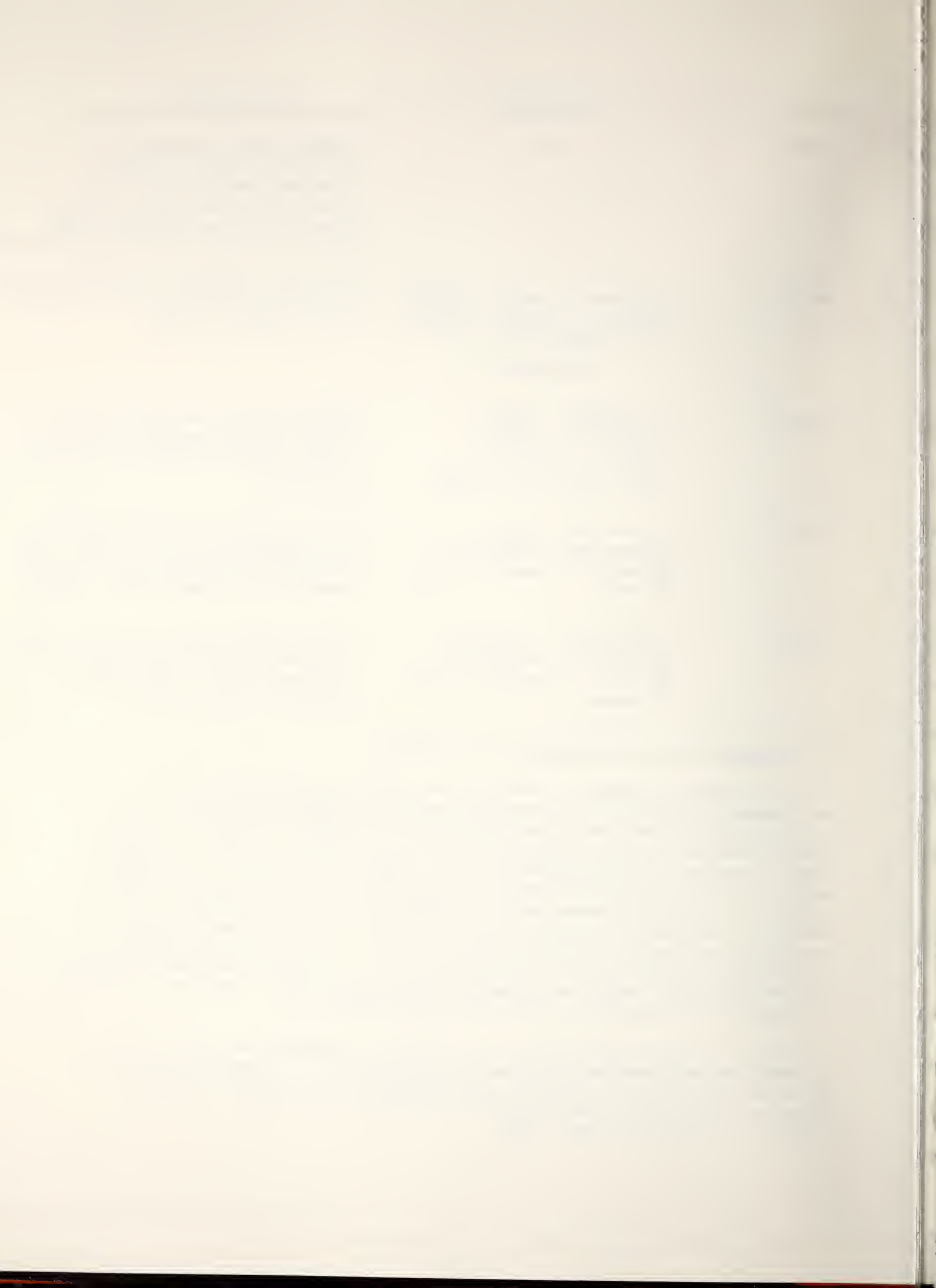
Table 1.   SPRAYABLE POWDERS

Material	From	Supplier	Description	X-ray Diffraction	Comments on Availability
$_{.95}Mg_{.05}CrO_3$	NBS 6500 A-1A	CERAC	Crushed aps powder -200 +25μ mesh 1% excess Cr_2O_3 added	single phase $LaCrO_3$-crystallinity fair to good	Special order 2-3 weeks delivery any mesh size
$_{.95}Mg_{.05}CrO_3$		Trans-Tech	spray dried aps powder		6-8 weeks delivery special order, any mesh size
rO_3	Westinghouse (Kochka) LC-GRO2	Gen. Refract.	no details supplied. aps powder crushed	med. good crystallization, no parameter shifts, no 2nd phases	
rO_3	Westinghouse (Kochka) LC-CEO1	CERAC	aps powder, crushed no further details given	med. crystallization, no parameter shifts, no other phases	
Al_2O_4-Fe_3O_4 F-31	NBS	Trans-Tech	aps powder spray dried -140 +325	single phase-good crystallization	Off shelf item
rO_3	Westinghouse LC-CEO2	CERAC	fines from 6500 A-1A	single phase, good crystallinity	2 to 3 weeks del.
l_2O_4	NBS S-71	Trans-Tech Type 1	aps spray dried powder, -140 +325	single phase, good crystallinity	Off the shelf
l_2O_4	Westinghouse (Kuszyc) MA-CEO2	Not stated	aps powder crushed 98% pore, -150 +325 mesh	single phase good crystallinity	
rO_3	NBS Lot. No. 4283	CERAC	aps powder crushed, -150 +325 mesh	cubic perovskite single phase	Off shelf-stock # 1128
rO_3	NBS Lot. No. 3451 B	CERAC	aps powder crushed, -325 mesh	cubic perovskite single phase	Off shelf-stock # 1129
rO_3	Westinghouse (Kuszyc) SZ CEO2	No origin given	aps powder, -150 +325 mesh	single phase, good crystallinity	
rO_3	Westinghouse (Kuszyc) SZ UMO2	no origin given	powder-no details given	single phase, poor crystallinity	
rO_3	NBS Lot No. 3757	CERAC	aps crushed powder -150 +325 mesh	orthorhombic perovskite + second phase of 10-20% cubic Ca stabilized ZrO_2	Off shelf-Stock No. 1021
rO_3	NBS Lot No. 375	CERAC	aps crushed powder, -325 mesh	orthorhombic perovskite plus 5 to 10% Ca stabilized ZrO_2	Off shelf - Stock No. 1022
O_2-$12Y_2O_3$	NBS 202NS	METCO	aps power mechanical mix of ZrO_2-Y_2O_3		Off Shelf
O_2	NBS	CERAC	aps powder crushed -150 +325	single phase CeO_2 good crystallinity	Off shelf - Stock No. 1282
O_3	NBS	CERAC	aps powder crushed -150 +325	single phase Y_2O_3 fair crystallinity	Off shelf - Stock No. 1584
O_2-$5Y_2O_3$	NBS	CERAC	aps powder crushed -150 +325 mesh	cubic HfO_2 plus 5-10% monoclinic HfO_2 - crystallinity very poor	Off shelf - Stock No. 1547
O_2-12 m/o O_2 - 3 m/o O_3	Westinghouse (Kuszyc) CZ-CEO1	no origin given	aps powder, no mesh given	broad peaks, mostly cubic - small amount tetragonal poor crystallinity	

$LaCrO_3$	Westinghouse (Kochka) LC-GRO5	Gen. Refract.	sinterable powder	good crystallization no parameter shifts no 2nd phases
$SrZrO_3$	Westinghouse (Kochka) ZA	no powder source given	sintered 1650 °C no time, atmosphere given	single phase crystallinity very good
$SrZrO_3$	Westinghouse (Kuszyk) 3A-SZ UMO2	no powder source given	sintered 1650 °C no further data	single phase crystallinity very good
CeO_2-Y_2O_3-ZrO_2 on $Ca(Mg)CrO_3$	Westinghouse (Kuszyk)	no source given	flame sprayed piece, no proportions given for CeO_2-Y_2O_3-ZrO_2	top surface CeO_2-Y_2O_3-ZrO_2 broad peaks perhaps single phase cubic type, possibly some tetragonal ZrO_2 type lower -LaCrO -poor crystal-linity +2 to 5% unknown phase as in LC CE 0201
MgO, Al_2O_4 ($MgAl_2O_4$)	Westinghouse (Rossing) MA-CEO301	CERAC	plasma sprayed piece made from Cerac MgO-Al_2O_3 powder -325 +10μ mesh	single phase crystallinity medium to good
$SrZrO_3$	Westinghouse (Rossing) SZ-CEO301	CERAC	plasma sprayed piece made from Cerac $SrZrO_3$ powder -325 +10μ mesh	SrZrO +5-10% tetragonal ZrO_2 crystallinity $SrZrO_3$ good ZrO_2 poor
$La_{.95}Mg_{.05}CrO_3$	Westinghouse (Rossing)	CERAC	plasma sprayed piece made from Cerac powder LC-CEO201	LaCrO +unknown+La_2O_3 unknown phase 10% La_2O_2 5% crystallinity poor
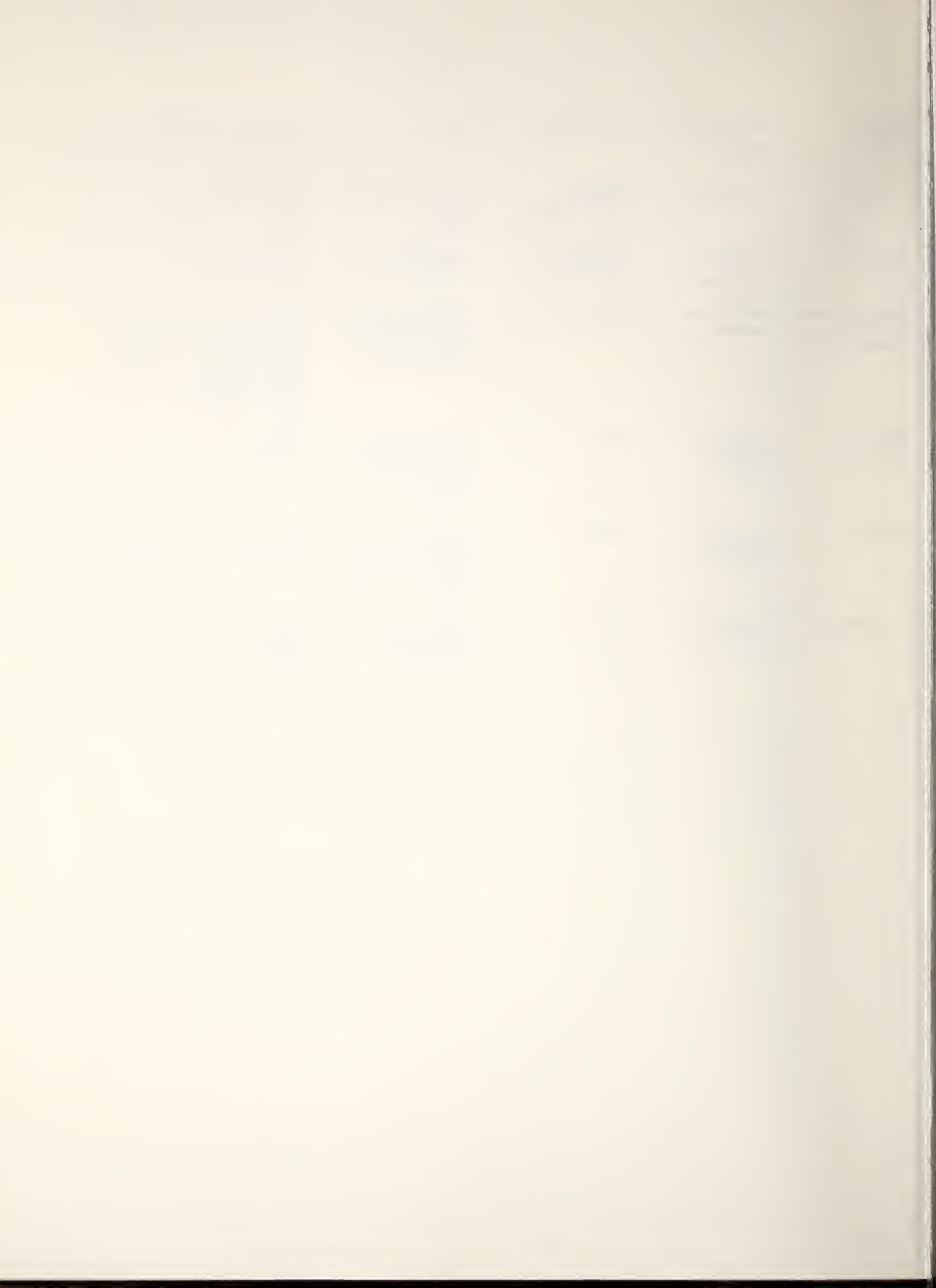
The electrodes (22) for the AVCO test in a slagging environment are in various stages of fabrication. Six electrode pairs have been completed by APS Materials, Dayton, OH. Five more electrode pairs are in progress at Technetics, Division of Brunswick, Milford, CT and should be completed soon. No date has been set for the test run, but it should occur during the next reporting period. A complete description of the design and test configuration will be given later.

4a. Examination of NBS LaCrO$_3$ Electrodes (E. N. Farabaugh)

Anode and cathode material of cermet bonded LaCrO$_3$ with a ZrO$_2$ cap has been examined by SEM and EDX techniques. These electrodes were the subject of test #166 on the MIT test rig on 2-18-77. The test ran for 3 hr. and 52 min. at temperatures of 1700 °C. The electrodes were under power and seed conditions for 2 hr. and 41 min. of the test. A drawing of the electrode assembly and cooling strip is shown in Fig. 1.

A cathode, after potting in epoxy, was cut along its length to provide a cross section of various positions along the long direction of the electrode. Areas where the ZrO$_2$ cap plus a little LaCrO$_3$ had come free from the main LaCrO$_3$ body as well as areas where the cap was well attached to the LaCrO were observed. Generally, the bond between the cap and the LaCrO$_3$ had held up well under testing. However, the entire cathode assembly had come free from the copper cooling strip leaving a thin layer of the Cu-Al alloy paste, used to bond the electrode to the cooling strip, on the bottom of the electrode.

Fig. 2a is an optical micrograph showing a typical cross section near the center of the electrode. The ZrO$_2$ ($\sim$.78 mm) is the top white layer. Next is the LaCrO$_3$ ($\sim$2.3 mm) and at the bottom is the Cu-Al alloy. There is no evidence of the cap coming loose in this area.

Fig. 2b shows an area where the cap has come free from the LaCrO$_3$. This is from a part of the electrode next to that shown in Fig. 2a. It is noted that there is some LaCrO$_3$ with the cap suggesting the failure came in the LaCrO$_3$ instead of at the ZrO$_2$-LaCrO$_3$ bond. Again, the Cu-Al alloy is seen at the bottom indicating the apparently poor bond of the paste to the cooling strip.

Fig. 2c is a 20X SEM picture of the cathode showing the separation of the cap and main body. There are several interesting areas to discuss. The first, A, is the cap and a little of the LaCrO$_3$ which has separated. There is no obvious definition of the boundary between the ZrO$_2$ and LaCrO3, indicating a good bond. Some K was detected in this area using EDX methods. B is a narrow layer in the LaCrO$_3$ which has a K concentration not much different from that in layer A. Area C is a layer in the LaCrO$_3$ which has a much higher concentration of K than either the material just above it (B) or just below it (D). The material in C also shows a much different microstructure than either B or D. D is the last of the LaCrO$_3$ before the Cu-Al alloy layer, layer E. K has been detected throughout the entire assembly. Some K was found even in the Cu-Al alloy layer.
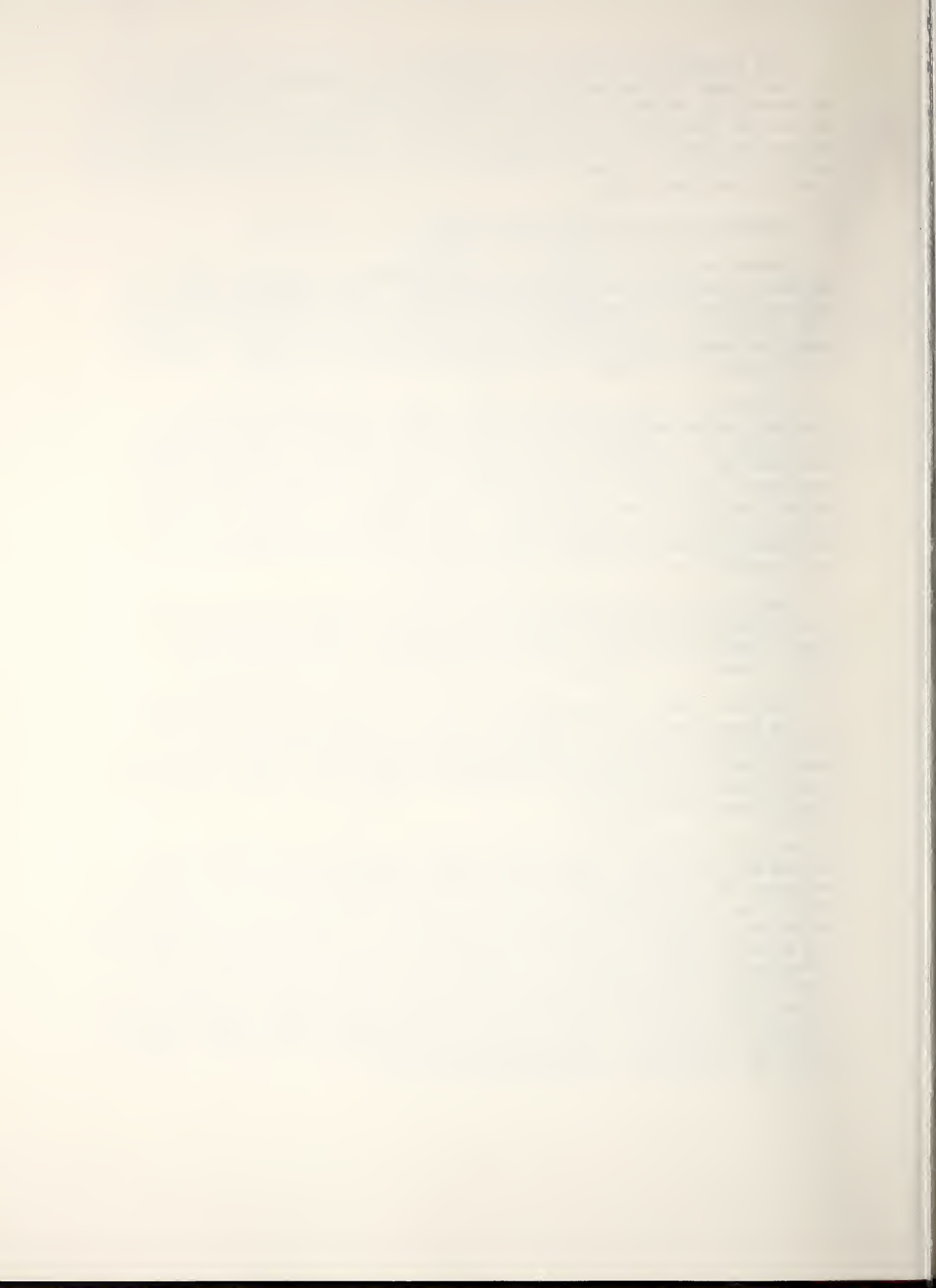
Close examination of EDX spectra showed a decrease in the Cr peak in layer C relative to layer B. This could be explained by the K reacting with the Cr and reducing the presence of Cr in the $LaCrO_3$. An exact analysis of the spectra is complicated by the overlapping of CrK_α and LaL_β lines, and other elements (i.e., scandium). In layer C it seems reasonably safe to say that higher K concentrations are accompanied by lower Cr concentrations.

It was noted that the separation of the cap occurred above where a well defined, K-rich layer was formed in the main body. It was further determined that the place where the ZrO_2 cap and $LaCrO_3$ broke free from the rest of the $LaCrO_3$ appeared to be where the Zr concentration has dropped to near zero.

We must consider two results: (1) a K-rich $LaCrO_3$ layer is found where the cap has parted; (2) the separation has occurred where the graded ZrO_2 has little Zr concentration. One cannot say which has occurred first. It may be that the separation started because of some thermo-mechanical strain, allowing K to easily get to the $LaCrO_3$ through the porous ZrO_2 causing expansion which caused the cap to break away carrying part of the $LaCrO_3$ with it.

The top part of the electrode was exposed to temperature from 1300 °C to 1700 °C at the top of the cap. At these temperatures, K will not condense, hence, the small concentration of K in A and B. Layer C could correspond to the temperature range of 1100 ° - 1300 °C where K is a liquid. (K_2CO_3) The band C had the largest concentration of K and the most microstructural changes which might be expected if the K-salt was liquid in that region.

Anode material, after potting, was cut to give a cross section at right angles to its length. Optical examination of the anodes showed that in none of them did the cap come free from the main $LaCrO_3$ body. However, some Cu-Al alloy was still on the bottom edge of the electrode showing that the anodes, as well as the cathodes, came free from the copper cooling strip at the alloy paste-copper bond.

EDX examination of the anode indicated the presence of K, Si, Mg, Zr, La, Cr, Y and Sc. There was not as much K present as in layers A and B of the cathode.
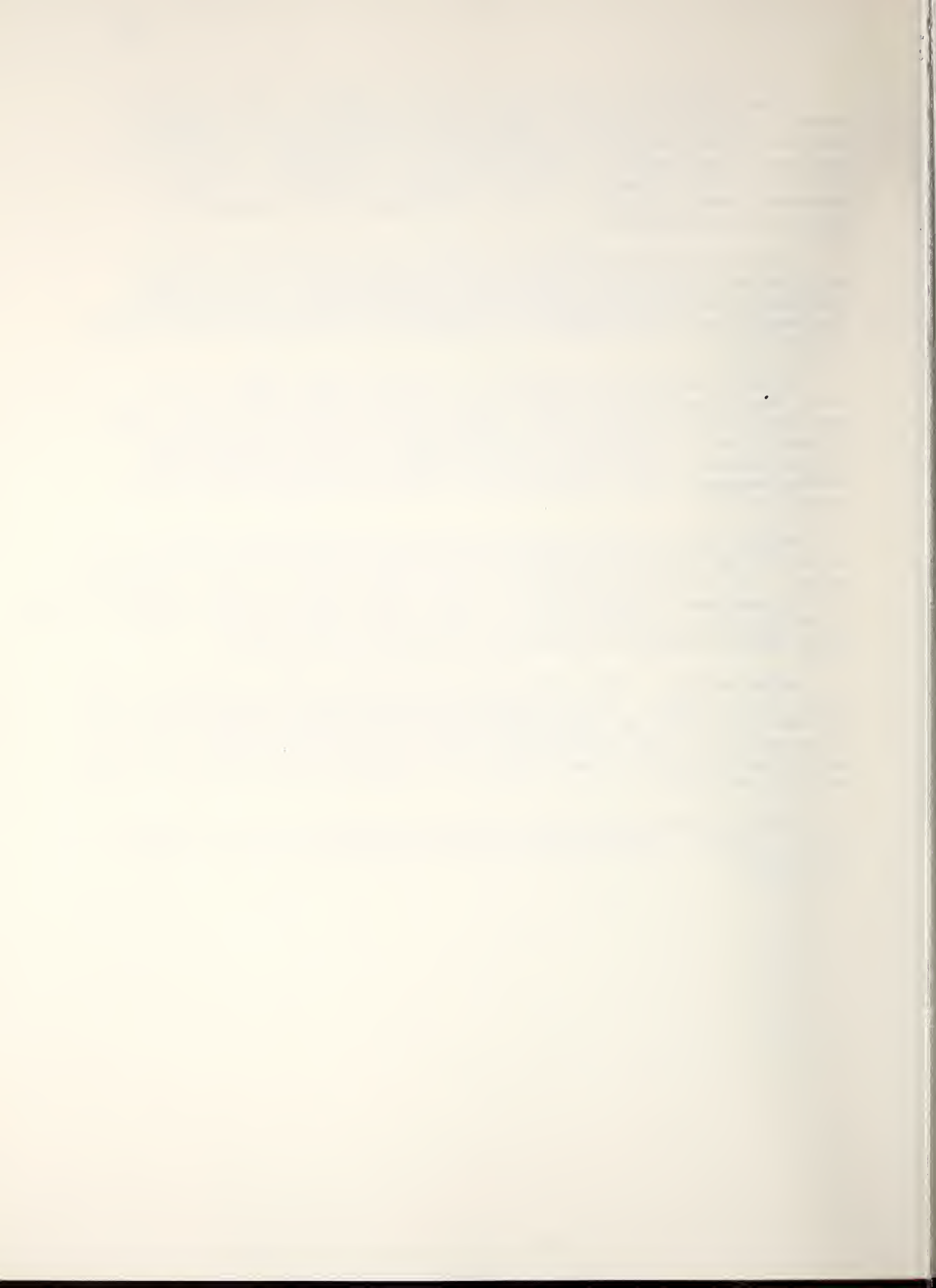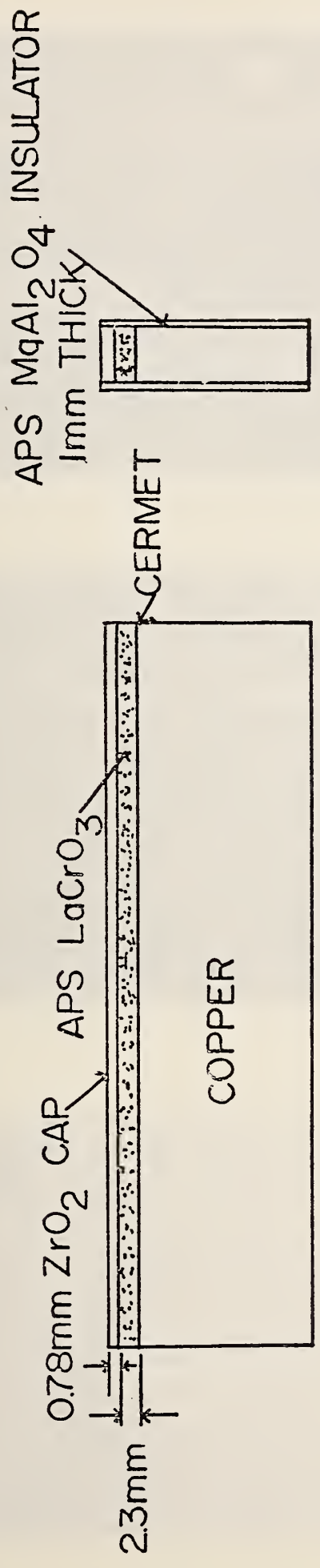
CERMET BONDED LaCrO₃ WITH ZrO₂ CAP

Fig. 1. Drawing of electrode assembly.

Fig. 2a. Optical micrograph of $LaCrO_3$-ZrO_2 cathode.

Fig. 2b. Optical micrograph of $LaCrO_3$-ZrO_2 cathode.
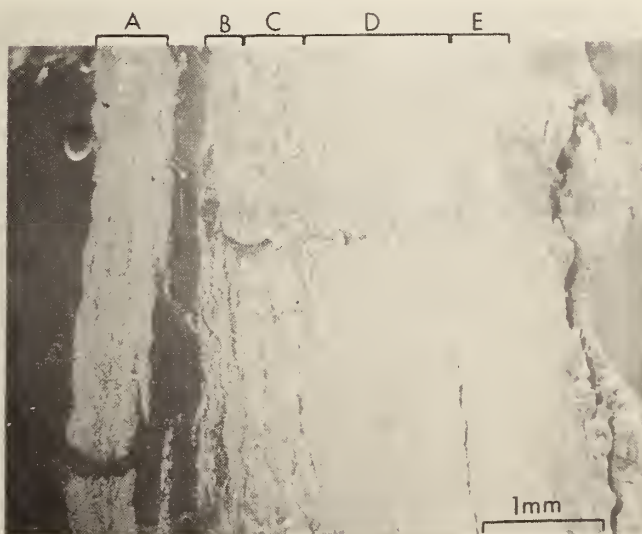
Fig. 2c. 20X SEM micrograph of cathode.

4b. <u>Post Test Analysis of ANL Electrode Test at MIT</u> (T. Negas)

On March 18 we received four electrode assemblies, including virgin specimens from ANL. These were tested in the MIT facility, March 8. The test was terminated after 30 minutes and no seed (or current) was utilized. Only one electrode remained intact partly as a result of difficulties related to the set-up and the running of the test as well as the incompatibility of the ANL electrode design (originally for the Reynold's facility) with the MIT test facility. These considerations together with observations during the test are documented by an ANL report, "Synopsis of ANL Electrode Test at MIT 8 March 1977."

The electrodes had a configuration illustrated in Figure 3 (provided by ANL). The ceramic portion consists of $82HfO_2$, $8Y_2O_3$ and $10CeO_2$ (HYC). Three of the electrodes incorporated a mesh of Nb (1% Zr) wire (apparently clad with an Au/Pt combination) while the remainder contained nichrome wire. Only the latter survived the test basically intact. Figure 3 suggests that the insulation is Al_2O_3 (plasma sprayed). X-ray diffraction and SEM/EDX data indicate that this material is actually $MgAl_2O_4$ (spinel). Zirconia castable was used to fill gaps between electrodes when stacked.
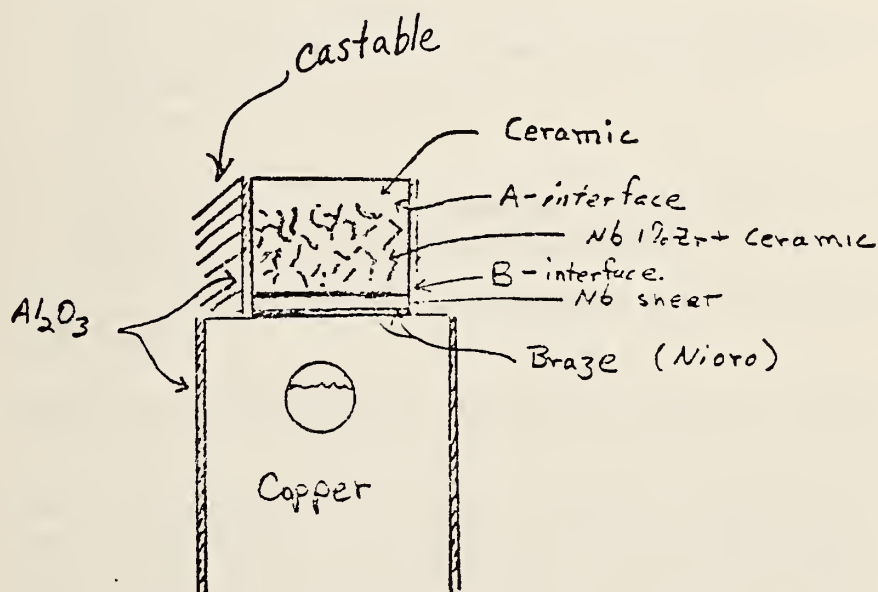
Figure 3. Schematic configuration of ANL electrodes (provided by ANL).

A separate report (11 figures) of our analysis was submitted to ANL. Conclusions based on this report are summarized below.

1a. The basic ANL electrode appears encouraging from a thermal design standpoint. Combining wire metal within an integral cohesive electrode unit is a sound approach for two reasons:

1. the wire, well into the ceramic, provides for electrical conductivity and,

2. means of attachment to an underlying metal is provided.

1b. The design was not subjected to potassium and E field, conditions which may alter the electrode structure.

2. The ceramic oxide-nichrome electrode survived the test in relatively good condition (see Figure 4).

3. The ceramic oxide-Nb (1% Zr) wire electrode (3 of 4) were damaged extensively (see Figure 5).

a. The Nb wire oxidized and reacted with adjacent ceramic components. Localized melting followed and some liquid was injected into the side insulation.

b. "Hot spots" (>1900°C) observed during the test contributed to localized heating and oxidation.

4. Fissures (and detachment) are apparent at the ceramic-braze interface.

5. The plasma sprayed $MgAl_2O_4$ insulation appears to bond well to the ceramic oxide but poorly to metallic components.

6. The ceramic oxide as fabricated contains coarse grains (HfO_2, monoclinic) surrounded by a finer matrix (CeO_2, Y_2O_3-rich). This matrix may provide avenues for seed penetration and subsequent corrosion of construction materials.
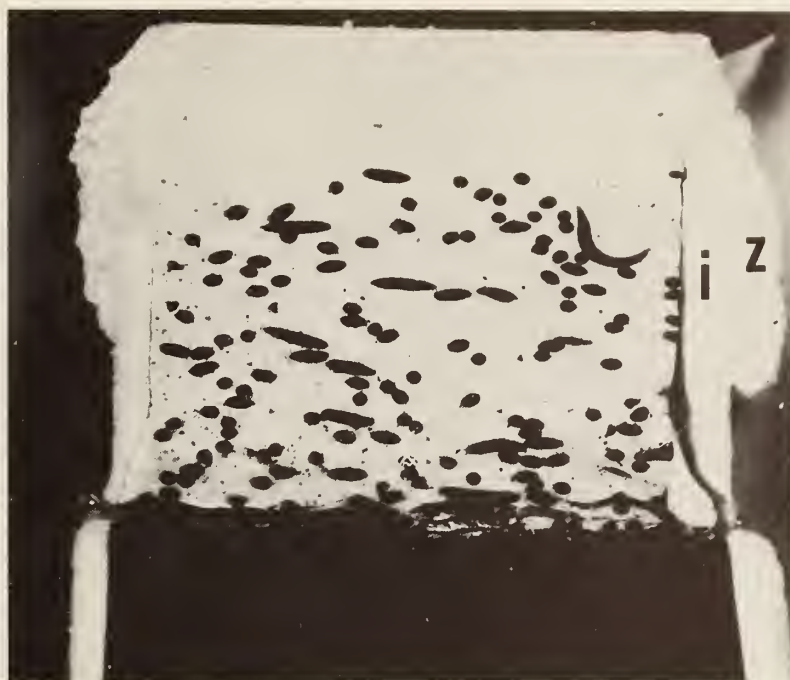
Fig. 4. Post-test ANL electrode (∿9X) fabricated from ceramic oxide (see text) plus nichrome wire. Z = zirconia castable; i = $MgAl_2O_4$ insulator.
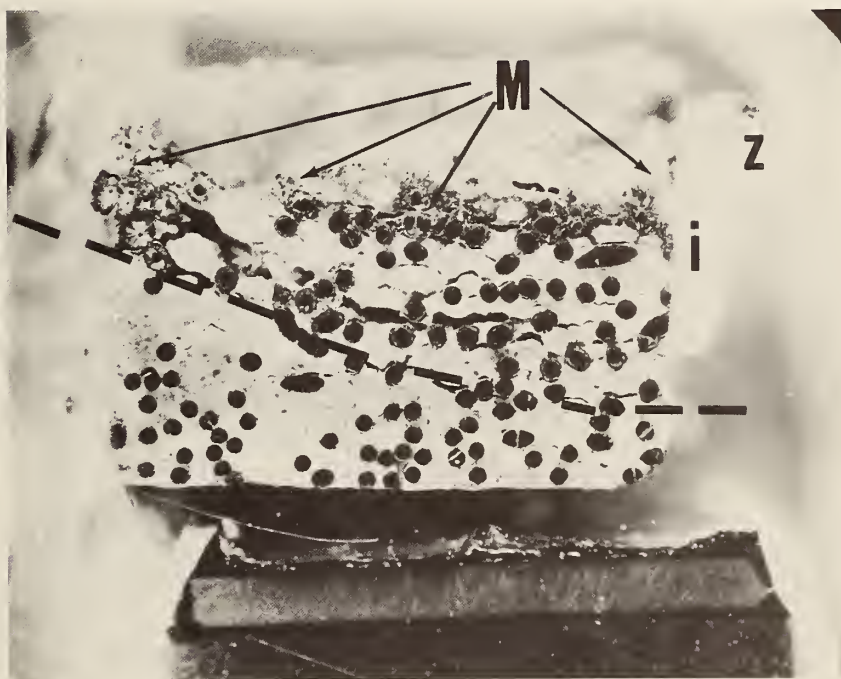
Fig. 5. Post-test ANL electrode (∿9X) fabricated from ceramix oxide (see text) plus Nb (1% Zr) wire. Oxidation of the wire is evident above the dashed line. Z = zirconia castable; i = $MgAl_2O_4$ insulator; M = several areas wherein chemical interaction including melting have progressed.

4c. <u>Post-test Analysis of G.E. Electrode Assembly Tested in MIT Rig.</u>[*]
    (L. Cook)

    A cathode assembly (#154-CA) and anode assembly (#154-A2) from a
4 hr test performed by M.I.T. on January 13, 1977 were provided by the
General Electric Company for materials characterization. Potassium
carbonate was the seed material and no slag was introduced. Other details
of the test and unused specimens for comparison were not available. The
electrodes are of a "proprietary design." For purposes of characterization
the essentials are: 1) (Mg,Al,Fe) - spinel of 2 mm thickness bonded to
2) Mo-sheathed, finned copper lead-out, in turn bonded to 3) a nickel
base with 4) (Mg, Al) - spinel slabs as insulators between electrodes.
The entire electrode assembly is attached in a complicated way to a copper
cooling block.

    The anode and cathode assemblies appear to have behaved similarly in
the 4 hr test, except: the anode may have been slightly more resistant to
corrosion; the anode insulator underwent markedly stronger attack than the
cathode insulator. Whether these differences are significant or are a
peculiarity of sampling is unknown. The spinel insulator material appears
to have withstood the test well (Figure 6), with the exception of local
breakdown in the anode insulator.

    It is estimated that a minimum of 25% of the spinel electrode material
was removed during the test. In some areas 100% has been removed. On the
average probably 50% was removed. Once degradation to the level of the
lead-out assembly occurred, corrosion of the lead-out fins, possibly by
local melting, was rapid in some areas. The ceramic-metal bond at the
spinel/lead-out junction appears to have survived the test.

    The mechanism of degradation of the spinel electrodes may be largely
thermo-mechanical. This suggestion cannot be evaluated without knowledge
of the thermal history, but is given support by the observation of partly
developed cracks which do not appear to be due, for example, to any chemical
process related to penetration of seed. They do appear related to the
highly porous areas in the spinel. To what extent textures in the spinel
(Fig. 7) are a function of fabrication vs. MHD operation cannot be evaluated
without comparison with fresh electrodes.

----

*Substantial portions of this report have been deleted, as they divulge
details of a proprietary nature. The material presented is done so with
the permission of Dr. M. Noone, General Electric Corporation.

Fig. 6. Secondary electron image of insulator surface, G.E. cathode assembly (800X), Plasma flow was from top to bottom.

Fig. 7. Polished surface of spinel near lead-out, G.E. anode (5000X).
a) Secondary electron image.
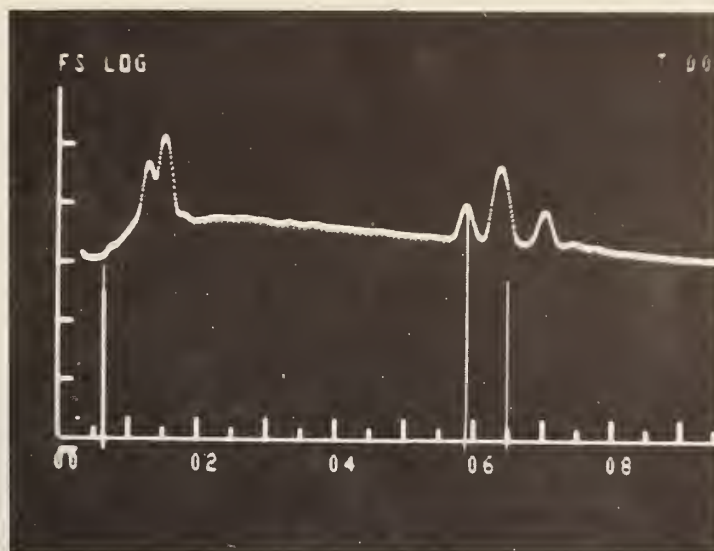
b) EDX spectrum of area in a), 20 KV. Marker shows Mn, Kα, Kβ.

c) Fe Kα, area in a).
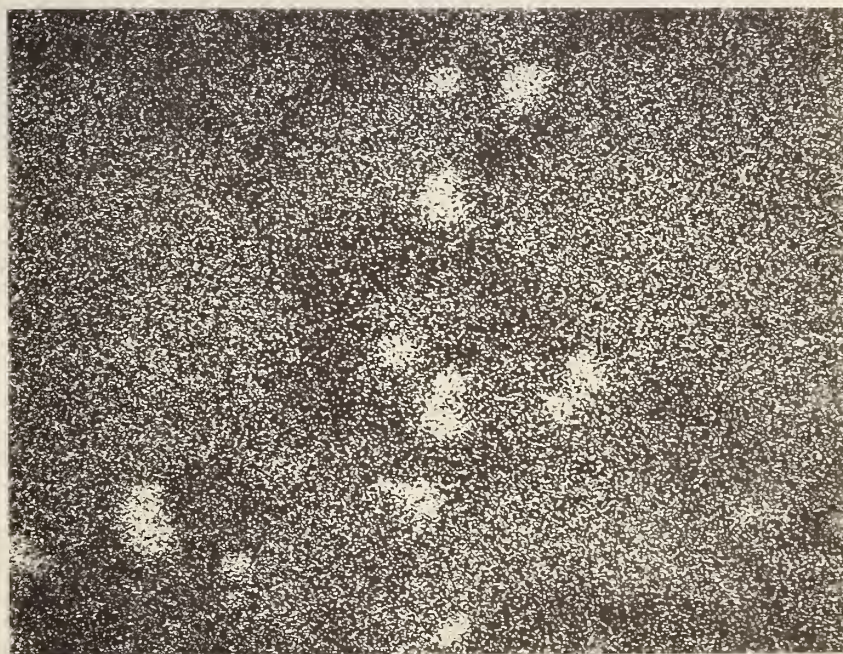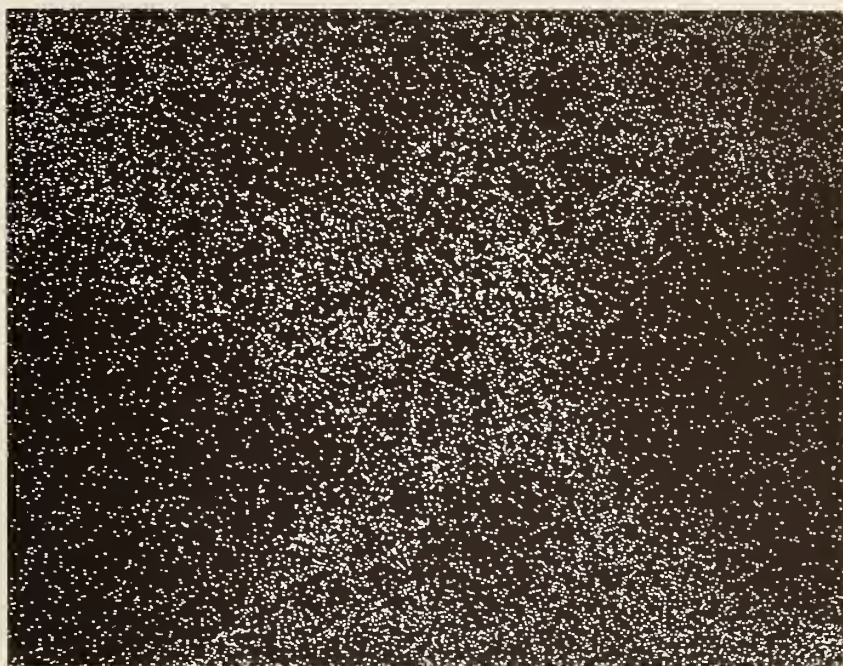
d) Mn Kα, area in a).

5a. Examination of Fluidyne RFG Samples (A. Perloff and E. N. Farabaugh)

Three samples of a chrome-magnesia refractory material were examined by x-ray powder diffraction techniques. The samples were (1) original (untested) material, (2) FN-96 cycled for 30 hours between 1800-1600°C with ash but no seed and, (3) FN-91 cycled between 1850-1700 °C with ash and K_2SO_4 seed. For the tested samples the material to be examined was chipped from the reacted surface layer.

Original Material:

The sample is predominantly well-crystallized MgO (a = 4.212Å) and a single phase spinel (a = 8.278Å). This spinel is very close in cell size to that reported for magnesiochromite [(Mg, Fe)(Cr,Al)$_2$O$_4$], but the intensities do not correspond very well. This suggests that the cation distribution may be a variation of the magnesiochromite. There are traces of materials which are reminiscient of forsterite (Mg$_2$SiO$_4$) and monticellite (CaMgSiO$_4$) but the fit is far from perfect and the identification must be considered tentative.

A sample of untested rebonded chrome-magnesia refractory (RFG) was characterized by SEM and EDX techniques. SEM micrographs showed the material is to be composed of many large grains. EDX spectra from these large grains revealed the presence of Mg, Al, Si, Ca, Cr and Fe. This suggests the presence of several phases in the grains. Further examinations of the large grains showed well-defined smaller grains of phases rich in Mg, Al, and Cr suggesting a chrome-spinel phase. X-ray analysis also indicated Si and Mg concentrated in areas surrounding the chrome-spinel phase. Thus, it is possible that MgSiO$_4$ is present between the chrome-spinel grains. MgO was easily seen in the structure when Mg mapping was done.

The untested structure is typified by large grains composed of several phases. MgSiO$_4$, MgO and chrome-spinel were predominately seen.

Tested RFG will be examined next and EDX characterizations will be used together with X-ray powder data to better describe the phase structure.

FN-96

This sample consists primarily of MgO (a = 4.218Å) and two spinel phases. The proportion of MgO relative to the spinel seems to be somewhat smaller than in the untested material, but the difference is small enough that it could be accounted for by intensity variations due to differences in crystallinity (likely) or preferred orientation (unlikely). The increase in cell size of the MgO relative to the other samples is small but real. The larger cell in this sample suggests some substitution of larger cations, probably Ca and/or Fe, which has not occurred in the other tested sample.

The two spinel phases have much broader peaks than the untested material spinel. This could indicate a much smaller crystallite size, a lower degree of crystallinity or possibly each phase represents a narrow range of cell sizes clustered around the average values of 8.25Å and 8.19Å. Both cell sizes are smaller than the cell for the original material which indicates the loss of some of the larger cations (Fe and Cr). There is more of the 8.25Å material than of the 8.19 Å phase (contrast with results on FN-91). This may indicate a smaller loss of Fe and Cr than in the FN-91 sample. However, it could also be due to the greater thickness of this sample providing proportionately more lower temperature material.

There is significantly more forsterite (Mg_2SiO_4) in FN-96 than in the other two samples. In addition, there are two weak lines (d = 2.55, 3.21) not explainable by any of the above phases. These lines could be due to an enstatite-like phase ($MgSiO_3$) which contains some Fe substitution for the Mg, but this identification is highly uncertain.

FN-91

This sample is predominately a two phase spinel system ($a_1 \sim 8.23Å$, $a_2 \sim 8.18Å$) plus some MgO with traces of other material. The most striking difference relative to the other samples is the reduced amount of MgO compared to the amount of spinel. This difference must be due to reaction with seed material. The MgO that is present has the same cell as pure MgO which indicates no substitution of Fe or Ca has taken place in contrast with the FN-96 sample.

The spinel peaks are broad as in the FN-96 sample which suggests the same possibilities with regard to crystallite size, crystallinity and variation of cell sizes. The spinel cells are similar or slightly smaller than those found in FN-96. In the FN-91 there is more of the 8.18Å material than of the 8.23Å phase. This could indicate a greater loss of Fe and Cr due to the presence of seed or the slightly higher temperatures. However, this sample was not as thick as for FN-96 so this difference could be simply indicative of a greater proportion of surface material in the sample.

The impurity levels are too low to make identification certain, but there is probably forsterite (Mg_2SiO_4) and moniticellite-like ($CaMgSiO_4$) material. Additional possibilities include traces of $KAlSiO_4$ and potassium magnesium silicates.
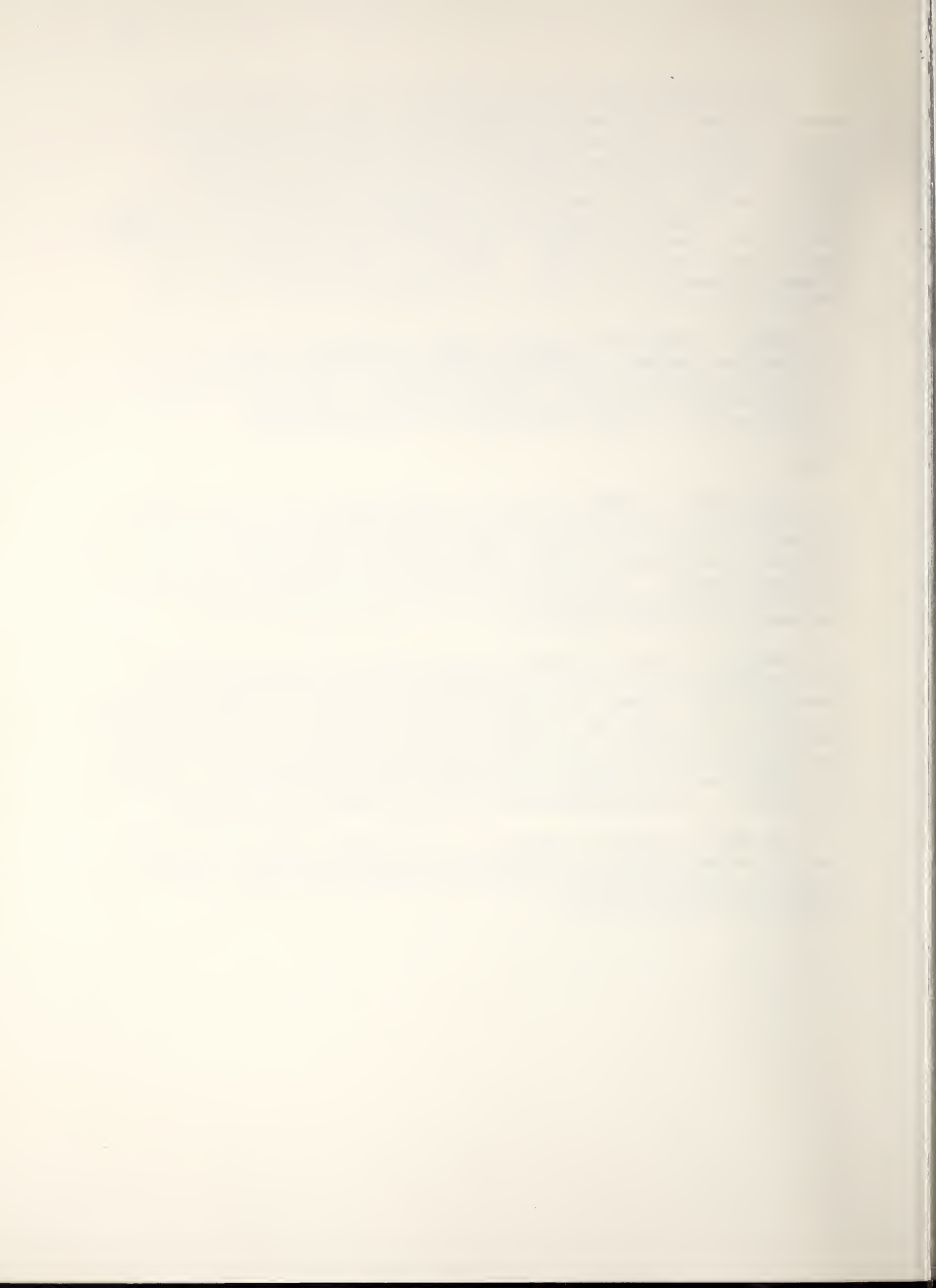
5b.   X-ray results on slags from AVCO generator using Montana Fly Ash and New Hampshire Fly Ash slags (A. Perloff)

We received from AVCO specimens of generator slag originating from Montana and New Hampshire fly ash. It was requested that these be analyzed for phase distributions, segregations, inhomogeneities, etc. which could account for observed polarization phenomena during testing.

Our first step has been to identify the crystalline phase assemblage of each slag specimen in bulk (see below). SEM/EDX analysis of these materials have not been concluded.

Six slag samples were examined by x-ray diffraction techniques. They are derived from two sources of fly ash and were identified as New Hampshire fly ash (anode and cathode) and Montana fly ash (front anode and cathode; rear anode and cathode).

ANODES

There is more general similarity between the N.H. fly ash pattern and the Montana fly-ash from the front electrode. Both are primarily orthorhombic $KAlSiO_4$ patterns. Impurity lines are d = 3.73, 3.27, 3.00, 2.90, 2.88, 2.72, 2.53 (N.H.), 2.38 and 1.936. The Montana fly-ash from the rear electrode contains orthorhombic $KAlSiO_4$, but the intensities are not normal for many of the lines which could be due to more substitution of other elements or different K, Al, silicate phases (hexagonal and tetragonal phases are possibilities). There are some lines appearing which are not significant in the other anode patterns, e.g., (d = 4.46, 2.83, 2.75, 2.66, 2.59, 1.912, and 1.880).

The complexity of the patterns make it impossible to unambiguously identify the impurity phases. A number of silicates of Ca, Mg, Al, and K are possible contributors. The probable presence of the tetragonal potassium aluminum silicate in the Montana fly ash rear anode suggests this may be richer in potassium than the others (lower temperature?, greater accumulation in rear of channel?).

The only anode sample which could contain significant amounts of iron oxide is the New Hampshire fly ash (d = 2.53).

CATHODE

All three cathode slags contain orthorhombic $KAlSiO_4$ but in reduced amounts relative to the anode slags. The cathode slags seem to be richer in the cubic and tetragonal phases which are higher in potassium. This is more pronounced in the Montana slags than in the New Hampshire one. The New Hampshire slag, although containing less of the potassium rich aluminosilicates is the only pattern to show a clear indication of $KHCO_3$ lines. No iron oxides or β-alumina phases appear to be present.
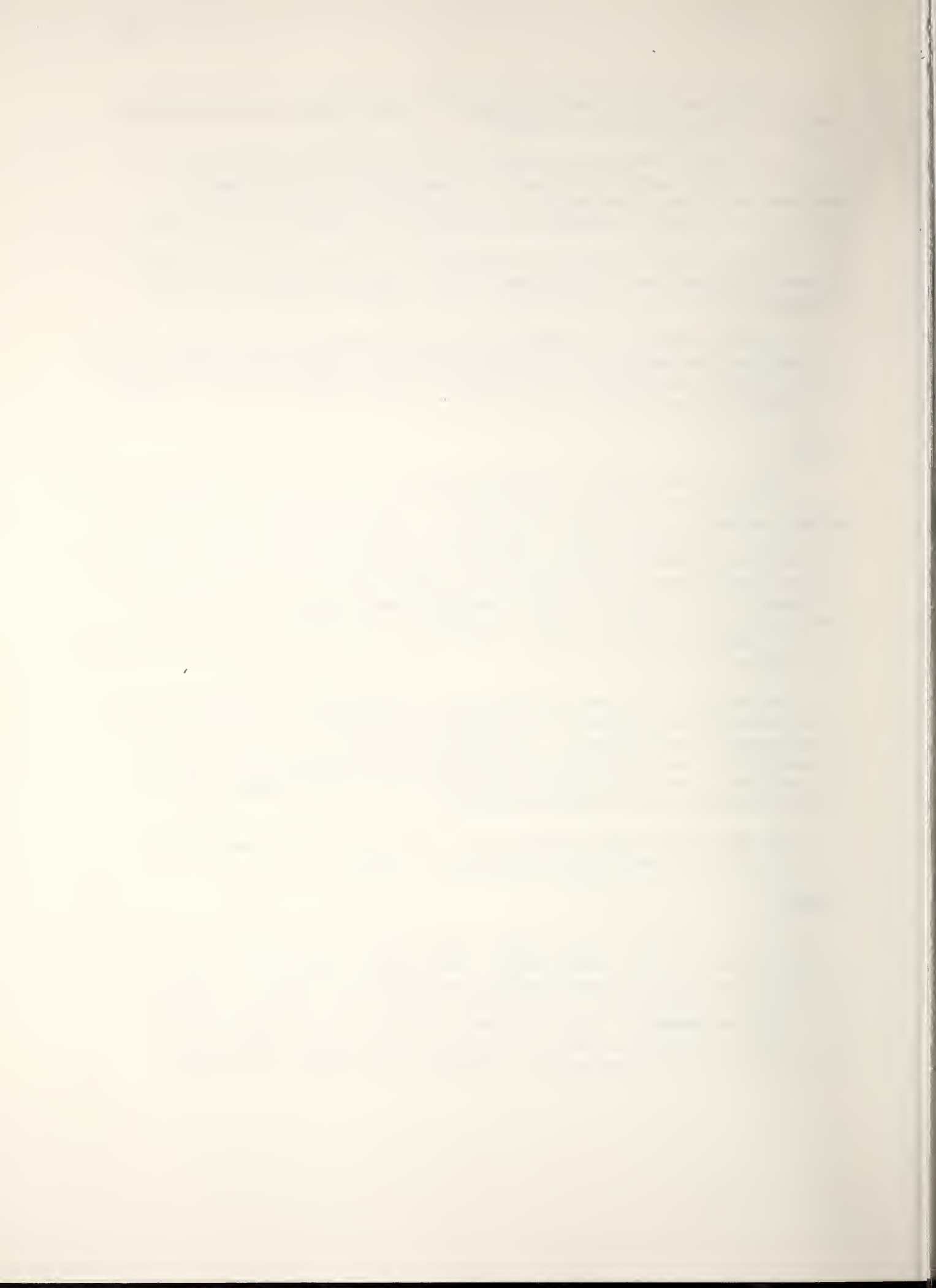
Task L. Assessment of Steam Plant Components (J. R. Cuthill)

This is the 8th quarterly progress report since the initiation of Task L. The overall objective of Task L is the recommendation of commerical alloys for critical components downstream of the MHD generator. The assessment of these commerical alloys is being made on the basis of data in the literature, including research papers, handbooks, data compilations, producers bulletins, specifications, and the ASME Boiler and Pressure Vessel Code. If specific construction alloys for these critical components cannot be recommended per se on the basis of the data in the literature, promising alloys will be cited and recommendations made for further testing. Such testing will be carried out under this Task to the extent possible.

Table 1 is a compilation of mechanical properties of some promising wrought alloys with the steam superheater tube application principally in mind. Table 1 is an extension of the corresponding Table 2 in the previous quarterly report. (Table 2 in the present report gives the corresponding alloy compositions). Each of these alloys has been included because of relevance to downstream component applications, i.e. simulation corrosion test data is available on them, or they are commonly used construction materials for steam plant components, or on the basis of related performance they appear to have promise of withstanding the unique service conditions imposed by the presence of the potassium compounds, which has been explored in previous quarterly reports. Also, in the quarterly report for Jan. 1 to Mar. 31, 1977, a relative alloy ranking is given in respect to anticipated ability to resist the hot corrosion attack. Conversion factors are given as a footnote to Table 1 for converting the mechanical property values in the Table, given in SI units, to the English units which continue to be used in the ASME Boiler and Pressure Vessel Code. (1)

ASME Boiler and Pressure Vessel Code

Many of the alloys in Tables 1 and 2 have been tabulated in the ASME Boiler and Pressure Vessel Code. These alloys are listed in Table 3 together with their respective ASME Specification No. After each alloy there is listed for comparison the maximum tensile stress allowed by the Boiler Code at 1200°F, the estimated external surface temperature of the steam superheater tubes. The maximum temperature at which the alloy can be used is also given together with the corresponding maximum allowable design stress. Note that in some cases this maximum allowable service temperature is below 1200°F (648 C).

Hard Facing and Wear Resistant/Corrosion Resistant Alloys

There are applications such as the mating surfaces of the valves on the high temperature air preheaters, that will require alloys to withstand metal-to-metal sliding wear as well as high temperature oxidation and hot corrosion. Some pertinent properties of two selected

alloys are given in Table 4. Stellite 21 can only be cast or applied as a weld overlay and then ground. Haynes Stellite Alloy no. 6B is a wrought alloy. These two alloys appear to be representative of the best of the stellite alloys in their respective categories for the combination corrosion/wear application being considered here. Heywood and Womack(2) suggest "Stellite facing" in their proposed valve design for the high temperature air heater unit.

Resistance of Alloys to H_2S

The update report on the Baseline Plant design by Jackson, et al (3), at the recent 16th Symposium on the Engineering Aspects of Magnetohydrodynamics, indicated that the proposed potassium seed recovery system will require the handling of high-temperature gases containing high concentrations of H_2S. (See Figure 1 composed from data in the above paper by Jackson, et al.)

In respect to this requirement for alloys to resist attack by H_2S at high temperature, some relevant data is given in Table 5a which was obtained in Phase I of the materials program of the Metal Properties Council, Inc. for coal gasification plants.(4) Only their 1500° data, which corresponds to the 1060°K reactor temperature (Fig. 1) are included in Table 5a . The alloys are arranged in the order of increasing thickness loss. Although these absolute values of loss rates cannot be assumed to apply in the atmospheres experienced in the MHD application, the relative alloy ranking in respect to H_2S attack can probably be assumed to hold. This assumption is supported by data reported by Hungtington Alloys Division of INCO (5) on thickness loss rate in a different H_2S-containing atmosphere. (The actual data are reproduced in Tables 5b and 5c .) Although there are very few alloys that are listed by both sources, the three that are, i.e. Incoloy 800 and type 309 and type 304 stainless steels fall in the same general relationship. There probably is no basis to make a distinction between types 309, 310, 446 stainless steels, 50 Ni-50 Cr and Incoloy 800 on the basis of these data, but Incoloy 600 and 9 Cr-1 Mo alloy appear to be distinctly inferior in their ability to resist H_2S attack, with the others falling somewhere in between the first 5 and these last 2 alloys.

References

1. ASME Boiler and Pressure Vessel Code, 1977 edition, Amer. Soc.
    Mech. Engrs., 345 E. 47th St., NY, NY 10017.

2. J. B. Heywood and G. J. Womack, Open Cycle M.H.D. Power Generation,
    p. 38, Pergamon Press, Oxford, 1969.

3. W. D. Jackson, R. L. Lawit, R. A. Stoudt, M. G. Klett, J. C. Cutting,
    and C. D. Maxwell, Status of the Reference Dual-Cycle MHD - Steam
    Power Plant, 16th Symposium, Engineering Aspects of Magnetohydro-
    dynamics, Pittsburgh, 1977.

4. A. O. Schaefer, C. H. Samans, M. A. Howes, S. Bhattacharyya, E. R.
    Bangs, V. L. Hill and F. C. Chang, A Program to Discover Materials
    Suitable for Service under Hostile Conditions Obtaining in Equipment
    for the Gasification of Coal and Other Solid Fuels, Annual Report
    to ERDA 1/1/75 to 12/31/75, The Metal Properties Council, Inc.,
    345 E. 47th St., NY, NY.

5. "INCOLOY Alloys", Huntington Alloy Products Division, INCO,
    Huntington, WV.
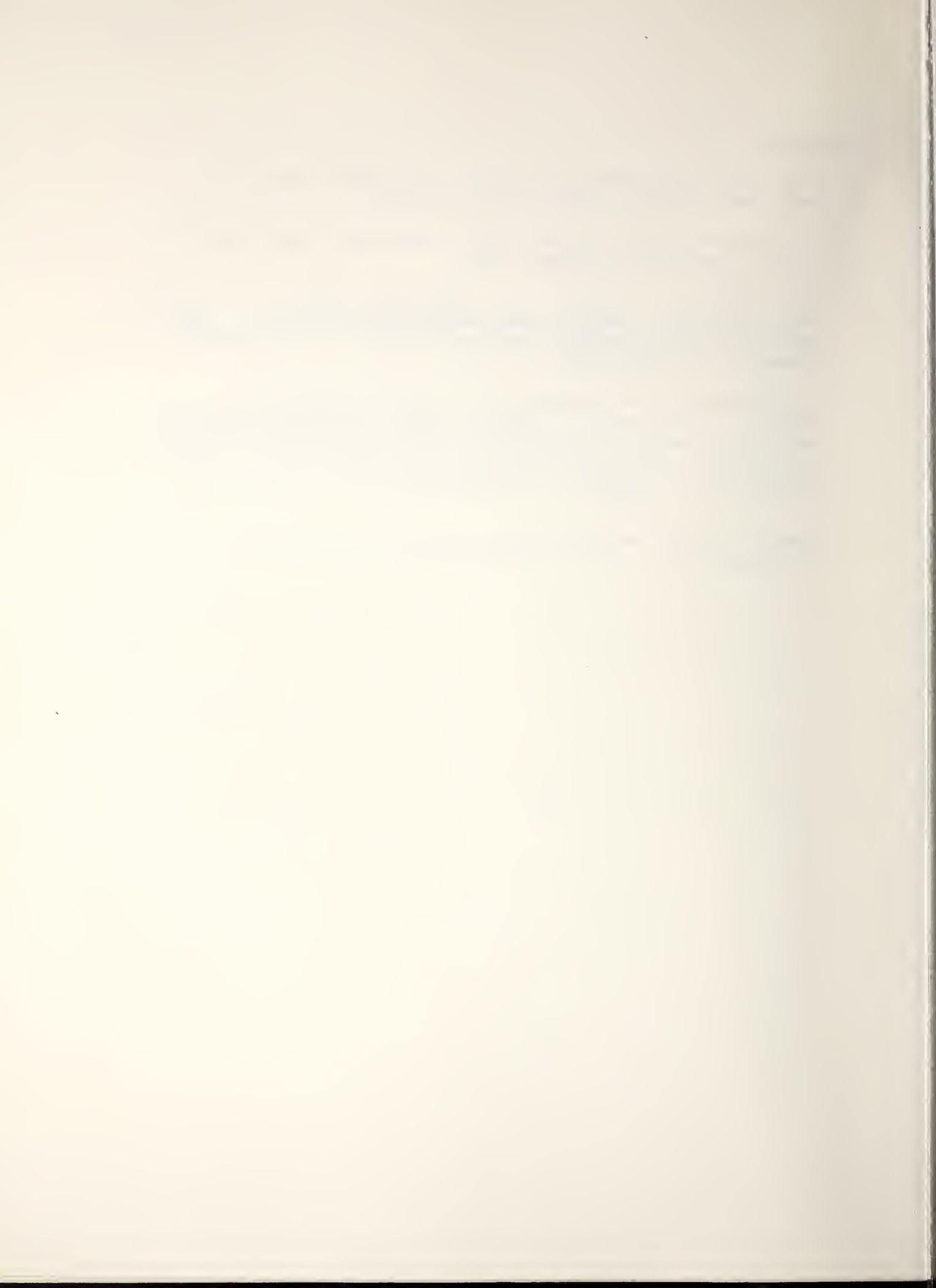
Table 1. Mechanical Properties of Wrought Alloys

Item #	Alloy	1000 hr. Rupture Str. MPa=10⁶N/m²	Yield Str. 0.2% offset MPa	Tensile Strength MPa	Elastic Modulus GPa=10⁹N/m²	Creep Str. 1% @ 10⁴ hr. MPa	Fatigue Str. 10⁸ Cy MPa	Charpy V Impact Str. joules
	STAINLESS STEELS							
1	304 S.S.	97 (649°C)	110 (649°C)	317 (649°C)	145 (649°C)	55 (649°C)	200 (649°C)	170 (RT)
2	310 S.S.	172 (593°C)	138 (593°C)	448 (593°C)	200 (RT)	103 (649°C)	217b (RT)	121 (RT)
3	316 S.S.	241 (593°C)	172 (593°C)	414 (593°C)	193 (RT)	83 (649°C)	269b (RT)	106 (RT)
4	446 S.S.	39 (593°C)	155 (593°C)	442 (593°C)	200 (RT)	17 (593°C)	324b (RT)	--
	Ni & Fe-Ni BASE ALLOYS							
5	Hastelloy C-276	276 (649°C)	261 (871°C)	394 (871°C)	176 (538°C)	--	--	--
6	Hastelloy X	214 (649°C)	272 (649°C)	572 (649°C)	164 (500°C)	152 (649°C)	310 (649°C)	39 (816 °C)
7	Haynes 556	276 (649°C)	219 (649°C)	589 (649°C)	156 (649°C)	--	--	--
8	Inconel 601	193 (649 °C)	172 (649 °C)	538 (649 °C)	206 (RT)	--	--	163 (RT)
9	Inconel 617	325 (649°C)	171 (649 °C)	568 (649 °C)	--	--	--	56 (RT)
10	Inconel 718	586 (649 °C)	738 (760 °C)	952 (760 °C)	165 (760 °C)	483 (649 °C)	490 (649 °C)	61 (649 °C)
11	Inconel X750	470 (649 °C)	450 (760 °C)	550 (760 °C)	165 (760 °C)	427 (649 °C)	400 (649 °C)	--
12	Incoclad 671/800H							
13	Inconel 671	97 (649 °C)	290 (649 °C)	552 (649 °C)	--	--	--	--
14	Incoloy 800 H	172 (649 °C)	100 (649 °C)	343 (649 °C)	139 (816 °C)	--	207 (649 °C)	244 (649 °C)
15	Incoloy 800	159 (649 °C)	179 (649 °C)	414 (649 °C)	154 (649 °C)	76 (649 °C)	152 (760 °C)	244 (649 °C)
16	Incoloy 802	193 (649 °C)	186 (649 °C)	517 (649 °C)	163 (649 °C)	117 (649 °C)	310 (649 °C)	--
17	Udimet U500	145 (871 °C)	241 (982 °C)	317 (982 °C)	142 (982 °C)	69 (371 °C)	331 (816 °C)	10.8 (649 °C)
	COBALT BASE ALLOYS							
18	Haynes 25 (a)	124 (816 °C)	238 (871 °C)	322 (871 °C)	181 (760 °C)	172 (659 °C)	83 (982 °C)	163 (871 °C)
19	Haynes 188	110 (816 °C)	303 (649 °C)	731 (649 °C)	181 (649 °C)	90 (760 °C)	290 (760 °C)	171 (704 °C)
	LOW ALLOY HIGH STRENGTH STEELS							
20	Croloy 9M	48 (649 °C)	207 (RT)	159 (649 °C)	--	16 (649 °C)	--	--
21	HCM9M (Japan)	60 (650 °C)	179 (649 °C)	255 (649 °C)	--	--	--	--

a - same as L605, WF11

1 ksi = 6.895 MPa
1 MPa = 0.1450 ksi

b - for 10⁸ cycles

1 ft. lb. = 1.356 J
1 joule = 0.737 ft. lb.

Table 2. Chemical Compositions of Selected Wrought Alloys

Item No.	Mfgr. Designation	Cr	Ni	Co	Fe	Al	Ti	Nb	Ta	Mo	W	Mn	Si	C	Other
	Stainless Steels														
1	304 S.S.	18-20	8-12	-	bal	-	-	-	-	-	-	2.0	1.0	0.08*	0.045P .03S
2	310 S.S.	24-26	19-22	-	bal	-	-	-	-	-	-	2.0	1.5	0.25*	0.045P .03S
3	316 S.S.	16-18	10-14	-	bal	-	-	-	-	2.0-3.0	-	2.0	1.0	0.08*	0.045P .03S
4	446 S.S.	23-27	0.50*	-	bal	-	-	-	-	.	.	1.5	1.0	0.35*	0.04P .025N
	Ni & Fe-Ni Base Alloys														
5	Hastelloy C-276	14.5-16.5	bal	2.5*	4-7	-	-	-	-	15-17	3-4.5	1.0*	0.05*	0.02*	0.35V .03P*
6	Hastelloy X	20.5-23.0	bal	0.5-2.5	17-20	-	-	-	-	8-10	0.2-1.0	1.0*	1.0*	1.15*	0.02La 0.2N
7	Haynes 556	22.0	20.0	20.0	bal	0.3	-	0.1	0.9	3.0	2.5	1.5	0.40	0.10	0.02La 0.2N 0.02Zr
8	Inconel 601	23.0	60.5	-	14	1.35	-	-	-	-	-	0.5	0.25	0.05	0.5Cu* 0.007S
9	Inconel 617	22.0	54	12.5	-	1.0	-	-	-	9.0	-	-	-	0.07	--
10	Inconel 718	17-21	50-55	1.0	bal	0.2-.8	0.9	(4.75-5.5)a	-	3.0	-	0.35	0.35	0.08	0.3Cu* 0.006B
11	Inconel X750	14-17	70 min.	-	5-9	0.4-1.0	2.5	(0.7-1.2)a	-	-	-	1.0	0.5*	0.08	0.5Cu 0.01S
	Incoclad 671/800H														
12		see below for compositions of cladding (671) and substrate (800H)													
13	Inconel 671	48	bal	-	-	--	0.35	-	-	-	-	-	-	0.05	--
14	Incoloy 800H	21	32.5	-	46	0.38	0.38	-	-	-	-	0.75	0.50	0.1	0.38Cu -.008S
15	Incoloy 800	21	32.5	-	46	0.38	0.38	-	-	-	-	0.75	0.50	0.05	0.38Cu -.008S
16	Incoloy 802	21	32.5	-	46	-	--	-	-	-	-	0.80	0.40	0.35	0.4 Cu
17	Udimet U500	15-20	bal	13-20	4.0*	2.5-3.2	2.5-3.2	-	-	3.0-5.0	-	-	--	0.15	0.008B
	Cobalt Base Alloys														
18	Haynes HS25	19-21	9-11	bal	3.0*	--	--	--	--	--	14-16	1-2	1.0*	0.10	--
19	Haynes 188	20-24	20-24	bal	3.0*	--	--	--	--	--	13-16	1.25	0.2-0.5	.05-.15	0.05-.15La
	Low-Alloy High Strength Steels														
20	Croloy 9M	8-10	--	--	--	--	--	--	--	0.9-1.1	-	0.3-0.6	.25-1.0	0.15*	0.03P 0.03S
21	HCM 9M (Japan)	8-10	--	--	--	--	--	--	--	1.8-22	-	0.3-0.7	.50*	0.08*	0.03P 0.03S

* = max

a() = Nb + Ti

Table 3.

ASME Boiler and Pressure Vessel Code, Maximum allowable Tensile Stresses

Alloy	ASME Spec. No.	Shape	Max. allow. tensile stress, psi		
			@ 1200°F (648°C)	@ Max. allowable temp. (temp. in parenthesis)	
304 SS	SA 213	tube	6,000	1,400	(1500°F/815°C)
304L SS	SA 213	tube	-----	9,000	(800°F/427°C)
		plate	-----	11,000	(800°F/427°C)
310 SS	SA 213	tube	6,000	700	(1500°F/815°C)
316 SS	SA 213	tube	7,400	1,300	(1500°F/815°C)
446 SS	SA 213	tube	-----	14,300	(650°F/343°C)
Incoloy 800	SB 163	tube	7,900	1,700	(1500°F/815°C)
"	SB 408	bar	7,900	1,700	(1500°F/815°C)
Incoloy 800H	SB 407	tube	8,400	2,500	(1500°F/815°C)
Inconel 617	(Has not been entered into the Boiler Code)				
Hastelloy X	SB 435	plate	11,300	4,800	(1,400°F/760°C)
	SB 572	bar	11,300	4,800	(1,400°F/760°C)
Hastelloy C-276	SB 574	bar	------	21,800	(1,000°F/538°C)
Hastelloy G	SB 582	plate	------	19,000	(1,000°F/538°C)
	SB 581	bar	------	6,000	(1,000°F/538°C)
Haynes 25	(Has not been entered into the Boiler Code)				
Haynes 188	(Has not been entered into the Boiler Code)				
9Cr-1Mo	SA 213	tube	1,500	1,500	(1,200°F/648°C)
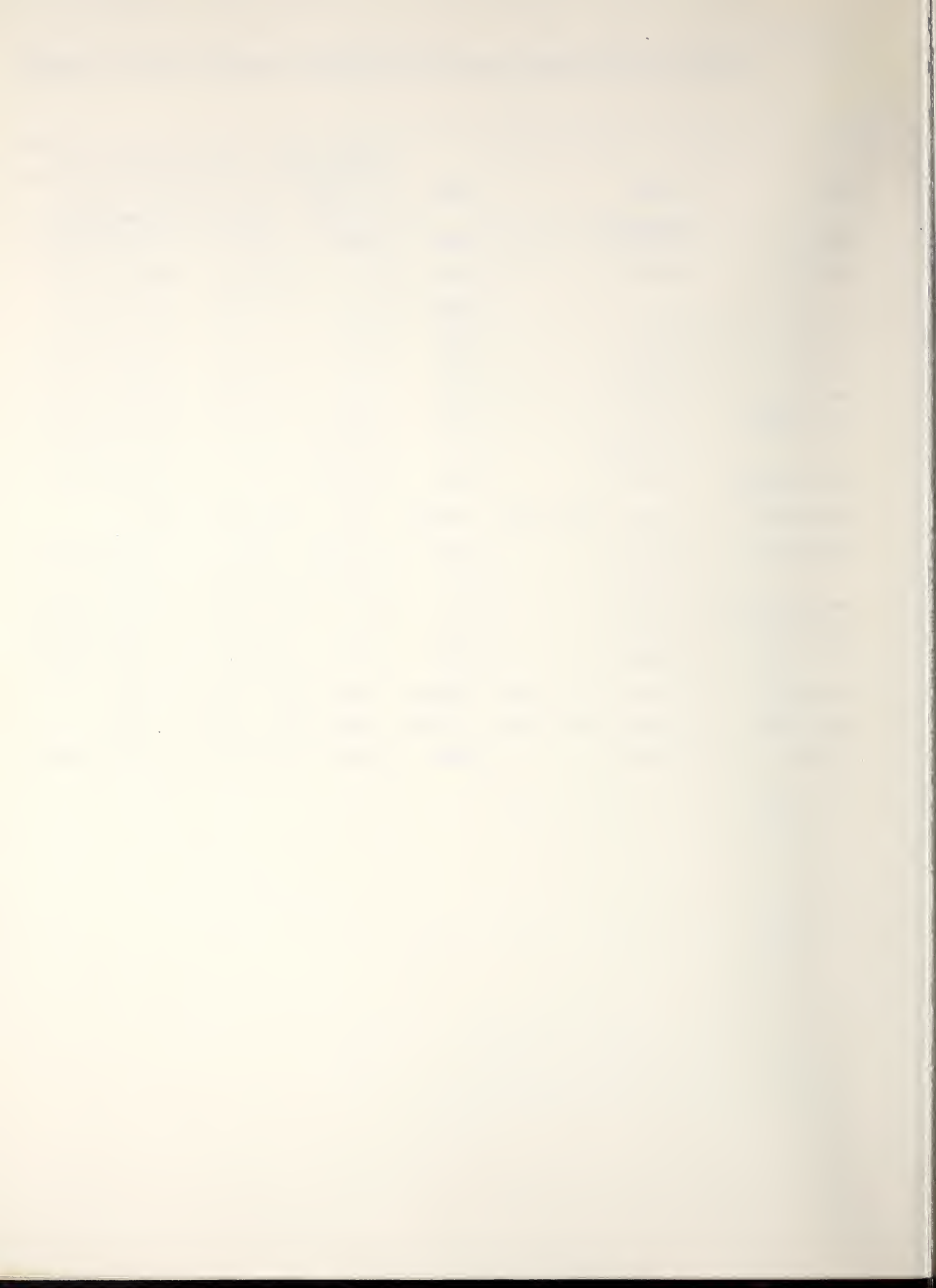
Nominal Composition

Alloy	Cr	Ni	Co	Mo	W	Fe	Si	Mn	C
Haynes Stellite (a) Alloy No. 21	27.0	2.8	bal.	5.0	-	-	-	-	0.25
Haynes Stellite (b) Alloy No. 6B	28-32.0	3.0	bal.	1.5 max	3.5-5.5	3.0 max	2.0 max	2.0 max	.9-1.4

(a) Covered electrode for Hard-facing by weld overlay and grinding.

(b) Wrought Alloy.

Mechanical Properties

Alloy	Temperature	Hardness ROCKWELL	Ultimate tensile ksi+	Yield Strength ksi	Elongation %	Izod Impact ft-lbs.	1000 hr Rupture stress ksi
Haynes Stellite (c) Alloy No. 21	R.T.	C30*	101	82	8		
	1200°F (648°C)		71	39	16		42
Haynes Stellite (d) Alloy No. 6B	R.T.	C38	148	88	7	62	
	1250 °F (675°C)		115	60.6	9		

(c) Data on Investment Cast material in lieu of data on weld overlay, -except Hardness value.

(d) Data on ½" rolled plate material

*Work-hardens to C45

+ Ksi = 1000 lbs/sq in.; to convert to MegaPascals (MPa), multiply by 6.895

Table. 5a. Corrosion Rates in H_2S from The Metal Properties Council data (Ref.4)

Alloy	Loss of sound metal in./ yr.*
310 S.S.	.004
309 S.S.	.006
50 Ni-50Cr	.006
446 S.S.	.008
Incoloy 800	.015
304 S.S.	.039
316 S.S.	.041
INCONEL 601	.657
INCONEL 600	4.9

*based on 1000 hr. test at 1500°F(815°C) in 1% H_2S, 24% H_2, 18%CO_2,12%CO,

5% CH_4, 1% NH_3, bal. H_2O, except Inconel 600 which was a 100 hr. test.

Table 5b.
Corrosion Rates in H_2S from Huntington Alloys data (Ref. 5)[2] in 7.0% H_2S, bal. H_2.

Alloy	Temperature, °F	Corrosion Rate, mpy	
		330-hr Test	Long Term [b]
INCOLOY alloy 800	600	1.1	0.6
	750	8.7	2.3
	900	28.2	5.8
Type 321 Stainless	600	1.9	0.9
	750	14.6	3.3
	900	38.1	5.3
Type 304L Stainless	600	2.1	0.9
	750	15.1	2.6
	900	36.8	5.7
9 Cr-1 Mo	600	37.9	17.1
	750	172.2	64.7
	900	383.2	128.0

[a] 5 to 7% by volume hydrogen sulfide in hydrogen at 2000 psig.
[b] Calculated from slope of weight-loss/time curve.

Table 5c.
Corrosion Rates in H_2S from Huntington Alloys data (Ref. 5) in 1.5% H_2S, bal. H_2

Alloy	Corrosion Rate, mpy
INCOLOY alloy 800	2.9
Type 309	4.9
INCOLOY alloy 804	5.0
Type 204 ELC	5.0
Type 202	7.7
Type 304	7.9
INCONEL alloy 600	10.1

[a] Test duration, 730 hr Test temperature, 750° F. Hydrogen pressure, 485 psig. H_2S concentration in H_2, 1.5% by volume.

Fig. 1 Schematic of Seed Regenerator Function (from Ref.3)